If I have seen further it is by standing on the shoulders of Giants

To my own giants, my parents, **Professor Dimitris Gikas** and **Mrs. Margarita Gika**, for their support and patience throughout my career so far. They are and have been my source of strength and guidance on the all too many occasions where I found myself frightened and lost.

And to two people who have in their own ways inspired me in my career so far; **Professor Briggs** for helping me become a good clinician and a safe orthopaedic surgeon and **Professor Flanagan** for teaching me how to be a good academic.

“Would you tell me, please, which way I ought to go from here?"
"That depends a good deal on where you want to get to," said the Cat.
"I don’t much care where--" said Alice.
"Then it doesn’t matter which way you go," said the Cat.
"So long as I get SOMEWHERE," Alice added as an explanation.
"Oh, you’re sure to do that," said the Cat, "if you only walk long enough.”

Lewis Carroll, *Alice's Adventures in Wonderland*

A Study of the Subchondral Bone in Human Knee Osteoarthritis using Raman Spectroscopy

Thesis submitted for the degree of M.D. (Res)

Panagiotis D. Gikas

Institute of Orthopaedics and Musculoskeletal Science

University College London

Declaration

I, Panagiotis Gikas, confirm that the work presented in this thesis is my own.

Where information has been derived from other sources, I confirm that this has been indicated in my thesis.

Abstract

Osteoarthritis (OA) is a common, debilitating disease, involving degeneration of cartilage and bone in synovial joints. Subtle changes in the molecular structure of subchondral bone matrix occur and may precede gross morphological changes in the osteoarthritic joint.

In this thesis, the analytical technique Raman Spectroscopy (which uses a monochromatic light source to probe chemical composition) is used to explore the hypothesis that subchondral bone changes occur prior to and during joint degeneration.

The question is approached by looking at excised tibial plateaus from patients undergoing total knee replacement for advanced OA of the knee and comparing them with tibial plateaus from healthy joints. The samples were analysed with Raman spectroscopy, peripheral quantitative computed tomography (pQCT) and chemical analysis, to compare collagen alpha chains.

The results show that bone matrix changes, related to OA, can be detected in the subchondral bone prior to overt cartilage damage, by Raman spectroscopy. These data provide support that chemical changes in bone can be related to the initiation of, or predisposition towards, joint degeneration. The results demonstrate that Raman spectroscopy should be further developed as a future tool to provide screening for early detection of joint degeneration based on correlating molecular-specific modifications in the subchondral bone.

Acknowledgements

I would like to thank my supervisors, **Professor Goodship** and **Dr. Kerns**. **Professor Goodship** has always given me encouragement and useful feedback during preparation of this thesis. **Dr. Kerns** has been an inspiration in terms of her knowledge, organization and commitment. Without her this thesis would not have been completed and I am sincerely grateful to her.

I would also like to thank **Dr. Birch** for her help with the collagen biochemistry, **Professor McCarthy** for his help with the pQCT machine and **Professor Parker**, **Professor Matousek** and **Dr. Buckley** for their help with Raman spectroscopy. Furthermore, **Mr. Miles** for providing samples.

Abbreviations, Conventions and Formulae

Abbreviations

NCP	Non-Collagenous Protein
OA	Osteoarthritis
MMP	Matrix MetalloProteinase
TGF-β	Transforming Growth Factor – beta
TIMP	Tissue Inhibitors of Matrix MetalloProteinase
CT	Computed Tomography
pQCT	peripheral Quantitative Computed Tomography
DXA	Dual energy X-ray Absorptiometry
MRI	Magnetic Resonance Imaging
µMR	Magnetic Resonance Microscopy
PET	Positron Emission Tomography
AFM	Atomic Force Microscopy
EM	Electron Microscopy
DNA	Deoxyribonucleic Acid
RNA	Ribonucleic Acid
CCD	Charged Coupled Device
SORS	Spatially Offset Raman Spectroscopy
iSORS	inverse Spatially Offset Raman Spectroscopy
PCA	Principal Component Analysis
PC	Principal Component
LDA	Linear Discriminant Analysis
SDS PAGE	Sodium Dodecyl Sulphate PolyAcrylamide Gel Electrophoresis
vBMD	volumetric Bone Mineral Density
aBMD	area Bone Mineral Density
QA	Quality Assurance
EDTA	EthyleneDiamineTetraAcetic acid
LWD	Long Working Distance
IQR	Inter-Quartile Range
SD	Standard Deviation

Formulae

1. Stress = Force/Area

2. Strain = (Elongated length-Original length)/Original length

3. Young's Modulus of Elasticity stress/strain (N/m^2)

4. General Form of PCA model:

$$X=TP^T+E$$

where X matrix is decomposed by PCA into two smaller matrices, one of scores T and other of loadings P

$$\sum_{i=1}^{I} t_{ia} t_{ib} = 0$$

where t_a and t_b are the a^{th} and b^{th} columns of T matrix, respectively

$$\sum_{i=1}^{I} p_{ia} p_{ib} = 0$$

where p_a and p_b are the a^{th} and b^{th} rows of P matrix, respectively

Conventions

Raman Spectra – only Stokes shifted spectra are shown. They are plotted with shift (in wavenumber) increasing from left to right.

The terms "**normal**" and "**control**" when referring to specimens is used interchangeably throughout this thesis; "**fresh**" refers to control samples acquired directly from the operating theatre from living subjects, whereas "**cadaveric**" refers to control samples acquired from cadavers.

Publications and Presentations Produced during the Course of this Thesis

Peer Reviewed Publications

JG Kerns, **PD Gikas**, K Buckley, A Shepperd, HL Birch, I McCarthy, J Miles, TWR Briggs, R Keen, AW Parker, P Matousek, AE Goodship. *Raman spectroscopy supports a putative link between inherent bone matrix chemistry and degenerative joint disease, In Preparation*

Conference/Meeting Presentations

The levels of Mineralisation, Carbonate Accumulation and Bone Remodelling in Osteoarthritic Subchondral Bone
Mohidin B, **Gikas P**, Kerns J, Birch H, Miles J, Briggs T, Goodship A
Accepted to the *ORS 2013*

Raman Spectroscopy: A Novel Technique for the Diagnosis of Osteoporosis and Predicting Fragility Fractures
Smith C, **Gikas P**, Kerns J, Buckley K, Corner T, Parker A, Matousek P, Goodship A; Accepted to the *ORS 2013*

Subchondral Bone quality in human hip osteoarthritis
Mohidin B, **Gikas P**, Kerns J, Birch H, Miles J, Briggs T, Goodship A
Seddon Society Prize 2012; *Best of the Best session BOA 2012, Manchester*

Raman Spectroscopy: A Novel Method for the detection of molecular changes in human knee osteoarthritis
Gikas PD, Kelly J, Perera JR, Buckley K, Birch H, Miles J, Briggs T, Parker A, Matousek P, Goodship A
Prize for best oral presentation RSM Presidents Prize session, May 2011

Spatially offset Raman spectroscopy towards diagnosing bone disease – an update

Parker A, Buckley K, Kerns J, **Gikas P**, Briggs T, Matousek P, Goodship A; *14th ECSBM, Lisbon 2011*

Spatially offset Raman spectroscopy and its potential use as a diagnostic tool

Parker A, Buckley K, Kerns J, **Gikas P**, Briggs T, Matousek P, Goodship A; *'Inside Raman', Natural History Museum, London, September 2011*

Raman Spectroscopy shows that Human Subchondral Bone in Osteoarthritis is Hypermineralised

Mohidin B, **Gikas PD**, Kerns JG, Birch HL, Miles J, Briggs TWR, Buckley K, Parker AW, Matousek P, Keen R, Goodship AE

European Orthopaedic Research Society, Amsterdam 2012

Raman Spectroscopy: A Novel Method for the detection of molecular changes in human knee osteoarthritis

Kelly J, **Gikas PD**, Perera JR, Buckley K, Birch H, Miles J, Briggs T, Parker A, Matousek P, Goodship A

British Orthopaedic Research Society, Cambridge June 2011

ORS, San Francisco Feb 2012

Table of Contents

CHAPTER 1 – INTRODUCTION

1.0 Overview

The goal of this thesis is to examine the chemical composition and molecular structure of components in subchondral bone. Early-stage osteoarthritis is characterized by chemical structure changes to extracellular matrix macromolecules, many of which have not been reliably measured by current histology, imaging or clinical methods. These subtle, inherent changes that occur in subchondral bone will provide the markers for diagnosis of knee joint damage. We propose to develop Raman spectroscopy techniques to examine molecular structure and chemical composition of subchondral bone. We further propose that Raman spectroscopy will complement current strategies for imaging subchondral bone by providing insight into the chemistry of joint degeneration.

1.1 Composition of Bone Material

Bone material (connective tissue composed of cells and extracellular matrix) has remarkable mechanical properties and the structures made from it (bones/skeleton) remain rigid even after being subjected to many thousands of cycles of immense force e.g. for a 70 kg individual, the head of the femur experiences a force of over 1600 N (≈350 lb) or 2.4 times the body weight during normal walking(Currey 2006). Bone is able to sustain these immense forces repeatedly

because it is a composite material with two phases that both contribute to its performance; they are a fibrous scaffold of collagen fibrils (which give the material its toughness) and a stiff solid matrix of tiny hydroxyapatite crystals (which give the bone material its stiffness)(Currey 2006).

1.1.1 Collagen

The organic scaffold of bone consists of the fibrillar protein collagen; it is secreted along other non-collagenous proteins by bone cells, becomes mineralised and develops as bone material(Boivin 2002). Collagen type I, which accounts for 95% of the collagen in bone is coded as three polypeptide chains; two identical peptide chains (α_1 chains) and one other similar peptide chain (α_2 chain)(Viguet-Carrin 2006). One end of each alpha chain terminates in an amino functional group (-NH_2) group and the other end terminates in a carboxyl group (-COOH)(Veis 1997). In humans, the COL1A1 and COL1A2 chains, are encoded by genes on chromosome 17 and 7, respectively(Huerre 1982). Each chain is roughly 1000 amino acids long and consists of a repetitive triplet pattern defined by the presence of glycine (Gly) at every third position, along most of its length(Glanville 1983). Usually the second (X) and often the third position in the collagen triplet (Gly-X-Y) are occupied by proline(Viguet-Carrin 2006). After the collagen polypeptide chains have been translated, proline and lysine amino acids become hydroxylated and subsequently the chains fold to form helices along most of their length(Lees 1977).

The presence of glycine at every third position along the alpha chains causes them to fold and form left-handed helixes along most of their length (there are non-repetitive, non-helical regions at each end). The three helical chains subsequently aggregate and intertwine to form a quaternary structure called tropocollagen (**Figure 1.1**)(Lees 1977). Tropocollagen molecules aggregate to form bundles called micro-fibrils (formed through covalent crosslinks between lysine residues) and then these aggregate further to form fibrils, which have typical diameters of 50-200 nm and are the fibrous structural unit in the bone material(Smith 1968; Lees 1977; Thurner 2009).

Figure 1.1: Structure of tropocollagen; three helical polypeptide chains aggregate and intertwine to form a quaternary structure. (adapted from http://www.sciencedaily.com)

The tropocollagen to collagen-fibril aggregation is an ordered process with the adjoining 300nm long tropocollagen molecules being offset from each other by 67nm along the long axis (**Figure 1.2**). Since the 300 nm is not divisible by 67 nm, a periodic banding pattern is created along the long axis where the 'remainders' line up, these holes are called gap regions and are thought to be where most of the mineral crystal nucleation occurs in the bone(Hulmes 1995). The neighboring tropocollagen molecules are joined together by covalent cross-links

found within and between the micro-fibrils. They are formed when one lysine residue in a tropocollagen's helical region joins with a lysine residue from the non-helical (non-repetitive) region of another tropocollagen(Knott 1998). These crosslinks are of vital importance because when their function is inhibited using drugs, the bone material loses most of its strength (Bailey 1999).

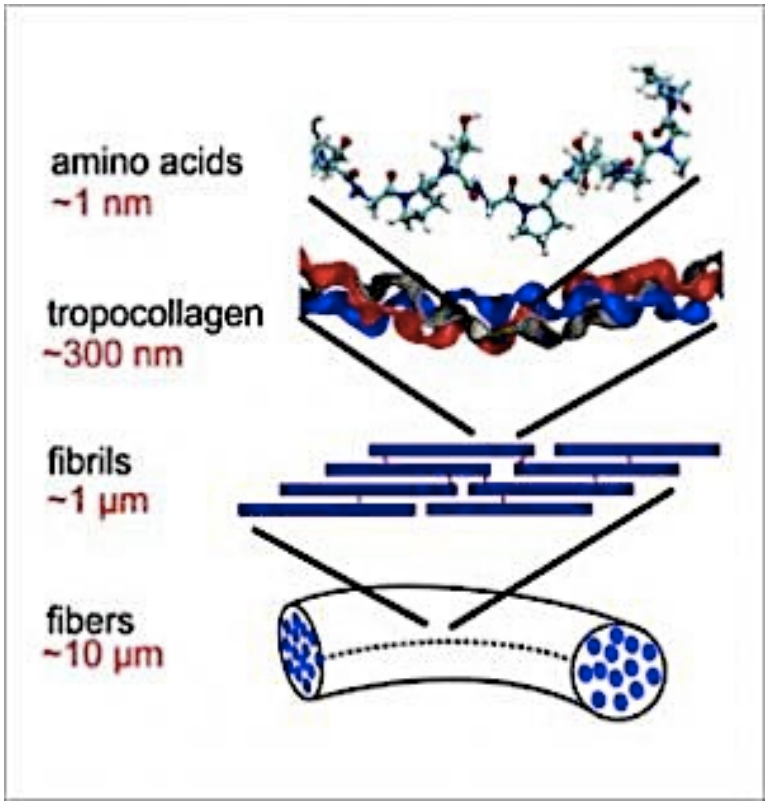

Figure 1.2: Tropocollagen to collagen-fibril aggregation is an ordered process. (adapted from http://www.sciencedaily.com)

The tensile strength of the collagen framework is provided by the intermolecular crosslinking of the collagen molecules making up the fibres of the framework. Despite its role as the fundamental framework of bone few attempts have been made to include the nature of the collagen crosslinks in the prediction of the mechanical properties of

bone. Stability of the collagen may vary depending on the nature and extent of the collagen crosslinks. Even a partial reduction in the extent of crosslinking produces a significant loss of mechanical strength in the bone.(Lees 1990; Oxlund 1995; Knott 1998)

Initial attempts to correlate mechanical strength and intermolecular crosslinking revealed a surprising relationship between the tensile strength and the pyrole cross-link rather than the pyridinoline cross-link. These studies were carried out on avian tibiotarsus bone employing three-point bending to determine the tensile strength(Knott 1998). A more detailed study of the mechanical properties of human vertebral cancellous bone and the nature of the intermolecular cross-linking of the collagen demonstrated that the hydroxylysyl-pyridinoline/lysyl-pyridinoline ratio appeared to be a significant predictor of strength (p = 0.001) and stiffness (p = 0.001), samples with a high ratio being stronger and stiffer(Banse 2002; Banse 2002). The ultimate strain correlated with the hydroxylysyl-pyridinoline or lysyl-pyridinoline concentration.

Further studies on the vertebral cancellous bone compared the nature of the collagen with the structural organisation of the trabecular network. Subjects with high pyrole and low pyridinoline in their bone collagen had a thicker and simpler structure, whereas those with a low pyrole and a high pyridinoline content possessed thin trabeculae that were more numerous(Banse 2002). This indicates a relationship between the structure and the stability of the collagen fibre controlling the micro-architecture of the bone.

1.1.2 Mineral Inorganic Phase

The collagen fibrils are surrounded by a solid matrix of closely packed mineral crystals. These crystals are shaped like small plates, with thickness in the range of 2 to 7 nm, a length of 15-200nm and a width of 10-80nm. The mineral is analogous to naturally occurring hydroxyapatite, ($Ca_{10}(PO_4)_6(OH)_2$) but substitutions occur frequently with cations such as Mg^{2+}, Sr^{2+}, Fe^{2+}, Pb^{2+}, Na^{+}, K^{+} take the place of calcium and anions such as CO_3^{2-}, HPO_4^{2-}, H_2PO^{4-}take the place of phosphate groups or hydroxyl groups(Boskey 2001; Fratzl 2004).

1.1.3 Water and Non-Collagenous Proteins

Water accounts for 5-20% of the weight of bone material(Lees 1987). It fills pores where it acts as an interstitial fluid, diffusing nutrients, removing waste etc(Wilson 2006). It affects the mechanical properties of bone with dry bone being more brittle than wet bone even when the ration of organic material to mineral remains constant(Sedlin 1966; Fratzl 1993; Cowin 1999).

A number of non-collagenous proteins (NCPs) have been shown to be important in controlling the mechanical properties of bone(Viguet-Carrin 2006). Fibronectin, one of the most abundant NCPs, is thought to have a critical role in bone development and function; in particular it may regulate the mineralisation of bone by binding to other matrix proteins and also regulate osteoblast function. Another NCP, osteonectin, has a strong affinity for both collagen and mineral, may have an important role in mineralisation(Young 2003).

1.2 Bone at Higher Levels of Organisation

1.2.1 Bone Microscopic Structure

The mineralised collagen fibrils, which constitute the basic unit of bone matrix, can be arranged in many different ways to create bony materials that differ at the micro-scale and are better suited to specific functions. Many types of microstructure have been proposed(Weiner 1992; Wagermaier 2006). However, in broad terms the microstructure of bone can be classified into two types, with time being the main determinant. In circumstances where bone needs to be created very quickly e.g. at fracture sites, osteoblasts lay down collagen fibres without regard to its structural order. This woven bone is inefficient, being highly mineralised yet having poor mechanical properties(Ritchie 2009). At the other extreme is lamellar bone in which the mineralised collagen fibrils line up in one direction to form an ordered sheet (2-6μm thick) of bone. As alternate sheets (lamellae) are laid down the long axes of fibrils are tilted so that the material takes a plywood-like arrangement. Lamellar bone takes longer to form but is superior mechanically(Weiner 1998; Webster 2001).

1.2.2 Bone Macroscopic Structure

At a macroscopic level, bone material can be seen to be arranged in one of two distinct architectural states; cortical bone (compact solid bone such as the one found along the shaft of long bones) or cancellous bone (network of struts and plates, called trabeculae, forming a porous structure on the mm scale)(Webster 2001).

The larger scale structures formed from cortical and cancellous bone i.e. the whole bone organs, do not have fixed shapes but can be modelled and sculpted into new forms when they grow or when they have to adapt to new loading patterns or heal after an injury (fracture)(Goodship 1979).

Even when the shape of the whole bone as a structure is static, the bone as a material itself can be turning over (constantly being removed and reformed), this process is called remodelling. The remodelling cycle begins when osteocytes (cells) living in lacunae (small cavities) in the bone material sense damage in their surrounding area, undergo apoptosis and release signalling molecules(Webster 2001).. These signalling molecules activate and summon large multi-nucleated cells called osteoclasts, which burrow into the bone surface by releasing H^+ ions and dissolving the bone material. Next the resorption cavity is filled in with lamellar bone by specialised bone forming cells called osteoblasts (**Figure 1.3**).

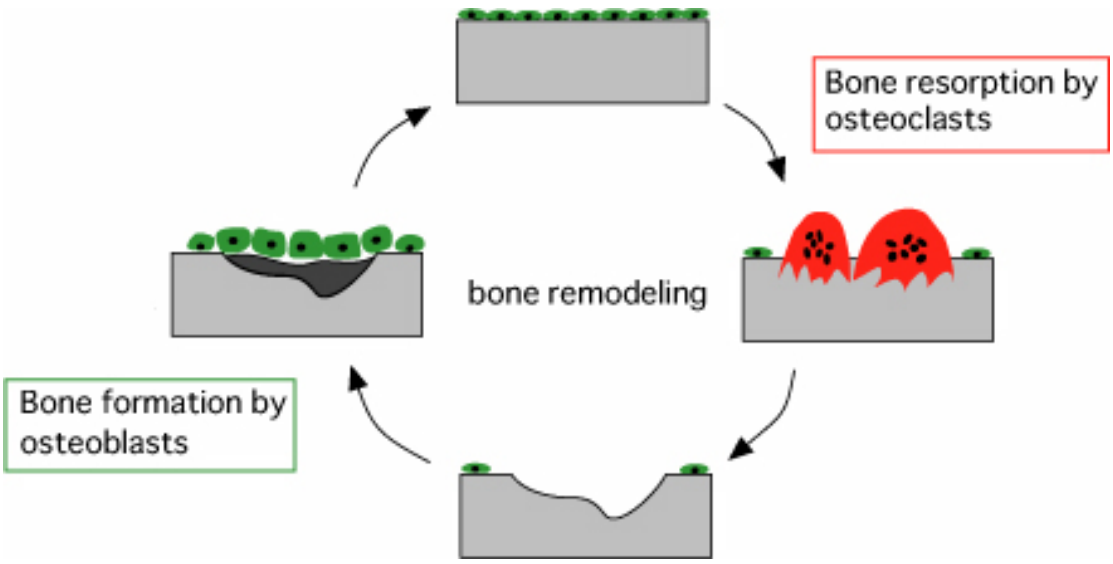

Figure 1.2: The Bone Remodelling Cycle. (adapted from www.coe-stemcell.keio.ac.jp)

1.2.3 Mechanical Properties of Bone Material

When bone material is subjected to a force it deforms. As the force increases, the deformation increases, until it reaches the point where the material breaks. For some forces, the removal of the applied force will allow it to go back to its original shape (i.e. will behave elastically) but for other larger forces, the material will remain deformed even after the force has been removed; the transition point between these two types of behaviour is known as the yield point(Turner 1993). **Figure 1.4** shows a diagram representing this behaviour.

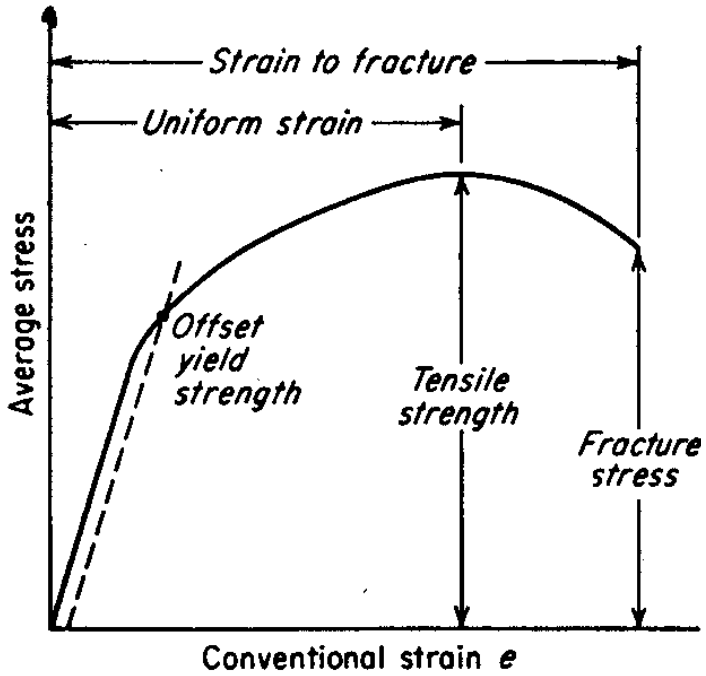

Figure 1.4: Stress/Strain curve. Stress (force/area), strain (elongated length-original length/original length), tensile strength (maximum stress that a material can withstand while being stretched or pulled before failing or breaking), yield strength (maximum stress that a material can withstand without developing plastic deformation), fracture stress (stress upon which material fails) (adapted from www.keytometals.com).

The ‘stress’ and ‘strain’ labels refer to concepts from material science, which allow comparison between samples of different sizes and shapes. The area under the curve represents energy; the area under the whole curve gives the amount of energy the sample can withstand before breaking (toughness) and the area under the curve before the yield point, is the elastic energy. The Young’s modulus of elasticity is defined as the stress/strain ratio (N/m^2; Pascals) in the elastic (pre-yield) region of the curve (cancellous bone: 0.5-1.5 GPa; cortical bone: 10-30 GPa).

1.3 Knee Joint Composition, Chemical Structure and Function

The knee joint is a complex biological organ comprised of non-mineralized cartilage, mineralized cartilage, bone, synovial fluid and a synovial membrane (also known as synovium). A schematic of knee joint anatomy is shown in **Figure 1.5**. Within the synovium, cartilage is attached to the joint surface of the patella, femur and tibia, and the cavity between and around the joint is filled with synovial fluid(Cohen 1998). Synovium encapsulates the joint. Additional fibrous and ligament layers outside the synovium further contain the entire joint and help to stabilize the joint during motion. The knee joint is avascular and delivery of nutrients is controlled by diffusion through the synovium. Intricate biological, chemical and mechanical properties of cartilage, synovial

fluid and subchondral bone within the knee joint underscore its complexity in health and disease.

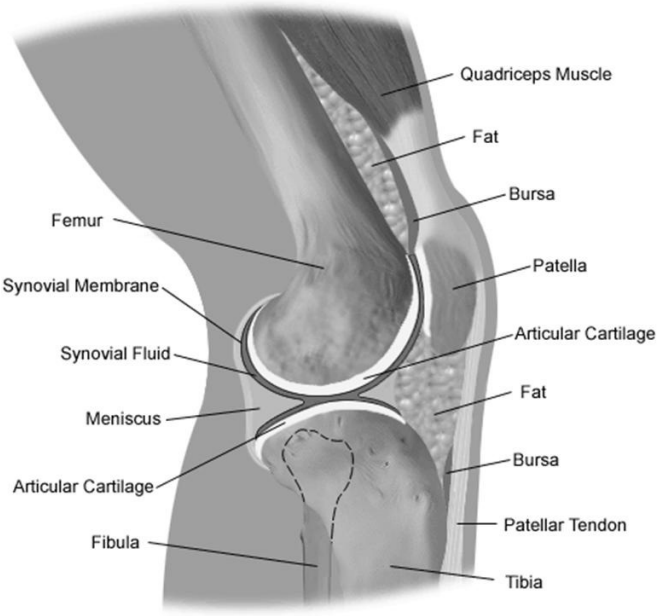

Figure 1.3: Schematic of Knee Joint [adapted from Netter's Concise Orthopaedic Anatomy (Thompson 2010)]

Cartilage is a connective tissue located throughout the body and varies in physiological function, chemical composition and mechanical properties. There are three types of cartilage: hyaline, elastic and fibrocartilage. Hyaline cartilage is the focus of many studies because it is the type covering the ends of bones at the joints (as articular cartilage), and comprises epiphyseal plates where bones grow(Marieb 1998). Articular cartilage provides a lubricated surface for joint movement and resists compressive forces. Chondrocytes, the cells which are responsible for the maintenance and repair of cartilage, are primarily found in the superficial layer near the articular surface and are surrounded by an extracellular matrix consisting of water, type II

collagen, proteoglycans, and glycoproteins, Water is a major component in cartilage, comprising between 60-80% of its total weight.

The extracellular matrix of cartilage regulates nutrient diffusion, provides resistance to compressive forces, and adds tensile strength to cartilage. Type II collagen, glycoproteins, and proteoglycans intertwine to form the extracellular matrix. Articular cartilage is heterogeneous in the axial (vertical) direction in both the relative abundance of chondrocytes and type II collagen orientation. A cross-sectional view of articular cartilage is shown in **Figure 1.6**. The three zones of articular cartilage are defined primarily by type II collagen orientation. The superficial zone, located at the articular surface, contains the highest density of chondrocytes in cartilage tissue and type II collagen fibers are oriented parallel to the joint surface. In the tangential, or mid, zone collagen fibers are not preferentially oriented. Type II collagen is ubiquitous in the deep zone and is oriented perpendicular to the cartilage surface. Glycoproteins bound to type II collagen provide structural integrity and influence type II collagen fibrillogenesis(Kucharz 1992). Proteoglycans consist of a hyaluronic acid backbone with core protein side chains. Sulfated glycosaminoglycans, chondroitin sulfate and keratin sulfate, are attached to the core protein. At physiological pH glycosaminoglycans are negatively charged and are highly hydrated. The unique viscoelastic properties of glycosaminoglycans, in addition to the high degree of hydration, renders to proteoglycans a sponge-like quality that provides compression resistance properties to cartilage. Aggrecan is the most abundant proteoglycan in cartilage.

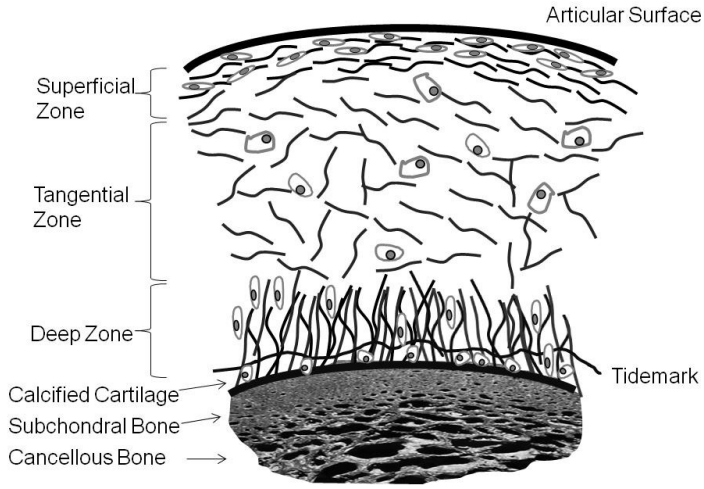

Figure 1.6: Collagen Orientation and Chondrocyte Distribution in Articular Cartilage (Thompson 2010)

Articular cartilage is unmineralized in the surface layers, but contains a layer of calcified tissue adjacent to subchondral bone. Calcified cartilage intertwines with subchondral bone to form a mineralized plate beneath cartilage and serves as the source of cartilage attachment to bone. Calcified cartilage provides additional structural integrity to the joint and limits diffusion across the bone/cartilage interface. The organic matrix of calcified cartilage is similar to non-mineralized cartilage and the mineral composition of the calcified layer closely resembles hydroxyapatite. The chemical composition of calcified cartilage resembles both cartilage and bone. Because the mineral in calcified cartilage is similar to the carbonated apatite in bone, it exhibits unique mechanical properties(Kim 1996; Ferguson 2003). In disease processes, like OA, it has been shown to hypermineralise and may therefore function as a hard, grinding abrasive, accelerating wear rates. The cortical bone that directly

underlies cartilage is called subchondral bone and it is composed primarily of type I collagen and a carbonated apatite mineral.

Synovial fluid, a dialysate of plasma, fills the joint cavity space in diarthrodial joints and is essential to maintaining joint health and function. Synovial fluid is primarily composed of water, proteins, glycosaminoglycans, lipids, small inorganic salts, and metabolites such as amino acids or sugars. Synovial fluid functions include resistance to compression, nutrient diffusion, molecular signaling, and lubrication of cartilage surfaces(Fam ; Jay 2007).

Synovial fluid molecules often have multiple functions and exhibit a large degree of interaction with other synovial fluid and cartilage molecules. For example, hyaluronic acid is responsible for the complex viscoelastic properties of synovial fluid but has also recently been found to regulate the biological activity of advanced glycation endproducts and cytokines and enzymes associated with late-stage osteoarthritis(Neumann 1999; Cowman 2005; Wang 2006)

1.4 Osteoarthritis

Arthritis is a disease or group of diseases/degenerative processes that are marked by the degradation of components in the synovial joint leading to an increase in fluid shear and hydrostatic pressure between two adjacent bones. The main form of arthritis, osteoarthritis (OA), is a degenerative joint disease with greater than 30% prevalence among individuals over 65 years(Guccione 1994; Gabriel 2001). The first and second decades of the new millennium have been designated Decades

of the Bone and Joint by the World Health Organisation and the United Nations, and the US National Institute of Health has set up the Osteoarthritis Initiative for the detailed study of human osteoarthritis. In 2012, osteoarthritis is the disease with the fourth greatest impact upon the health of women and has the eighth greatest impact for men (Hochberg 2012).

Primary osteoarthritis occurs without an obvious cause or refers to the accumulation of mechanical damage that accompanies aging. Secondary OA occurs as a response to trauma, previous injury, obesity, or metabolic disease. The percentage of adults afflicted with OA increases with age, and results in an economic burden in lost wages and early retirement(Felson 2000). OA is one of the most common causes of disability in the elderly, and therefore has a high prevalence in an aging society(Guccione 1994).

To date, there are no evidence based clinical treatments to reverse the cartilage damage characterized by osteoarthritis or to induce cartilage regeneration. Identification of osteoarthritis in its early stages is critical to disease management because minimally invasive therapies such as diet, exercise, non-steroidal anti-inflammatory drugs, or intra-articular injections can be effective in delaying disease progression and ameliorating pain. However, by the time patients present with symptoms or once radiographic changes are evident, then OA is typically in an advanced stage. The challenge is to detect OA progression, especially for sub-clinical patients. There is a real need for new technologies able to detect and characterize OA at pre-symptomatic stages of disease and

to identify at risk individuals.

The pathogenesis of OA is exceedingly complex, involving genetic and environmental factors as well as local biomechanical factors. OA was historically defined pathologically as focal and progressive loss of hyaline cartilage with concomitant changes in underlying bone. More recent studies have shown that osteoarthritis may be considered a whole joint disease and involve a range of constituent tissues and structures. Biological, chemical and viscoelastic changes affect cartilage, synovium, subchondral bone, synovial fluid, and surrounding muscles and ligaments(Radin 1986; Burr 1997; Oegema 1997; Felson 2004; Dieppe 2005). Degradation of extracellular matrix molecules, such as cleavage of glycosaminoglycans or a loss of collagen cross-linking, is implicated in a complex series of biological, mechanical and chemical events that lead to loss of articular cartilage function. At the level of the articular chondrocyte, an altered composition of matrix, a pathological response to mechanical stress and programmed cell death contribute to the pathologic syndrome, with alterations in cartilage extracellular matrix proteins likely occurring early.

The role of subchondral bone has been examined in current models of OA. A common consequence of osteoarthritis is thickening of the subchondral bone plate and increased apparent bone mineral density but significantly reduced material density associated with an altered composition of the bone in which the mass fraction of mineral is 12% less than normal (Li 1997; Li 1999; Day 2004). Radiography and other imaging studies have shown alterations in bone architecture and

chemistry in addition to plate thickening(Matsui 1997; Bruyere 2003; Hunter 2003; Lahm 2004). Material properties in subchondral bone are also compromised, as observed by a less mineralized tissue and altered architecture in the cancellous and cortical bone regions(Bailey 2004). These studies support the idea that osteoarthritis is a disease that affects the entire joint.

Clinical symptoms, such as pain, swelling or loss of function, are observed in most patients with osteoarthritis. However, these symptoms vary across patient populations, do not adequately correlate with disease stage and are non-specific to osteoarthritis. In 2004, Webb and colleagues reported the results of a population-based cross-sectional survey of knee pain(Webb 2004). The survey population included approximately 4,500 people living in the urban area of Manchester, England, divided into eight groups defined by age and gender. Symptomatically, OA is defined as pain with joint use; however, the cause of joint pain in OA has yet to be elucidated.

Several bone changes occur in osteoarthritis, with osteophyte formation and, more importantly, subchondral plate sclerosis. Radin postulated that increased bone mass and thickening of the subchondral bone plate would cause stiffening of the bone and, as a consequence, cartilage destruction on repeated loading(Radin 1986). The initiation of cartilage destruction would be secondary to steep stiffness gradients in the subchondral bone. The most likely cause of such stiffness variations, according to the authors, is failure of the musculoskeletal peak dynamic force attenuation mechanisms. More recently, studies have re-

emphasized the importance of bone changes. In patients with osteoarthritis of the knee and hand, Buckland-Wright reported thickening of the subchondral bone(Buckland-Wright 2004), while Carlson et al., using histological techniques, detected increased bone thickening with osteoarthritis progression in the cyanomolgus macaque model(Carlson 1996). Both techniques revealed a marked increase in bone formation before cartilage fibrillation. Using labelled bisphosphonate in a scintigraphic study, Dieppe et al. demonstrated elevated bone turnover in those human patients that progressed to severe osteoarthritis(Dieppe 1993; Dieppe 2005), while Mansell demonstrated increased turnover of the subchondral bone collagen(Mansell 1998) by measuring the carboxy-terminal propeptide content and alkaline phosphatase activity.

The occurrence of these bone changes is not disputed, but, their importance in the pathogenesis of osteoarthritis remains contentious, and the mechanisms involved in these changes have received scant attention. There is now emerging evidence to suggest that changes in bone precede changes in cartilage, so that bone rather than cartilage may be the site of the causally most significant pathophysiological events(Mansell 2007). New treatments, focused on the cartilaginous component of the joint, such as injections to lubricate the joint or cartilage implants may therefore be at best short-term palliative measures.

Resolution of the question of the importance of bone in osteoarthritis requires a multidisciplinary approach, including the disciplines of biomechanics, imaging, collagen biochemistry and cell

biology, as well as the development of animal models and the use of tissues from natural disease.

1.5 Bone Structure and Metabolism in Osteoarthritis

1.5.1 Collagen structure

Simplistically, bone can be considered as a two-phase system of a collagenous supporting framework that provides strength and calcium apatite that confers rigidity, both phases being replaced during remodelling. Biochemical studies have revealed a several-fold increase in metabolism of the subchondral bone collagen in osteoarthritis, along with decreased mineralization in human femoral heads.

Bailey et al have reported changes in the composition of collagen, with the type I collagen α_1 homotrimer identified in osteoarthritic subchondral bone, indicating a changed phenotypic expression in the osteoblasts(Bailey 2002). Studies of transgenic mice with deleted α_2 chain have shown that such changes cause loose packing of the collagen chains and could therefore have a deleterious effect on the mechanical properties and mineralization of bone(Chipman 1993). However, the authors did not comment on whether these transgenic animals exhibited any clinical features of OA.

1.5.2 Cellular activity

Many growth factors, which act to promote cell differentiation and activity, are stored in bone matrix, suggesting that these may be important in the coupling of the resorptive and formation processes of bone. Transforming growth factor β is related to bone turnover(Pfeilschifter 1998) and has been shown to be increased several-fold in osteoarthritic subchondral bone(Mansell 1998). Growth factors may also act as potential mediators of communication between bone and adjacent cartilage cells: for example, cells derived from osteoarthritic joints promoted the degradation of non-arthritic cartilage biopsies in vitro, whereas cells from normal joints did not do so(Westacott 1997).

The turnover of the collagenous network in bone involves collagenases of the matrix metalloproteinase (MMP) family (MMP-1, MMP-8 and MMP-13)(Shingleton 1996); this suggests therapeutic targets to block production of these enzymes(Cawston 1996). However, the cathepsins, particularly cathepsin K, are also involved in the degradation of bone collagen(Garnero 1998), and the relative importance of the cathepsins and the MMPs remains to be determined.

It has been proposed in the literature, that chronic hypoxia and anoxia, resulting in the generation of free radicals, initiate bone erosion, and that they should be considered a target for therapeutic manipulation in osteoarthritis(Jones 1987; Miller 1998). Hypoxia induces the production of xanthine oxidoreductase, which generates superoxide and nitric oxide, which leads to bone resorption.

1.5.3 Biomechanics of bone in osteoarthritis

The results of studies of the mechanical properties of bone in osteoarthritis are conflicting. Bone taken from patients with osteoarthritis varies both in its properties and according to location. The subchondral bone from such patients is less stiff and dense (material vs. apparent density), shows greater porosity, has a reduced mineral content(Li 1997) yet is thicker than normal bone. These results complement the findings of biochemical studies(Mansell 1998; Bailey 2002), but are contrary to those of earlier studies, which suggested that subchondral bone was stiffer(Radin 1986).

Bone is a dynamic mechanically sensitive tissue adapting to prevailing loading conditions. Disuse results in bone loss, allowing the skeleton to achieve sufficient strength without excessive mass, which would be energetically costly to build, maintain or use(Lanyon 1996; Skerry 1997). There is emerging evidence that different cell types in bone communicate though effector molecules and receptors that are similar to those that operate at synapses in the central nervous system. Studies, based on a differential display of osteocyte RNA following bone loading, have shown regulation of a glutamate transporter previously thought to be expressed only in the central nervous system(Mason 1997). Such an arrangement would allow response to rapidly changing transient strains. Manipulation of such signaling pathways could provide a way of controlling bone mass in disease.

In a different approach, bone cells cultured in vitro can be subjected to physiological levels of mechanical strain with resulting

changes to proliferative response and prostaglandin production(Murray 1990). Suggestive differences between cells from osteoarthritic and normal patients have been observed, for example, in proliferative responses and prostaglandin production(Fermor 1998). The mechanical effects on osteoprogenitor and osteogenic cells warrant further investigation.

Grynpas et al. measured the mineral content in bone through density fractionation, and found the OA subchondral bone (both the cortical plate and the underlying cancellous bone) to contain less mineral content than age-matched controls(Grynpas 1993). Therefore, from a material perspective, and contrary to intuition, bone mineral density actually decreases in OA. Burr suggests subchondral bone is constantly remodelling with a high turnover rate, preventing the matrix from fully mineralising. Consequently, subchondral bone has a lower material density in OA so the total volume, which is related to the apparent density, must increase significantly to provide a sufficient degree of structural stiffness. Therefore, the apparent density has to increase in OA, to compensate for the reduced material density, in order to provide an acceptable level of stiffness(Burr 2003).

1.5.4 Animal models

Bone changes occur in many non-human animal species (e.g. dog, horse), which also naturally develop osteoarthritis(Bailey 1997; Billingham 1998). These natural animal models allow the examination of the early stages of bone changes, as well as to test potential therapies. In macaques, where striking similarities to the slow human disease are

seen, Carlson et al. demonstrated histological evidence for thickening of the subchondral bone before cartilage fibrillation(Carlson 1996). Studies by Bailey and co-workers on spontaneous male Duncan Hartley guinea pigs suggest that bone density alterations accompanied by bone collagen remodelling are important in initiation and early disease progression(Quasnichka 2000).

The hypothesis that bone sclerosis results from a change in joint mechanics, which in turn could be due to metabolic changes in the cruciate ligament(Bailey 1997) is supported by evidence from mice and guinea pigs, where ligament remodelling is seen before cartilage fibrillation(Anderson-MacKenzie 1999; Quasnichka 2000).

The different animal models, both natural and induced, suggest that bone changes precede cartilage damage. Further studies are required to confirm that changes in the ligaments and subsequent changes in subchondral bone are major initiating events in idiopathic osteoarthritis.

The changed view of the pathogenesis of osteoarthritis from cartilage to the involvement of the whole synovial joint, and the recognition of early changes in the bone and ligaments, provide the potential for a new approach to the understanding and novel treatment targets for this prevalent, painful and debilitating disease.

Changes in bone and collagen play an integral part in osteoarthritis of the joint. Much work has already been done to clarify the changes in articular cartilage, but a greater effort must now be directed towards research into bone to redress the balance in our understanding of the

role of osteoarthritic changes at the osteochondral junction within synovial joints.

1.6 Role of Subchondral Bone in Osteoarthritis

The majority of the basic research into the pathogenesis of OA has concentrated on the mechanisms involved in the characteristic focal destruction of the articular cartilage. The initiating events of this destruction are believed to be changes in the proteoglycans followed by the collagenous framework, after which the disease is irreversible.

The well-recognised additional characteristics of bony osteophytes and subchondral bone thickening have to a large extent been considered secondary and unimportant in the pathogenesis of osteoarthritis: the potential involvement of bone has been overlooked. Over four decades ago Johnson postulated that subtle changes in bone remodelling might precipitate irregularities in the articular cartilage(Johnson 1962). Radin and Rose later proposed that sclerosis of the subchondral bone plate would cause stiffening of the bone and result in cartilage destruction(Radin 1986). Newer radiographic techniques(Buckland-Wright 1994) have demonstrated progressive thickening of the subchondral bone with joint narrowing and technetium-labelled bisphosphonate demonstrated that the heightened bone activity of the knee was related to the progression to severe OA, as monitored radiographically by joint space narrowing(Dieppe 1993).

The question then arises as to whether the bone thickening is a result of cartilage degradation, occurs at the same time, or precedes

cartilage degradation(Bailey 1997; Burr 1998; Senior 2000). If the latter, then the subchondral bone thickening is indeed important in the pathogenesis of OA, either as an initiating factor or, at the very least, important in the progression of OA. Thickening of the subchondral bone was shown to occur prior to cartilage destruction in elderly cynomolgus macaques and that the thickness of the subchondral bone was related to the onset of cartilage fibrillation(Carlson 1996). Similar findings have been shown during spontaneous OA in the guinea pig knee (Quasnichka 2006). In a mechanically induced model it was reported that sub-fracture impacts applied to the patellofemoral joint of rabbits resulted in subchondral bone thickening after 6 months whilst cartilage stiffness only decreased after 12 months(Newberry 1997). In an attempt to detect earlier changes ultrasonography was employed in a rodent inflammatory joint model and reported changes in both bone and cartilage before any histological evidence of cartilage damage(Saied 1997).

However, regardless of whether thickening of the subchondral bone occurs at a late stage or precedes cartilage destruction it is important to know the biochemical and mechanical characteristics of bone in osteoarthritis, as they may be important in its pathogenesis.

In an analysis of osteoarthritic human femoral heads it was found that collagen was turning over at a rate several fold greater than non-OA bone(Mansell 1998). The elevated type I collagen synthesis was accurately corroborated by the increase in alkaline phosphatase activity. The relative contribution of cathepsin K and the MMPs were not

determined. Transforming growth factor-beta (TGF- β) levels were increased 4-fold. TGF-β plays a major role in remodelling and recruitment of osteoblast precursors, stimulating collagen synthesis, inhibiting MMPs and increasing TIMPs thus leading to a net gain in collagen deposition(Pfeilschifter 1998). In contrast studies have shown that the mineral content of the new bone is significantly reduced (30%) with increased presence of osteoid(Grynpas 1991; Reinmann 1997). Higher turnover rate would lead to a higher proportion of immature bone suggesting a reduced mechanical strength. Cancellous bone from OA femoral heads is significantly weaker than age-matched controls(Li 1997).

The increased metabolism of bone collagen may be a feature of other bones in OA subjects. Interestingly, increased bone density and increased levels of TGF-β have been reported in the iliac crest bone of OA subjects(Dequeker 1993) and this suggests that the increased bone density of OA subjects protects them against osteoporosis(Dequeker 1993). Certainly spontaneous fracture of femoral heads tends not to occur in OA subjects.

Of additional importance is the fact that the increased turnover is not a function of age. Mature non-OA subjects have been investigated over a wide age range and did not show any changes in rate of turnover or the nature of the stabilizing collagen cross-links(Bailey 1999). Any changes found with increasing age are, therefore, likely to be due to disease processes.

The extremely rapid turnover of the collagen in OA subchondral

bone means that the environment of the osteoblasts is very different from normal bone, and the consequent change in cytokines and growth factors could lead to differences in their phenotypic expression. Indeed, osteoblasts isolated from the bone of OA subjects were found to be capable of degrading cartilage proteoglycans in contrast to osteoblasts from normal bone(Westacott 1997) and possessed an altered response to various cytokines and growth factors(Hilal 1998). Bailey investigated the phenotypic expression of the osteoblasts *in situ* and demonstrated the presence of collagen, type I homotrimer $(\alpha_1)3$, in OA femoral heads in addition to the normal type I heterotrimer $(\alpha_1)2\alpha_2$(Bailey 2002).The amount of the homotrimer, demonstrated by the ratio of the α_1 to α_2 chains varied considerably from subject to subject, from 4 : 1 to 17 : 1 compared with 2 : 1 for normal bone. The authors suggest that the amount of the excess α1 chain depends on the rate of turnover and hence the severity of the OA, but further studies are required on clinically classified samples to confirm this suggestion. Cyanogen bromide cleavage of the homotrimer derived from OA subchondral bone revealed an identical peptide profile to the α_1 chain of the heterotrimer isolated from the type I collagen of non- OA bone. The presence of the homotrimer is therefore due to a loss of the regulation controlling the α_1/α_2 ratio to produce an excess of α_1, rather than a genetically distinct type I collagen α_1-chain(Bailey 2002).

To determine the effect of increasing amounts of type I homotrimer on the mechanical properties of the OA subchondral bone researchers have studied the mouse model expressing a variant of osteogenesis

imperfecta (*oim*) in which the α_2 chain had been deleted (Chipman 1993). The mechanical strength of the bones of these animals is about half that of the wild type mouse with a significant decrease in collagen chain cross-linking. Quite why the loss of the α_2 chain should have such an effect on the cross-linking is not immediately obvious but could be related to an increase in hydroxyproline content on replacement of the α_2 chain by the α_1 which contains a higher hydroxyproline content, with 348 hydroxyprolines compared with 327 for the heterotrimer triple helix. The mechanism of stabilisation of the triple helix by hydroxyproline is still controversial. It may be form stabilising hydrogen-bonded water-bridges as originally proposed by Ramachandran(Ramachandran 1973), a proposal currently supported by recent X-ray studies defining the location of the water molecules on the triple helix (Bella 1995). Alternatively other workers have proposed that the hydroxyproline stabilises the *trans* configuration of the prolyl peptide bond by the inductive effect of its hydroxyl group suggesting that water hydrogen bonding plays no role in the stabilisation of the triple helix (Holmgren 1998).

Bailey proposes that the decrease in cross-linking and hence in mechanical properties, is due to the increased water content of the fibre rather than a distortion of the molecular structure(Bailey 2004). According to his theory, an increasing proportion of the weaker type I homotrimer fibres in the subchondral bone of OA subjects would have a significant effect on decreasing its mechanical properties.

In summary, the ability of bone collagen to provide a strong framework and to fully mineralise depends on the very precise alignment of the type I collagen heterotrimer. However, in osteoarthritis the increased narrowing of the fibre diameters, the reduced level of the pyrrole cross-link, the decreased mineralization, together with the increasing proportion of the homotrimer, all contribute to a weakening of the mechanical properties of subchondral bone.

1.7 Bone Imaging and Analysis

Bone has been imaged and analysed using many different analytical techniques. These can be classified into four general categories: radiographic techniques, other clinical in vivo techniques, ex vivo techniques and spectroscopic techniques.

1.7.1 Radiographic Techniques

1.7.1.1 Projection Radiography

X-ray radiation is the name given to electromagnetic radiation with wavelength in the range of 0.1-10nm. The simplest x-ray technique is projection radiography in which an X-ray source is placed at one side of the limb/bone and a detector is placed at the other. As the different tissues absorb the X-rays, an image (analogous to a shadow) is created at the detector. The limitation of projection radiography is the fact that it produces a 2D image of a three dimensional object.

1.7.1.2 Computed Tomography

This limitation is overcome with X-ray computed tomography (CT)(Mahesh 2002). Early CT scanners had an X-ray source which was aligned so as to be incident on the part of the body to be imaged e.g. the chest and a detector used to measure the signal at the other side of the chest. The source and the detector were then moved along the axis parallel to the original measurement and another reading was taken. This was repeated until data for a full slice of the chest was collected. The source and the detector were then rotated through a small angle and the same slice of chest was imaged from a slightly offset angle. This was repeated until the equipment was rotated for 180^0, resulting in a large number of cross-sectional attenuation paths, crossing at all angles. Mathematical manipulation of the data set enabled a model of the slice to be created.

In modern CT scanners, in order to speed up the measurement, the x-ray source and the detector are constantly moving through a helical path around the patient while the patient is moving headfirst through the helix in an opposite direction.

1.7.1.3 Peripheral Quantitative Computed Tomography (pQCT)

pQCT instruments work in a similar way as the older type CT scanners but have smaller sample space between X-ray source and detector. They are designed to create images of thin cross-sections and can give quantitative values for the amount of bone mineral present. The images obtained can be divided into trabecular and cortical regions

and by averaging the density across different topographical regions, the density of the trabecular or cortical bone can be obtained.

1.7.1.4 *Dual-Energy X-ray Absorptiometry (DXA)*

Compared to CT this technique is simpler and involves a much smaller dose of radiation. An X-ray beam is sent through the bone to be examined and the attenuation is measured, a second x-ray beam with a different wavelength is sent along the same path and its attenuation is also measured. This allows the mass per unit of projected bone to be calculated.

DXA is used for measuring bone density and is currently the gold standard for the diagnosis of osteoporosis(Blake 1997). However it is limited by its planar nature. The density values it produces are a measure of x-ray absorption along the path of travel of the x-ray; a thin portion of highly mineralized bone will stop as many photons as a thick portion of under-mineralised bone, yet these two portions will have significantly different mechanical properties. Moreover DXA measurements cannot be separated for trabecular and cortical bone(Heaney 2005). DXA measured bone mineral density accounts for 60-70% of the variation in whole bone strength (Rizzoli 2003).

Radiographic techniques are useful and widely used but have two main limitations:

1. X-rays are harmful; high-energy photons can ionize molecules they collide with and can create free-radicals which can damage DNA and/or destroy cells.

2. They do not allow for visualization of the organic phase of bone material. This normally accounts for 30% of the weight of the bone and is an integral part of the composite related to strength. This could explain some of the variation in whole bone strength that is not accounted for by DXA(Rizzoli 2003).

1.7.2 Alternative Techniques

1.7.2.1 Ultrasound

Ultrasound vibrations can be used a medical tool, the sound wave sent through the body part to be probed and the reflected or transmitted sound (echo) is collected and analysed. Quantitative ultrasound that looks at the percentage of the signal that was transmitted and at the time the vibration took to propagate has been used to study osteoporosis, osteogenesis imperfect and hyperparathyroidism(Gregg 1997; Danese 2001). Ultrasound techniques primarily probe the mineral phase of bone.

1.7.2.2 *Magnetic Resonance Imaging*

Magnetic Resonance Imaging (MRI) uses the magnetic properties of protons in different environments to distinguish between different tissues(Hendrick 1994; Pooley 2005). It can be used to probe a variety of connective tissues (e.g. bone, tendon, ligament, cartilage etc.) and the images produced give information about structure, function and pathology of bone and joints. Recently smaller MRI scanners have been developed, which have stronger magnetic fields and can produce

detailed localized scans (Magnetic Resonance Microscopy (μMR). They have enabled researchers to form in vivo images of bone microstructure and discriminate individual trabeculae(Genant 1996).

The principle of MRI can also be used for chemical analysis. If the behaviour of a certain nucleus in a certain biochemical is known upon application of a magnetic field then one can study that in vivo. Magnetic Resonance Spectroscopy has been used to investigate tumours of breast, prostate, cervix and bone(Kurhanewicz 1996; Kvistad 1999). Magnetic Resonance Imaging does not involve ionizing radiation, is however time consuming and expensive and contraindicated in patients with implanted metallic devices.

1.7.2.3 *Positron Emission Tomography*

Positron Emission Tomography (PET) is a medical imaging technique that can be used to create 3D images on internal organs and tissues(Votaw 1995). In PET a bio-compound is labelled with radioactive markers, injected into the patient and its distribution around the body is measured as a function of time. PET is a quantitative technique and data obtained complement other imaging modalities well especially in assessment of tumours and infections in bone(Miller 1996).

1.7.3 Ex-Vivo Imaging Techniques

1.7.3.1. Atomic Force Microscopy

Atomic Force Microscopy (AFM) is a technique in which the tip of a tiny probe needle mounted on a spring arm (cantilever) interacts with the

surface of the sample(Thurner 2009). It can also be used to measure the mechanical properties of samples (*nanoindentation*)(Donnelly 2010).

1.7.3.2 Electron Microscopy

Electron Microscopy (EM) can also be used to image the constituents of bone material(Boivin 1990). EM uses a beam of electrons in place of photons to image the sample. The electrons can be passed through a thin section of material and collected on the transmitted side (*Transmission Electron Microscopy*) or the signal they produce when they interact with the sample surface can be collected (*Scanning Electron Microscopy*)

1.8 Raman Spectroscopy

1.8.1 Background

The inelastic scattering of light from matter is called Raman scattering, after the Indian scientist Chandrasekhara Venkata Raman who first discovered it. Raman studied the scattering of filtered sunlight from various liquids during the 1920s at the Indian Association for the Cultivation of Science in Calcutta. The experiments culminated on the 28th February 1928 when he passed monochromatic light from a quartz mercury lamp through bulbs containing a series of liquid samples. Raman reported the results of this experiment to the South Indian Science Association on the 16th March 1928 in a talk titled “A New Radiation”(Raman 1928). He stated ‘…most liquids showed in the spectrum of the scattered light, a bright line in the blue-green region of

the spectrum, whose position was practically the same for chemically similar liquids such as pentane, hexane and octane. There was however, a recognizable difference in the position of the modified line when other liquids such as benzene were used…' (Raman 1928; Krishnan 1981). He was awarded the Nobel Prize in physics for his discovery in 1930.

1.8.2 Scattering

When light is incident on a molecule it can scatter, the scattering can be elastic with no energy exchanged between the photon and the molecule (Rayleigh scattering) or an inelastic process with energy exchanged between the photon and the molecule (Raman scattering). These scattering processes consist of two steps:

1. molecule and photon combine to excite the molecule to a higher energy virtual state which exists for a very short time
2. the photon is then released and the molecule returns to a vibrational state (either the original or a different one)

A Raman scattering event that creates a photon with less energy (longer wavelength) is called Stokes scattering and a Raman scattering event that creates a photon with more energy (shorter wavelength) is called anti-Stokes scattering(Carey 1982).

In order for anti-stokes scattering to occur the molecule must be in an excited state before the scattering event. Unless the scattering material is very hot and therefore in an excited state, most molecules will occupy the vibrational ground state; hence in normal conditions anti-

Stokes scattering events will be much less numerous than Stokes scattering events.

A scattering event from a molecule in its ground state can lead to Rayleigh scattering or to Stokes scattering but the probability of each event is very different. Rayleigh scattering is 10^{6}-10^{8} times more likely to occur; hence the number of inelastically scattered Raman photons is comparatively tiny and Raman signal is very weak(Smith 2005).

1.8.3 Intensity of Scattered Radiation

The factors, which are important in determining the intensity of the Raman radiation from a material with vibrational ground state and excited state, are the intensity of the incident radiation, the wavelength of the scattered radiation (1/wavelength^{4}) and the properties of the molecular vibration in question. These properties include the geometry of the molecule and the values of the electric dipole moment for each quantum mechanical state (vibrational or electronic)(Long 2002).

Any molecular vibrations, which affect the ability of a molecule to become polarized by an electromagnetic wave, will be a relatively strong Raman scatterer. Therefore:

- Stretching vibrations should scatter more than deformation vibrations
- Multiple bonds scatter more than single bonds
- Symmetric molecules with many conjugated electrons scatter more

1.8.4 Raman Spectroscopy Instrument

A Raman instrument consists of three main components (**Figure 1.7**):

1. A light source. The availability of bright monochromatic light sources was one of the factors preventing the widespread adoption of Raman spectroscopy for many decades. However, since the latter half of the 20th century, cheap, efficient laser light sources have been developed. Modern lasers (Light Amplification by Stimulated Emission of Radiation) can emit light as a single wavelength from the ultraviolet to the near infrared and beyond, can deliver high intensities and can maintain their performance for many thousands of hours.
2. A wavelength discriminator (filter). Firstly, a Raman spectrometer must have a component for separating the Raman signal from the light that has been elastically scattered from the sample; the much weaker Raman signal would otherwise be obscured. Secondly, the instrument must also be able to separate the different wavelength Raman photons in order to record a spectrum. Traditionally instruments use holographic notch filters (nowadays edge filters), made by imprinting inference patterns in optical media with laser beams, to remove the elastically scattered laser light. The Raman signal is then separated into its constituent wavelengths using dispersive techniques or interferometry techniques.

3. A detector. The current detector of choice is the Charged Coupled Device (CCD). A CCD camera consists of a semiconductor chip, which builds up electrical charge when electrons are incident on it; the charge is then read off by electrodes and recorded on a computer. The chip can have millions of electrodes on it and are designed so as to be more sensitive in the optical region of interest.

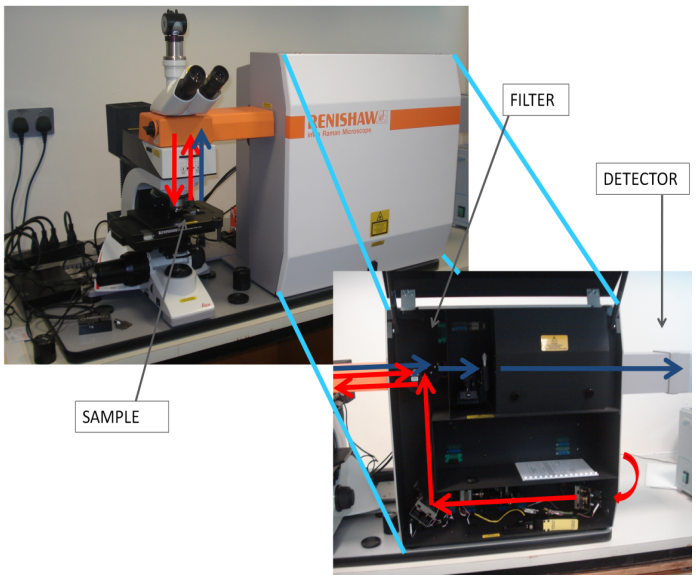

Figure 1.7: A Raman microscope with schematic of the laser pathway(Kelly 2010). The filter firstly removes elastically scattered light and then separates the light into its constituent wavelengths using dispersion grating

1.8.5 The Raman Spectrum

In a Raman spectrum the energy of the scattered photons (wavenumber shifts) is recorded on the x-axis and the intensity of the Raman signal is recorded on the y-axis (**Figure 1.8**). The energy of the x-axis is represented as a wavenumber shift from the laser wavenumber, rather than an absolute wavenumber, enabling comparison of spectra recorded with different instruments and with lasers of different wavelengths. The units are inverse centimetres (cm^{-1})

and enable comparison between spectra recorded with different excitation wavelengths. The spectrum in **Figure 1.8** shows the Stokes shifted side of the laser line, the anti-Stokes spectrum is to be found on the opposite side of the vertical axis and is much less intense. The intensity of the light is measured in detector counts and is associated with the charge coupled device (CCD) chip in the detector.

Each Raman spectrum has several bands and each band has a frequency signifying the energy at which a vibrational transition takes place in the scattering molecule. In **Figure 1.8** the phosphate band at 960cm^{-1} means that laser photons with energy X were inelastically scattered from the phosphate in a sample (in this case bone) and during this process the photons lost an amount of energy corresponding to wavenumber shift of 960cm^{-1}. The other bands correspond to other molecular vibrations and therefore their shape, position and intensity are different for each scattering molecule allowing for Raman spectroscopy to give a unique chemical fingerprint of the substance being studied.

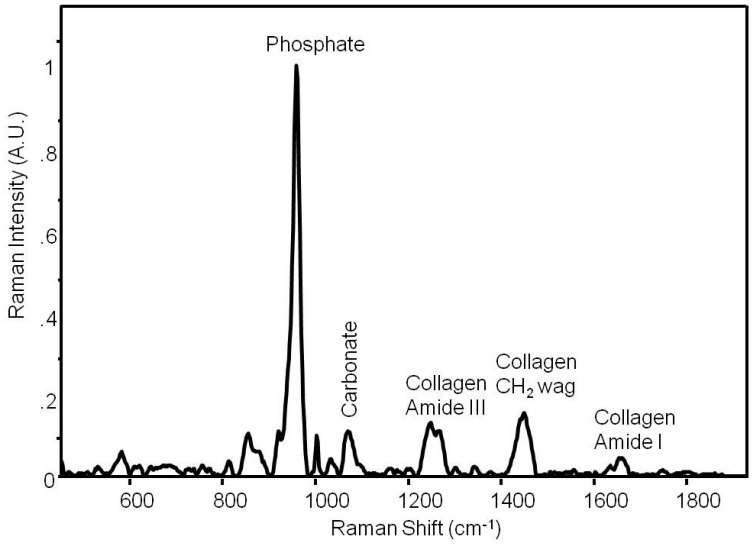

Figure 1.8: Example of Raman spectrum of bone with main peaks labelled (by P.D. Gikas).

1.8.6 Advantages of Raman Spectroscopy

1. Water is a weak Raman scatterer and therefore does not interfere strongly with Raman spectra. This means it can be used *in vivo.*
2. Laser beams are relatively easy to use in a wide range of experimental setups and hence a variety of samples can be analysed.
3. Lasers can be focused to very small points and hence photons can be scattered from well-defined areas with high spatial resolution.
4. Raman spectroscopy does not involve any ionizing radiation.
5. No need for sample preparation
6. It is a non-destructive/non-invasive technique
7. Specialized Raman techniques can be used non-invasively to depths of several millimeters with biological tissues, i.e., SORS and iSORS.

1.8.7 Disadvantages of Raman Spectroscopy

1. As the number of photons scattered inelastically from a material is a minority the Raman signals are inherently weak, which means that conventional Raman spectroscopy cannot be used to measure trace quantities and can also be overwhelmed by other sources of light.
2. Raman spectroscopy is not suitable for pure metallic samples.

3. The laser can sometimes increase the temperature of the sample to undesirable levels and can cause degradation.
4. Raman spectroscopy cannot be used on samples exhibiting strong fluorescence in the spectral region of interest. If the photon and the molecule's energy gap have matching energies then this interaction is much more favorable than Raman scattering.

1.9 Use of Raman Spectroscopy to Study Bone

As aforementioned, the bands in a Raman spectrum represent the intensity of a particular frequency of Raman scattered light. The bands are specific to the type and proportion of chemical bonds that are in the sample and thus form a unique chemical 'fingerprint' of the sample. In other words, by comparing the bands with reference values/pure samples you can potentially determine what a given sample consists of. Raman spectroscopy can therefore be used as a diagnostic tool.

Raman spectroscopy of bone is a relatively young field, with the possibility of obtaining Raman spectra from intact calcified tissue first demonstrated by Walton et al. in 1970(Walton 1970). The idea of using Raman as a diagnostic tool for bone disorders is undoubtedly attractive. What sets Raman spectroscopy apart from x-ray techniques and other imaging modalities is:

- its ability to probe both organic and inorganic phases of bone
- its ability to probe any single bone at different points
- its safety profile

1.9.1 Effect of Age and Exercise on Bone

Raman studies have demonstrated increased crystallinity of the hydroxyapatite phase i.e. degree of order and size of the crystals (v_1 phosphate band) with increasing age in mice(Freeman 2001; Akkus 2004). Age-related changes of the organic phase of bone material have also been investigated using Raman and it has been shown that the amide I band increases in intensity with age, something that may reflect changes in cross-linking of collagen and correlate with decreased fracture toughness(Akkus 2003; Ager 2005).

Raman spectroscopy has also been used to demonstrate that exercise causes compositional changes in tibial bone material, with mineralization (v_1 phosphate band to proline/hydroxyproline band) being significantly increased in exercised bones relative to controls(Kohn 2009).

1.9.2 Effect of Mechanical Loading on Bone Material

The response of the chemical structure of bone to large mechanical stresses has been studied with Raman spectroscopy. In one study(Carmejane 2005) pressure was seen to induce large shifts in the position of collagen bands. The CH_2 bands shifted towards higher wavenumbers (reversible) whilst the amide I band shifted towards lower wavenumbers (irreversible). All the mineral bands shifted reversibly. The authors suggested that the irreversible shifts in the amide I band are associated with changes in protein secondary structures such as cross-linking and helix pitch. On the other hand, the reversibiliy of the mineral

Raman bands has been taken as evidence that it is very hard for water to move out of the crystal lattice.

The response of bone to elastic deformation in the physiological range has also been examined using Raman, with the centre of gravity of phosphate bands shifting on tensional loading indicating that the bone mineral may not be a passive contributor to tissue strength but rather function as a local energy storage and dissipation mechanism, thus helping to protect tissue from catastrophic damage(Morris 2004).

1.9.3 Effect of Radiation on Bone Material

Raman Spectroscopy studies that look at the effect of ionizing radiation on bone material have shown that the organic phase suffers much more damage than the mineral phase(Kubisz 2007; Polomska 2010).

1.9.4 Raman Studies of Non-Collagenous Proteins in Bone

In a study using knock-out mice for fibrillin 2 it was found that the femora of the mutant mice had lower hardness and lower elastic modulus than the wild type controls. Raman however failed to demonstrate any significant difference, suggesting that fibrillin 2 may have a unique role in determine the mechanical properties of bone material (e.g. needed to control collagen fibril arrangement)(Kavukcuoglu 2007).

1.9.5 Raman Studies of Bone Microstructure

Raman spectroscopy has a theoretical spatial resolution of 1μm and can therefore probe collagen fibrils, which are aligned in specific directions. Studies have confirmed that the phosphate v_1 to amide I ratio is best for looking at the orientation of the lamellae whilst phosphate v_2 to amide III and phosphate v_2 to carbonate are best for bone material composition(Kazanci 2007). The composition versus orientation methods were used to look at anatomically identical regions of femur in mice of different ages, the results suggesting that there is an evolution of both orientation and chemical composition as a function of tissue age within the same specimen(Gamsjaeger 2010). Hence Raman spectroscopy can be used not only to gain information about composition (e.g. mineral to collagen ratio) but also to study the organization of bone constituents.

1.10 Use of Raman Spectroscopy to study Bone through Skin and Soft Tissue

The Raman studies summarized so far have all used excised bone material that had laser light shone directly onto its surface. More recently techniques have been developed which allow Raman spectroscopy of bone through skin and overlying tissue therefore permitting the potential development in the future of Raman spectroscopy as a non-invasive diagnostic tool in day to day clinical practice.

1.10.1 Kerr Gate

If a molecule that is in an excited electronic state relaxes back down to the electronic ground state and releases the energy as a photon, the process is called fluorescence. Skin, muscles and other soft tissues, unlike bone, consist of large biological molecules (small electronic energy gaps) and fluoresce strongly. The fluorescent photons along with the surface Raman signal will often saturate the detection equipment and drown out the Raman signal making transcutaneous analysis very difficult. The emitted fluorescence photons themselves can be collected and used as a spectroscopic signal however a fluorescence spectrum will have wide overlapping bands and hence much lower chemical specificity. The property that accounts for the differing chemical specificity between Raman and fluorescence is the timescale associated with each process. The Raman scattering event occurs so quickly that the photons capture ‘snapshots’ of the target molecule, whereas the longer timescales associated with the fluorescence process allow time for the excited electronic state to change energy due to thermal collisions with other molecules. Therefore, the gap between the excited and ground state varies during fluorescence and hence the emitted photon energy varies and hence the spectrum will have overlapping bands.

The temporal difference between the Raman and fluorescence processes has been exploited using Kerr-gate technology to produce fluorescence-reduced spectra. The technology has developed to enable the retrieval of Raman spectra of bone through 1mm of skin and tissue

and the discrimination between healthy and pathological bone material(Morris 2004; Morris 2005; Morris 2005). Draper et al. used this technology to analyse metacarpal bones of mice from two distinct genotypes: wildtype and oim/oim(Draper 2005). The oim/oim mice were used as a model for osteogenesis imperfecta as they only produce homotrimeric collagen, which is associated with poor mineralisation. The measurements were repeated with the overlying tissues removed and therefore measured bone directly. They found that the spectrum produced through skin contained more noise but essentially was the same as the spectrum produced through bone directly. They showed that the phosphate peak was less intense and the organic CH_2 wag peak was more intense in oim/oim specimen than the wildtype specimen. The phosphate:CH_2 band area ratio was higher in the wildtype specimen than the oim/oim specimen. All of the results obtained were therefore consistent with what was expected providing evidence that Raman spectroscopy could reliably detect the difference in bone quality in a non-invasive manner.

However, the inherent instrument complexity limits is applicability and this led to the development of spatially offset Raman spectroscopy (SORS).

1.10.2 Spatially Offset Raman Spectroscopy

SORS relies on the fact than laser photons that enter through the surface of a medium will increasingly diffuse in lateral directions the further they travel through the medium. This means that photons returning from deep in the medium will be more likely to emerge far from

their entry point than photons which made only a short journey to the surface from more shallow regions.

Shortly after the development of SORS, it was demonstrated that Raman spectra of bone material could be retrieved through skin and other overlying tissues using animal specimens and living human subjects (up to 4 mm of depth)(Matousek 2006; Schulmerich 2006; Schulmerich 2006).

SORS also has excellent capability to dampen melanin-induced fluorescence from skin and this further enhances its use in vivo. Matousek et al. performed the first transcutaneous Raman spectroscopy of human bone in vivo using SORS to provide a safe laser level(Matousek 2006). A further development to SORS is inverse SORS (iSORS), which enables the use of higher laser powers through a wider laser-exposed surface. The difference between SORS and iSORS is essentially the area of laser focus and the area of collection of Raman scattering. In SORS the laser beam is focused centrally and the Raman scattering is collected peripherally whereas in iSORS the situation is the opposite so the laser beam is focused peripherally and the Raman scattering is collected centrally.

1.11 Pre-processing

Following spectral acquisition the spectra must be pre-processed to account and correct for sample thickness, sloping baseline effects and to select the spectral region of interest. This is a current area of research.

1.11.1 Cut and smoothing

The region of interest in the study of biological specimens is 1800 cm^{-1} – 900 cm^{-1}, referred to as the *biochemical-cell fingerprint*. The spectral region usually selected in Raman spectroscopy is within 2000 cm^{-1} – 350 cm^{-1}.

1.11.2 Baseline correction

The raw data obtained from Raman spectroscopy need to be baseline corrected in order to account for fluorescence.

1.11.3 Normalisation

Normalisation is employed to scale the spectra and remove spectral changes accountable by the thickness of the sample.

1.12 Multivariate Analysis

1.12.1 Principal component analysis (PCA)

PCA is an unsupervised multivariate technique used to analyze the inherent structure of the data. PCA reduces the dimensionality of the data set by finding an alternative set of coordinates: principal components (PCs). PCs are linear combinations of the original variables, which are orthogonal to each other and constructed in such a way that each one successively accounts for the maximum variability of the data set. The PCs may be plotted as pseudo-spectra called loadings curves. They are also used for the axes of scores plots, where each spectrum is represented by an individual point, or score (**Figure 1.9**).

Scores plots allow the identification of segregation in the data set as clusters. The closer together two scores are the more similar they are biochemically, and vice versa. The interpretation of the scores, followed by the loadings allow the reasons for any segregation to be identified(Jollife 1986; Brereton 2003).

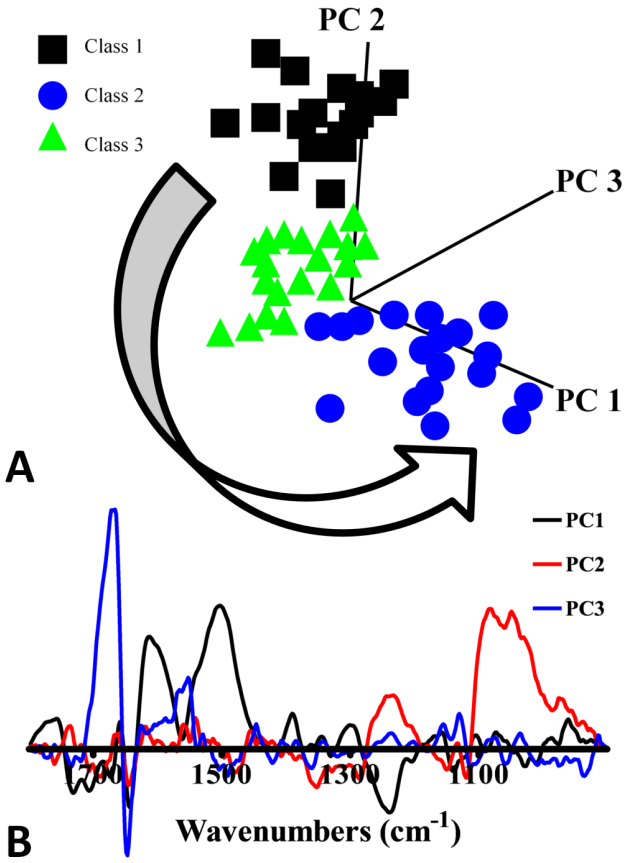

Figure 1.9: Example of PCA scores (A) and loadings (B) (Kelly 2010).

1.12.2 Linear discriminant analysis (LDA)

LDA is a supervised multivariate technique, meaning that information regarding how many groups there are and which samples correspond to each group is taken into account during the analysis process. This method maximizes the ratio of between-class variance to

the within-class variance in any particular data set thereby guaranteeing maximal separability.

The goals of LDA are somewhat similar to those of PCA. But different from LDA, PCA is an unsupervised technique and as such does not include label information of the data, effectively ignoring this often useful information. LDA explicitly attempts to model the difference between the classes of data. PCA on the other hand does not take into account any difference in class, and factor analysis builds the feature combinations based on differences rather than similarities.

LDA can be used to produce a scores plot, where relative distances correspond to dis(similarities) in the data. Additionally, a loadings plot may be produced and interpreted to provide wavenumbers (and corresponding biochemical) responsible for segregation between classes(Kelly 2010).

A downside of LDA is that it is a parametric method assuming unimodal Gaussian likelihoods. If the distributions are significantly non-Gaussian, the LDA projections may not preserve complex structure in the data needed for classification(Brereton 2003).

1.12.3 PCA-LDA

LDA may be performed on the output of data from PCA. This allows data reduction, and therefore removal of noise from the dataset prior to supervised analysis. Loadings/cluster vector plots may be interpreted to identify reasons for spread within the data and any biomarkers distinct to classes (**Figure 1.10**). This is true for both PCA

and PCA-LDA, although the latter may be more precise in determining inter-classes distinctions(Kelly 2010).

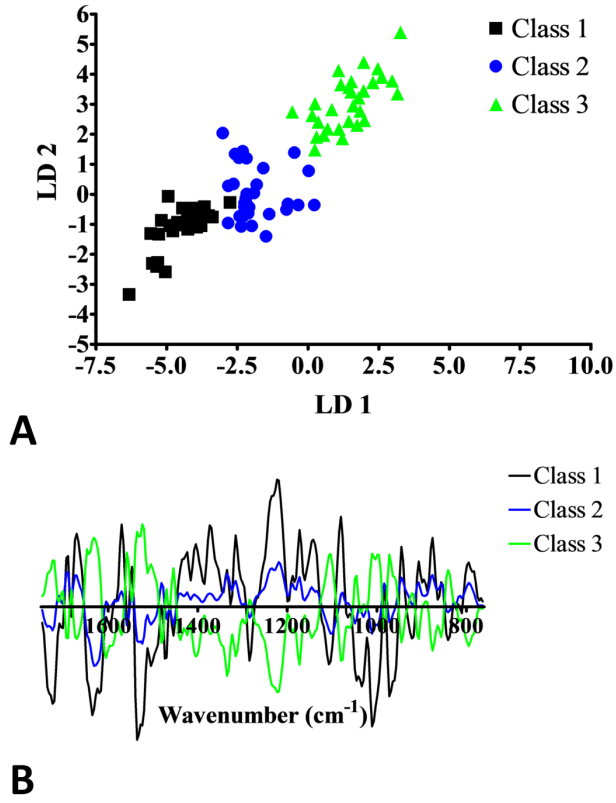

Figure 1.10: Example of PCA-LDA scores (A) and loadings (B) (Kelly 2010).

CHAPTER 2 – AIMS

2.0 General Aim

The general aim is to investigate the quality of subchondral bone in human osteoarthritic tibial plateaus. Normal tibial plateaus are used as controls so comparisons can be made. The term ‘bone quality’ is vague and cannot be measured directly. Instead, several parameters are used as markers for bone quality: mineral to matrix ratio, carbonate to phosphate ratio, carbonate to amide I ratio, amide I to amide III ratio and volumetric bone mineral density. These parameters have been used previously in the literature to define bone quality and the former two ratios are the most validated markers for bone quality in spectroscopy studies(Morris 2011). The phosphate to amide I ratio (mineral to matrix) indicates the degree of mineralisation and the carbonate to phosphate ratio indicates the extent of carbonate accumulation in the apatite crystals. The carbonate to amide I ratio may indicate bone remodelling(Morris 2011). Finally in our work we have used the amide I to amide III ratio as an indicator of collagen differences between our cohorts. This has not been previously validated and although the results will be cautiously interpreted, any differences nevertheless can potentially suggest quantitative and or qualitative collagen changes between healthy and diseased tissue.

The majority of the research done on subchondral bone has failed to accurately distinguish it from cancellous bone. In this study, subchondral bone is limited to within 3mm of articular cartilage. The

secondary aim is to investigate the presence of homotrimeric type I collagen in osteoarthritic bone using sodium dodecyl sulphate polyacrylamide gel electrophoresis (SDS PAGE).

2.1 Hypotheses

a) There is no difference in the vBMD and subchondral bone thickness in osteoarthritic tibial plateaus compared to controls.

b) There is no difference in the phosphate to amide I ratio, carbonate to phosphate ratio, carbonate to amide I and amide I to amide III ratios in osteoarthritic tibial plateaus compared to controls.

c) There is no difference in the levels of homotrimeric type I collagen in osteoarthritic and controls specimens.

2.2 Objectives and Study Design

a) To measure the subchondral bone density and subchondral bone thickness in OA and non-OA control specimens.

b) To acquire Raman spectra from OA and non-OA control specimens and to subsequently perform univariate and multivariate analysis

c) To quantify levels of homotrimeric alpha 1 collagen in bone form subchondral plate in OA and non-OA control specimens.

CHAPTER 3 – MATERIALS AND METHODS

3.0 Ethical Approval

Ethical approval was sought and granted from the Stanmore Biobank (09/H0304/78) for collection of human tissue at the Royal National Orthopaedic Hospital, Stanmore UK and transfer to the laboratories of the UCL Institute of Orthopaedics and Musculoskeletal Science at the Royal National Orthopaedic Hospital site (Stanmore, UK) for storage and analysis. Ethical approval was also granted for the collection of cadaveric lower limbs from The Vesalius Clinical Training Centre at the University of Bristol – www.bristol.ac.uk/vesalius (08/H0724/34), from people who had previously consented to donate their bodies for medical research.

3.1 Specimen Collection and Storage

Five cadaveric tibiae were obtained from the The Vesalius Clinical Training Centre at the University of Bristol, UK. There was no clinical and radiological history of osteoarthritis or metabolic bone disease in any of the donors. The tibial plateau was excised en bloc using a AEW Thurne 350 band saw (AEW Delford Systems, Norwich, UK) at a blade speed of 27m/s. All five cadaveric specimens were examined and confirmed not to have any macroscopic features of osteoarthritis (intact articular cartilage with absence of softening, fibrillation and fissuring; Grade O Outerbridge Classification, see **Figure 3.1**).

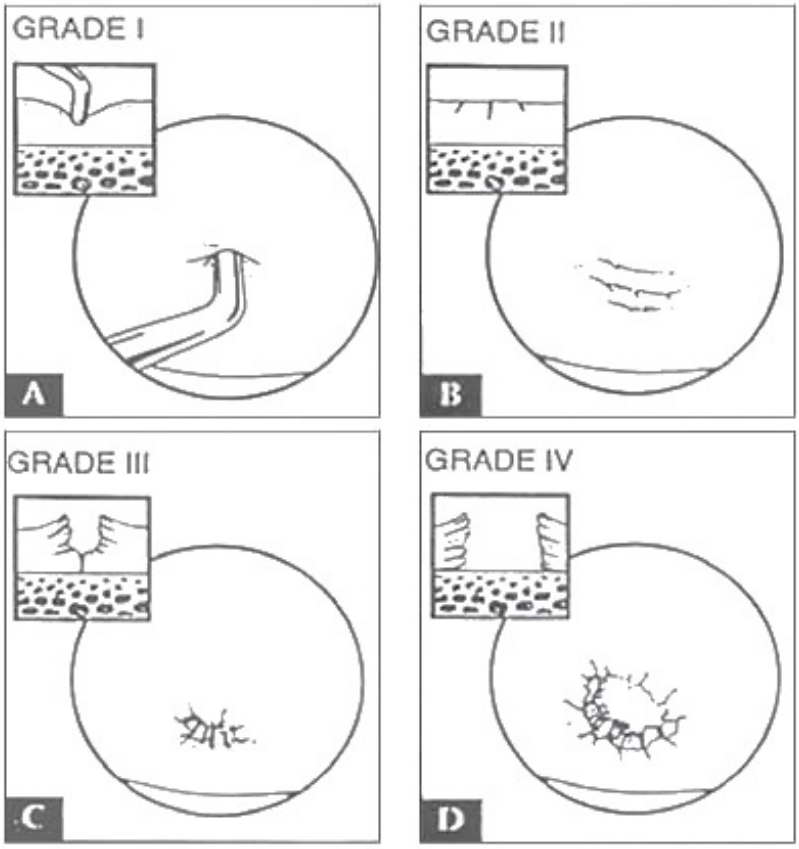

Figure 3.1: Outerbridge classification: Grade O = normal cartilage; Grade I = softening (A); Grade II = fissuring but < 50% (B); Grade = III fissuring and > 50% (C); Grade IV = full-thickness lesion (D) (adapted from www.healio.com).

Five normal tibial plateaus were retrieved following surgery at the Royal National Orthopaedic Hospital from patients undergoing oncological operations involving massive en bloc excision of the knee joint. There were no clinical or radiological signs of osteoarthritis and the primary disease process did not affect the tibias (distal femoral pathology). Weight bearing was not affected as a result of the primary disease process.

Ten tibial plateaus were retrieved at surgery from the Royal National Orthopaedic Hospital from patients undergoing primary total knee replacement for clinically and radiologically diagnosed

predominantly medial compartment osteoarthritis. Patients with post-traumatic osteoarthritis were excluded from the study.

All patients gave informed written consent to allow retention and analysis of their tibial plateaus for the purpose of the study. The samples were removed in the standard manner during the operation, briefly stored in a fridge before transportation to our laboratory the same day. All soft tissue was excised from around the specimens and they were stored in a Sanyo VIP series ultra low temp freezer (Sanyo Biomedical, Japan) at a temperature between -70 and -80°c.

3.2 Densitometry pQCT Measurements

Peripheral quantitative computerized tomography (pQCT) is a method of accessing bone mineral density, which uses multiple cross-sectional x-rays to reconstruct a volumetric model of the bone density distribution. The analyzed bone mineral density is presented as mg/cm^3.

Other densitometric technologies, using isotopes, x-rays, or ultrasound, yield results based upon a weighted average of combined trabecular and cortical bone. These older technologies employ a 2-D projection of the bone which super-imposes trabecular and cortical bone. They are, therefore, unable to isolate specific bone components.

Advantages of pQCT include:

1. Measurements of volumetric bone mineral density (vBMD, in mg/cm^3), as opposed to DEXA scanning, which provides area bone mineral density (aBMD, in mg/cm^2). Use of aBMD to assess samples does not take into account the third dimension and

therefore may lead to erroneous conclusions due to differences in bone size (Bennel et al.,2008).

2. The ability to analyse cortical bone and trabecular bone separately (Bennel et al.,2008). This is particularly relevant when scanning subchondral bone as the subchondral cortical bone and underlying trabecular bone can be distinguished.
3. Utilises thin cross-sectional slices, this is particularly important for studying the effects of OA, as variations in load across an articulating surface, such as the proximal tibial plateau, will probably result in heterogeneous subchondral densities (Bennel et al.,2008).

3.2.1 Validation of pQCT Apparatus

3.2.1.1 Quality Assurance

The quality assurance (QA) measurement is used to check all components of the pQCT apparatus. It is performed every working day to detect any possible defects. It is not a calibration of the system as the scanner is so stable that no drift is visible for several years.

QA measurement was performed by fixing the QA phantom in the phantom holder and placing it in the fixation for the measurement tube. The position of the CT scan and subsequent measurements are performed automatically by the system software. The software compares the measured values with the rated values and gives the message “QA successful” if the difference between measured and rated

values is smaller than 1%. QA measurements were always successful during the course of this work.

3.2.1.2 Repeatability

In order to confirm that the pQCT apparatus gave the same response to the same experimental conditions, repeated vBMD of a sample were recorded. A piece of diaphyseal cadaveric human femur sectioned along the coronal plane was used and cortical vBMD was calculated at 2 cm intervals along its length. Without changing anything another set of measurement was recorded. Five measurements were recorded five times in this way.

3.2.1.3 Reproducibility

Reproducibility was also investigated. A piece of diaphyseal cadaveric human femur sectioned along the coronal plane was placed on the sample stage and vBMD was measured at a location 5 cm from its proximal end (position marked). The sample was then removed, and subsequently placed back on the stage, so that the measurement was repeated on the same area 5 times.

3.2.2 pQCT Measurements

Samples were allowed to defrost at room temperature for a maximum of 2 hours. QA measurement of the pQCT XCT 3000 (Stratec, Pforzheim, Germany) scanner (**Figure 3.2**) was performed with a phantom.

Figure 3.2: The pQCT XCT 3000 scanner

XCT 3000 Stratec (version 6.00) software was loaded and details of the specimens entered. The samples were placed horizontally in a Stratec XCT 3000 pQCT scanner, ensuring same orientation and supported on a ruler base with low x-ray attenuation. Specimens were scanned in two mm increments; considered a small enough distance to gather data from specific sites. The images gathered allow the distinction between cartilage, subchondral cortical bone and subchondral trabecular bone. The x-ray beam width was 2mm and the voxel size was fixed at 0.3mm. The threshold for trabecular and cortical human bone was defined according to the manufacturer's specification as 280 and 710mg/cm^3 respectively. A measurement slice from the centre of each compartment of the plateau (red dashed line indicated in **Figures 3.3A** and **3.3C**) was used to calculate the vBMD (mg/cm^3) of the subchondral bone; the regions of interest (ROI) used for this were the same size and location across all measurements (**Figure 3.4**). Additionally, on the same slice, the thickness of the subchondral bone was also measured in mm, by drawing a line on the ROI image from

proximal to distal. The regions of interest (**Figure 3.4**) were used to calculate volumetric bone mineral density to an accuracy of ±5.0mg/cm^3.

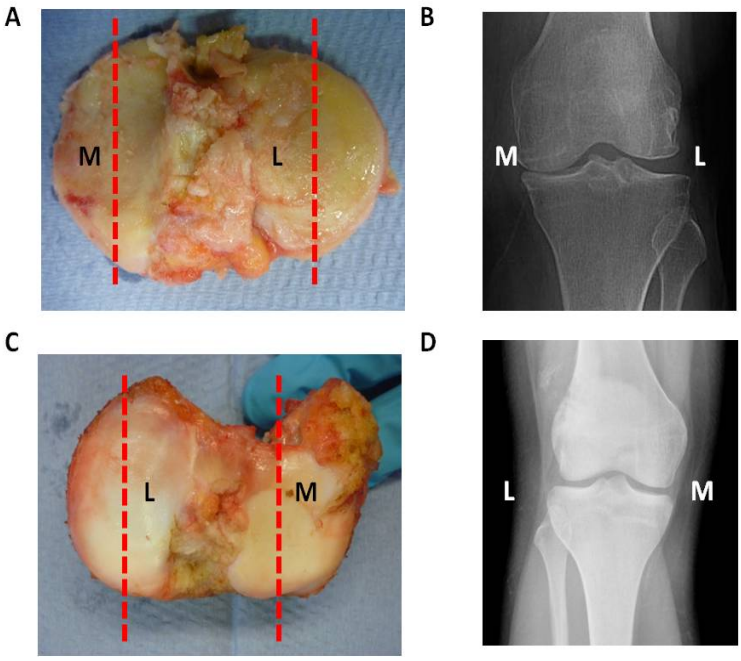

Figure 3.3: Tibial plateau post-operative photos and pre-operative radiographs [A] OA photo; [B] OA radiograph; [C] Photo of non-OA; [D] Radiograph of a non-OA knee. Red dashed lines indicate the plane the pQCT measurements were taken.

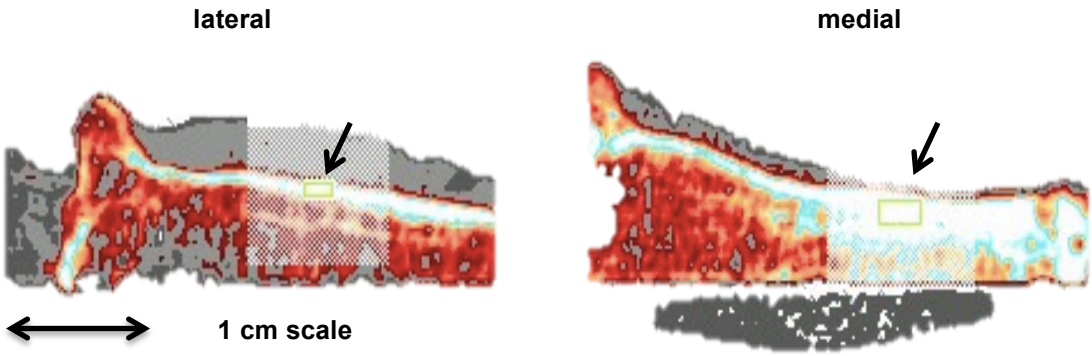

Figure 3.4: PQCT scan of the lateral side of a tibial plateau (left), showing cartilage (grey) overlying subchondral cortical bone, and the medial side of a tibial plateau (right), showing cartilage wear (thin, almost absent grey layer) and dense subchondral cortical bone exposed. Small yellow squares (arrows) demarcate region of interest (ROI) wherefrom density measurement is recorded.

3.3 Collagen Biochemistry to Determine Alpha Chain Ratios

3.3.1 Validation of Biochemistry Technique

A collagen and molecular weight standard was used in all gels giving reproducible results with an alpha chain ratio of two alpha 1:one alpha 2 chains equal to 2.476:1.

3.3.2 Tissue Preparation

Cores from specific sample regions were taken using a circular 2mm punch (Jamshidi needle). The cores were obtained from the centre of the medial and lateral plateaus. The cores were then defatted with 5ml of pure acetone and left for an hour at 37°C. This step was repeated twice more. The acetone was then washed off the cores with deionised water and dried. They were then weighed prior to decalcification. Decalcification involved immersing the cores in 10ml of 10% EDTA at a pH of 7.5. This was left to stir for 10 days at 4°C. The insoluble collagenous residues were then centrifuged at 4600 rpm for 10 minutes at 20°C. The cores were washed with deionised water (to remove excess EDTA) and freeze-dried. The cores were then re-weighed and the weight loss assessed. Five milligrams from each selected sample was isolated for further processing. The selected decalcified collagenous cores were each immersed in 1ml of 0.5M acetic acid with 25μg of pepsin added (0.5% w/w of 5mg cores). They were left to stir for 2 days at 4°C. The cores were then centrifuged at 13000 rpm for 15

minutes at 4°C. The supernatants were harvested and freeze-dried overnight.

3.3.3 Sodium Dodecyl Sulphate PolyAcrylamide Gel Electrophoresis

Samples prepared as above, were dissolved in 0.5ml of sample buffer and then heated in a water bath at 60°C for 10 minutes. The Mini-Protean II apparatus (Bio-Rad, Hemel Hempstead, UK) was assembled according to the manufacturer's instructions. The 7.5% polyacrylamide resolving gel matrix was prepared and immediately poured between the two glass plates and overlaid with a layer of deionised water. The gels were left to set for 30 minutes. The layer of water was discarded and filter paper used to dry the plates. The 4.5% stacking gel was then prepared and immediately poured between the two glass plates. Combs were inserted and positioned into the gels. The gels were left to set for 30 minutes and the running buffer prepared. Once the gels solidified, the combs were removed and running buffer added to the wells. The gel plates were clipped into the frame to make the upper reservoir and 10µl of each sample was loaded into the wells using specialised pipette tips. The upper reservoir was positioned into a tank and running buffer added to fill the upper reservoir and the majority of the tank. The lid was closed and the red and black leads plugged into their respective locations in the power pack. The gels were run at a constant current of 40mA (20mA/gel) and a starting voltage of 162V as per protocol. They were run until the dye front reached the end of the gel. After electrophoresis, the gels were stained overnight with Coomassie Blue and then

destained with 10% acetic acid and 20% methanol solution. The gels were photographed and the images analysed using Image J (version 1.45) software. This program was used to quantify the band intensities of type I collagen α1 and α2-chains. The α1: α2-chains ratio was subsequently calculated for each sample.

3.4 Raman Spectroscopy

3.4.1 Validation of Raman Apparatus

3.4.1.1 Calibration

The Raman instrument is calibrated prior to use with silicon and polystyrene. The former has the centroid of the peak at 520.5 cm^{-1} and the latter at 1001 cm^{-1} and 1031 cm^{-1}. The instrument is adjusted following silicon calibration until the peak obtained corresponds to the one expected. The polystyrene test is an additional check to confirm the calibration done with silicon and to ensure that it is accurate.

3.4.1.2 Repeatability

In order to confirm that the instrumentation gave the same response to the same experimental conditions, repeated spectra of a sample were recorded. A piece of bone from the midshaft of a human cadaveric femur was used and a spectrum was recorded. Without changing anything another spectrum was recorded. Ten spectra were recorded in this way.

3.4.1.3 Reproducibility

Reproducibility was also investigated. A piece of cadaveric human femur was placed on the sample stage and a spectrum was recorded. The sample was then removed, and subsequently placed back on the stage, so that the laser illuminated roughly the same area, and another spectrum was recorded. Ten spectra were obtained this way.

3.4.2 Raman Measurements

Cores from central portions of the medial and lateral parts were taken from each tibial plateau slice using a circular 2 mm punch (Jamshidi needle). A single core was taken from each area of interest and each one incorporated at least 3mm of subchondral bone. Cores were then defatted with 5ml of pure acetone and left for an hour at 37°C. This step was repeated twice more. The acetone was then washed off the cores with deionised water and dried and frozen for later use. All specimens were defrosted for a minimum of 60 minutes prior to Raman spectral analysis. The subchondral bone was analysed with the Renishaw inVia Raman microspectroscopy (Gloucestershire, UK), a class 3B laser with 300mW power and 830nm wavelength (**Figure 3.5**). A Leica 50x long working distance (LWD) microscope objective was used to focus the laser, ensuring accuracy and precision of the readings. The position of the microscope objective with respect to the bone tissue was manually controlled in the three axes during surface mapping. Ten independent Raman spectra were acquired from each sample allowing us to obtain average value of compositional and structural parameters of each tibial plateau core. The samples were

measured in room temperature. Cosmic ray artifacts were removed during acquisition and band spectral parameters were obtained by deconvolution in the WIRE 3.1 (Renishaw) software.

Figure 3.5: The Renishaw inVia Raman microspectroscopy apparatus.

3.4.3 Pre-processing

The data collected was pre-processed using INT13.exe, MATLAB (version 2007b) software. The raw data was baseline corrected to account for fluorescence. This was done in two steps. First the raw data was baseline corrected for wavenumbers in the range 350 – 1150cm^{-1} using a polynomial power of 3. The process was then repeated for wavenumbers in the range of 1150 – 1800cm^{-1}. The baseline corrected data were then normalised using Microsoft Office Excel 2007. This involved subtracting the lowest intensity (which was at the 1800cm^{-1} wavenumber) from the data and then dividing the resultant data by the highest intensity (which was at the 960cm^{-1} wavenumber) thus normalising all spectra to the v1 phosphate peak. The peaks of interest

are labelled in **Figure 3.6** and include the v_1 phosphate peak (961cm^{-1}), v_1 carbonate B-type peak (1070cm^{-1}), amide I (1658cm^{-1}) and amide III (1247cm^{-1}) peak (Penel 2005; Kazanci 2007; Morris 2011). The phosphate: amide I ratio, carbonate: phosphate ratio, carbonate: amide I ratio and the amide I: amide III ratio were the parameters investigated. They have been used previously in numerous studies for investigations of bone disorders (Tarnowski 2002; Kazanci 2007; Buchwald 2012) and the former three are the most validated markers for bone quality (Morris 2011). The phosphate: amide I ratio was calculated by dividing the height of the phosphate band by the height of the amide I band. The carbonate: phosphate ratio was calculated by dividing the height of the carbonate band by the height of the phosphate band. The carbonate: amide I ratio was calculated by dividing the height of the carbonate band by the height of the amide I band. The amide I: amide III ratio was calculated by dividing the height of the amide I band by the height of the amide III band. The height of the phosphate band was calculated by subtracting the average phosphate base (988 – 1000 cm^{-1}) from the average phosphate peak (958 – 963 cm^{-1}). The height of the amide I band was calculated by subtracting the average amide I base (1701 – 1705 cm^{-1}) from the average amide I peak (1653 – 1660 cm^{-1}). The height of the carbonate band was calculated by subtracting the average carbonate base (1108 – 1110 cm^{-1}) from the average carbonate peak (1064 – 1071 cm^{-1}). The height of the amide III peak was calculated by subtracting the average amide III base (1270 – 1280cm^{-1}) from the average amide III peak (1260 – 1265 cm^{-1}). It should be noted that the

baseline region for Amide III can include alpha-helix signals as this is not a spectrally quiescent region.

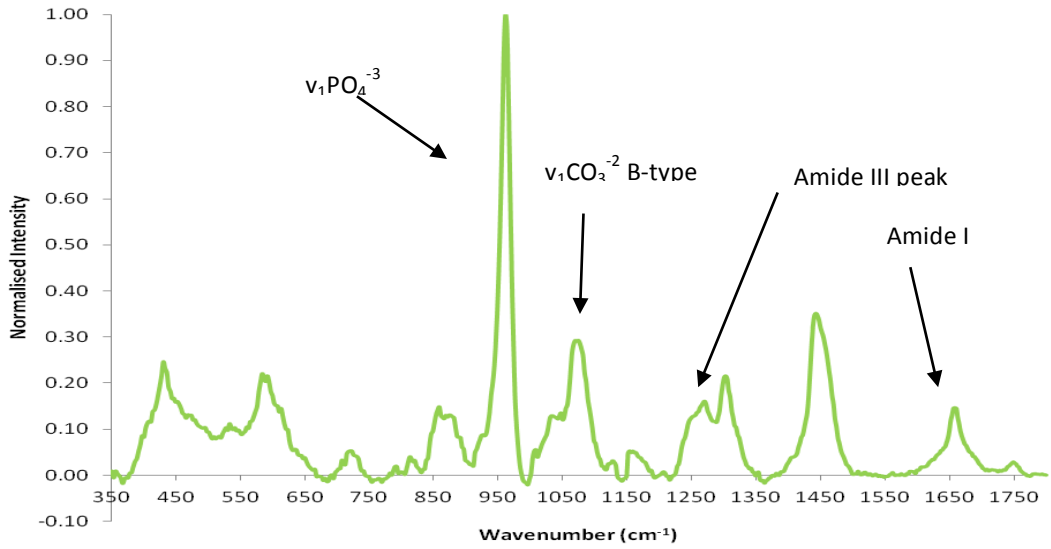

Figure 3.6: Typical Raman spectrum of normal subchondral bone with the peaks of interest labelled. The Raman intensity (dimensionless) has been normalised to the phosphate peak at wavenumber 961cm^{-1}.

3.5 Statistical Analysis Methods

3.5.1 Statistical Methods

Statistical tests were performed using SPSS Statistics (version 17.0) software. The sample sizes were insufficient to test for normality so the non-parametric equivalents to the t-tests were preferred. The Mann Whitney U test was therefore used to compare osteoarthritic samples with controls. Moreover, the Wilcoxon Signed Rank test was used to compare the different regions within OA and normal tibial plateaus. Differences were considered to be statistically significant where $p < 0.05$. The median and inter-quartile range (IQR) was considered the most appropriate measure to use for analysis due to the

skewed nature of the data. Unless stated otherwise, the data are expressed as the median (IQR).

3.5.2 Power Statement

This study is a pilot study that will explore a number of potential outcome measures to identify which is most sensitive and to gain an understanding of within patient variability. With 10 OA samples and 10 normal samples the study will have 80% power to detect a difference of 1.3 x Standard Deviation (SD) in the outcome measures of interest, using the two tailed 5% significance level. An effect size of 1.3 x SD constitutes a large effect size, (Cohen 1988). Sample size calculation was performed using Stata/IC version 12.1 (StataCorp, College Station, TC, USA).

3.5.3 Principal Component Analysis (PCA)

PCA is a multivariate technique that operates in an unsupervised manner and is used to analyze the inherent structure of the data. PCA reduces the dimensionality of the data set by finding an alternative set of coordinates, the principal components (PC's) (Martens 1989; Esbensen 2005). The general form of PCA model is:

$$X=TP^{T}+E \quad (1)$$

where X matrix is decomposed by PCA into two smaller matrices, one of scores (T) and other of loadings (P).

PC's correspond to a linear combination of the original variables, which are orthogonal to each other and constructed in such a way that

each one successively accounts for the maximum variability of the data set.

In other words, PCA involves a mathematical procedure that transforms a large number of correlated variables (i.e. Raman shifts) into a smaller number of uncorrelated variables called principal components. Numerically this means that:

$$\sum_{i=1}^{I} t_{ia} t_{ib} = 0 \qquad (2)$$

where t_a and t_b are the a^{th} and b^{th} columns of T matrix, respectively, and

$$\sum_{i=1}^{I} p_{ia} p_{ib} = 0 \qquad (3)$$

where p_a and p_b are the a^{th} and b^{th} rows of P matrix, respectively.

The first principal component (PC1) accounts for as much of the variability in the data as possible, and each succeeding component accounts for as much of the remaining variability as possible.

When PC-Scores are plotted, for example PC1 *vs.* PC2 or any combination of the PC's, they can reveal relationships between samples (grouping). It is important to remember that PCA does not act in a supervised manner, meaning that each number of the groups under study is not known *a priori.* PCA provides insight into the percentage of variance explained by each PC and how many PCs should be kept to

maintain the maximum information from the original data without adding noise to the current information. In addition, when the PC-loadings are plotted as a function of the variables, the plot reveals the most important diagnostic variables or regions related with the differences founded in the data set.

3.5.4 Linear Discriminant Analysis (LDA)

LDA computes linear combinations of variables to determine directions in the spectral space, discriminant functions (Linear Discriminants, LDs), that maximize the variance between groups and minimize the variance within groups according to Fisher's criterion (Hair 1998).

The LDs are used as axes in a scatter plot, to produce a *scores plot*; again relative distances correspond to dissimilarities/similarities in the data. A *loadings plot* may be produced and interpreted to provide wavenumbers (and corresponding chemical bonds) responsible for segregation between classes.

3.5.5 PCA-LDA

LDA was performed on the output of data from PCA. This allows data reduction, and therefore removal of noise from the dataset prior to supervised analysis.

CHAPTER 4 – RESULTS

4.0 Baseline Characteristics

Ten OA, five control fresh and five control cadaveric tibial plateaus were analysed. The ten OA samples were from six males and four females, the five control fresh samples were from four males and one female whereas the five control cadaveric were from five males. Both OA and control cadaveric groups had similar ages in the range of 58 – 88 years. The OA specimens had have average age of 68 years, cadaveric specimens had an average age of 74 years, while the fresh controls had an average age of 30 years. The difference between the age means of the OA and cadaveric specimens was not statistically significant ($p=0.08$) but significantly different when comparing OA and fresh controls ($p<0.0001$) and cadaveric with fresh controls ($p<0.0001$). None of the patients from whom samples were obtained had a known clinical history of metabolic bone disease, inflammatory arthritis, cancer, history of drug abuse, hepatic or renal pathology.

4.1 Volumetric Bone Mineral Density

4.1.1 Validation Results

In order to assess repeatability a piece of diaphyseal cadaveric human femur sectioned along the coronal plane was used and cortical vBMD was calculated at 2 cm intervals along its length. Without changing anything another set of measurement was recorded. Five measurements were recorded five times in this way. **Table 1** gives the

average vBMD for each area with standard deviation (this is of the order of 1%).

	REPEATABILITY
Area 1	1265 mg/cm^3 (12)
Area 2	1301 mg/cm^3 (15)
Area 3	1290 mg/cm^3 (14)
Area 4	1310 mg/cm^3 (11)
Area 5	1295 mg/cm^3 (12)

Table 1: Mean vBMDs for each area tested with standard deviations.

In order to assess reproducibility a piece of diaphyseal cadaveric human femur sectioned along the coronal plane was placed on the sample stage and vBMD was measured at a location 5 cm from its proximal end (position marked). The sample was then removed, and subsequently placed back on the stage, so that the measurement was repeated on the same area 5 times. The average vBMD (SD) was 1318 mg/cm^3 (14).

4.1.2 Experimental pQCT results

The median vBMD of OA samples was 112 mg/cm^3 higher ($p<0.001$) than the median vBMD of control samples (fresh and cadaveric) (**Figure 4.1**). The middle portion of both the medial and lateral tibial plateaus was used to obtain the most representative measurements subsequently used for statistical analysis. **Figure 4.2** highlights differences between OA, control fresh and control cadaveric specimens. The median vBMD of OA samples was 52 mg/cm^3 higher than cadaveric controls ($p=0.018$) and 187 mg/cm^3 higher than fresh controls ($p=0.001$). **Figure 4.3** demonstrates differences between OA and control medial and lateral tibial plateaus. The median vBMD of OA

medial plateaus was 78 mg/cm^3 higher than the OA lateral plateaus (p=0.005). The median vBMD of OA medial plateaus was 155mg/cm^3 higher than the control medial plateaus (p=0.003). There was no statistically significant difference between control medial and control lateral plateaus (p=0.241) and no statistically significant difference between OA lateral and control lateral plateaus (p=0.059).

The thickness of the subchondral bone is equal across both compartments of the non-OA samples but thicker in the medial compartment of the OA specimens (**Figure 4.4**).

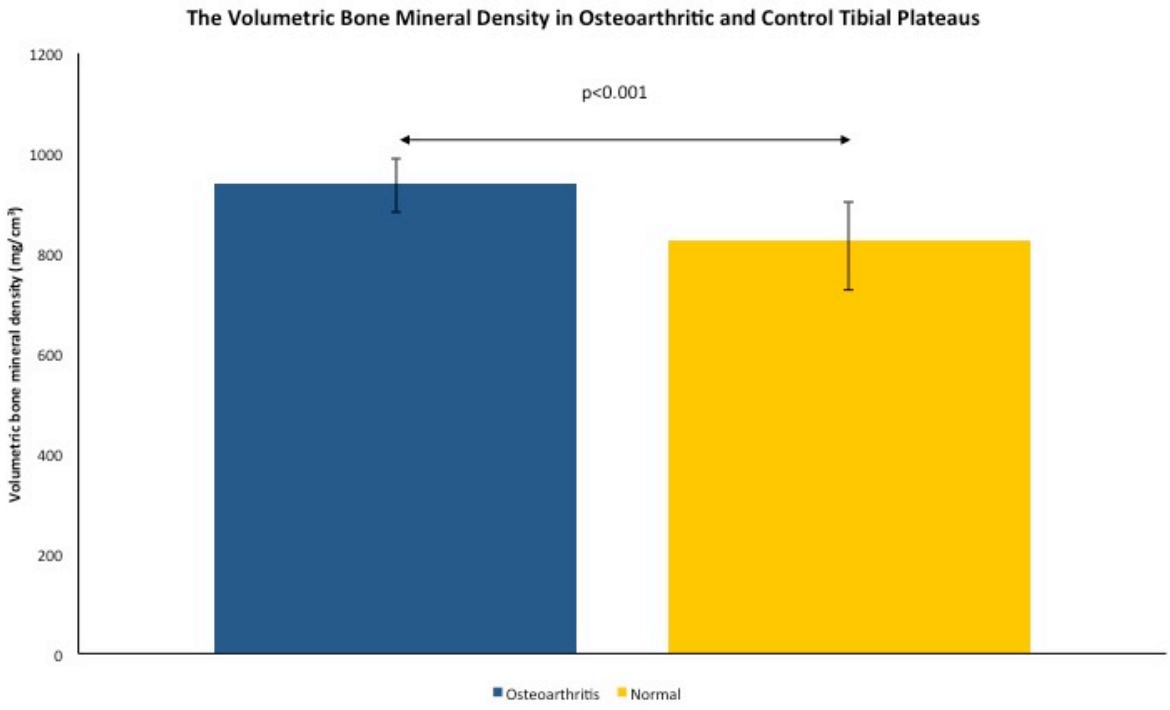

Figure 4.1: Volumetric Bone Mineral Density between osteoarthritic and normal (fresh and cadaveric) specimens irrespective of compartment. Measurements obtained from the central portion of the medial and lateral tibial plateaus. Median values are presented in mg/cm^3 to an accuracy of ±5.0mg/cm^3. Error bars represent the inter-quartile range.

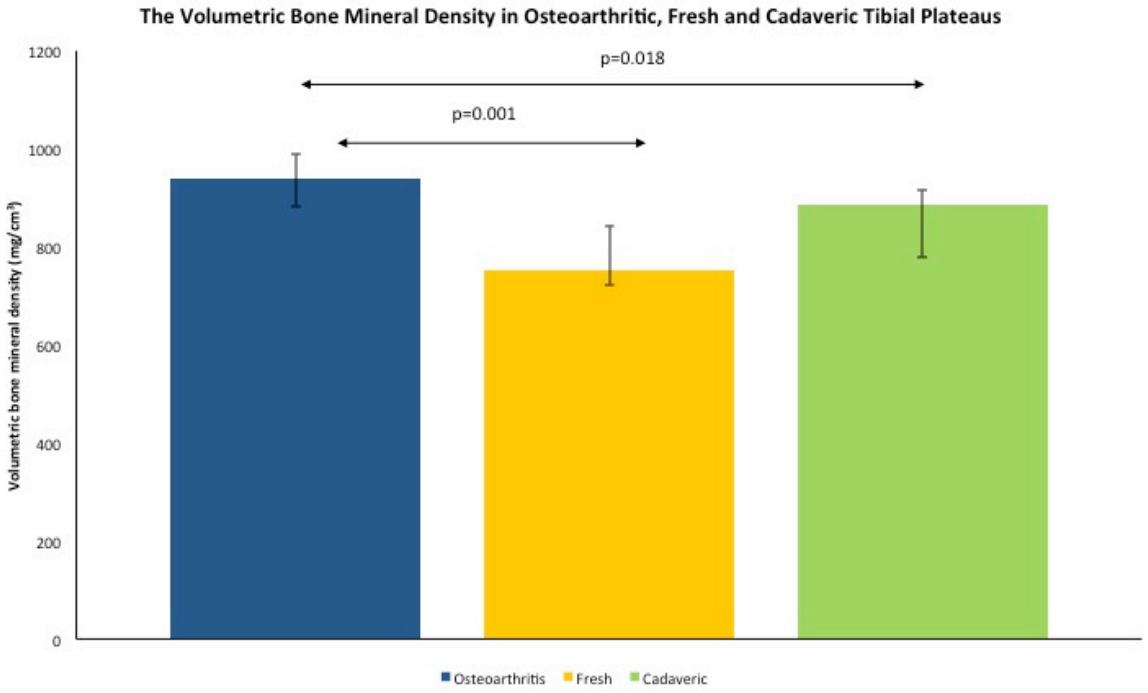

Figure 4.2: Volumetric Bone Mineral Density between osteoarthritic, control (normal) fresh and control (normal) cadaveric specimens. Osteoarthritic specimens are matched for age with control cadaveric. Median values are presented in mg/cm^3 to an accuracy of ±5.0mg/cm^3. Error bars represent the inter-quartile range.

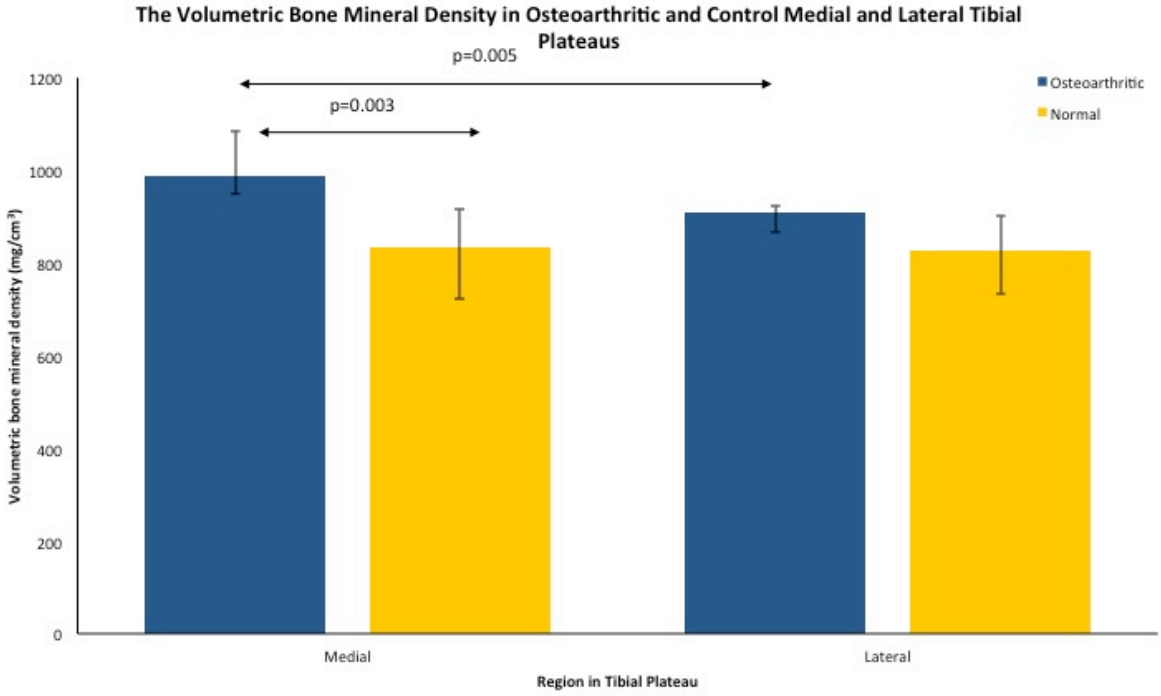

Figure 4.3: Volumetric Bone Mineral Density between osteoarthritic and control medial and lateral tibial plateaus specimens. Median values are presented in mg/cm^3 to an accuracy of ±5.0mg/cm^3. Error bars represent the inter-quartile range.

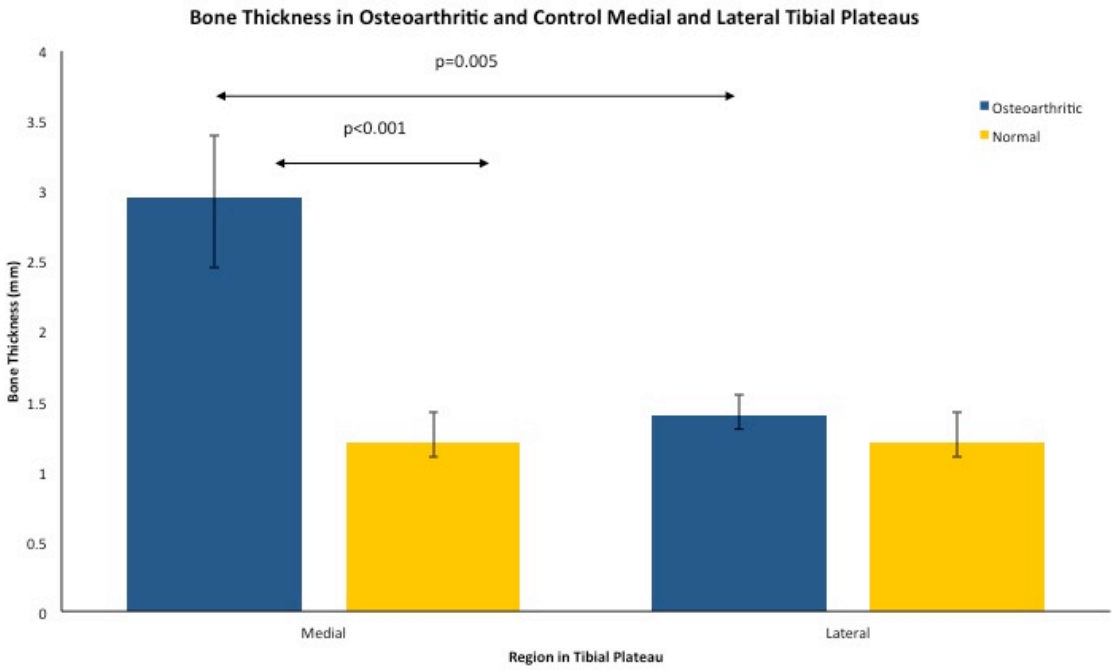

Figure 4.4: Bone Thickness between osteoarthritic and control medial and lateral tibial plateaus specimens. Median values are presented in mg/cm^3 to an accuracy of ±0.5mm. OA samples have statistically significant thicker subchondral bone in the medial compartment compared to both control medial and OA lateral compartments. Error bars represent the inter-quartile range.

Specimen	vBMD (mg/cm^3)	Subchondral bone thickness (mm)	Specimen	vBMD (mg/cm^3)	Subchondral bone thickness (mm)
OA 1	**Medial:** 984.5	3.2	Control (fresh) 1	**Medial:** 957.2	**1.8**
	Lateral: 916.2	1.2		**Lateral:** 927.0	**1.8**
OA 2	**Medial:** 841.2	3.3	Control (fresh) 2	**Medial:** 720.7	**1.1**
	Lateral: 810.0	1.3		**Lateral:** 737.2	**1.1**
OA 3	**Medial:** 956.1	4.9	Control (fresh) 3	**Medial:** 690.2	**1.2**
	Lateral: 869.3	1.5		**Lateral:** 703.0	**1.2**
OA 4	**Medial:** 988.6	2.5	Control (fresh) 4	**Medial:** 820.1	**1.1**
	Lateral: 914.2	1.4		**Lateral:** 818.0	**1.1**
OA 5	**Medial:** 997.4	3.2	Control (fresh) 5	**Medial:** 746.2	**1.2**
	Lateral: 950.0	1.7		**Lateral:** 752.3	**1.2**

OA 6	**Medial:** 1186.2	2.7	Control (cadaveric) 1	**Medial:** 843.7	**1.1**
	Lateral: 857.1	2.0		**Lateral:** 833.1	**1.1**
OA 7	**Medial:** 1052.3	2.6	Control (cadaveric) 2	**Medial:** 957.0	**1.3**
	Lateral: 904.5	1.4		**Lateral:** 928.6	**1.3**
OA 8	**Medial:** 928.1	1.6	Control (cadaveric) 3	**Medial:** 723.1	**1.5**
	Lateral: 874.9	1.3		**Lateral:** 718.2	**1.5**
OA 9	**Medial:** 1184.5	2.3	Control (cadaveric) 4	**Medial:** 887.2	**1.0**
	Lateral: 950.3	1.3		**Lateral:** 869.9	**1.0**
OA 10	**Medial:** 956.0	3.7	Control (cadaveric) 5	**Medial:** 903.0	**1.4**
	Lateral: 912.7	1.4		**Lateral:** 895.3	**1.4**

Table 2: vBMD and subchondral bone thickness in individual OA and control samples. Values represent single measurements taken from the central portion of the corresponding half of the tibial plateau.

Figure 4.5 illustrates the differences in the appearance of typical pQCT scans from control and OA tibial plateaus respectively.

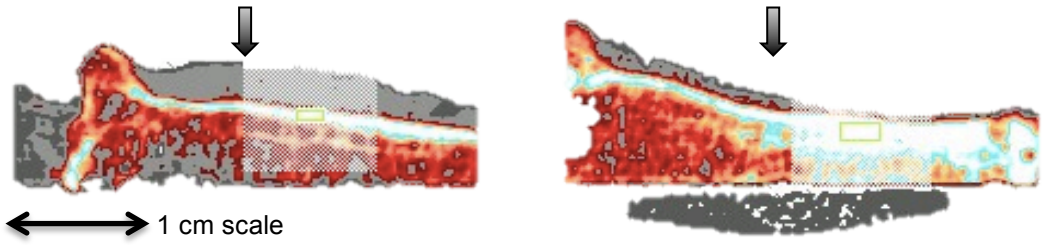

Figure 4.5: (a) left – typical appearance of pQCT from normal tibial plateau (sagittal section; posterior to anterior). Note the thickness of the normal articular cartilage (grey area) (b) right – typical appearance of pQCT from osteoarthritic tibial plateau (sagittal section; posterior to anterior). Note how thin the articular cartilage is and compare with (a) (grey area). Small yellow squares (arrows) demarcate area of interest wherefrom density measurement is obtained.

4.2 Raman Spectroscopy

4.2.1 Validation Results

In order to assess repeatability ten repeated spectra from the same location of a sample were recorded, pre-processed and plotted together (**Figure 4.6**). It can be seen that the variation is very small between each measurement and that the amide I band does not change shape. The average phosphate/amide I, carbonate/amide I and carbonate/phosphate ratios are given in **Table 3**, the standard deviation for each ratio is of the order of 1%.

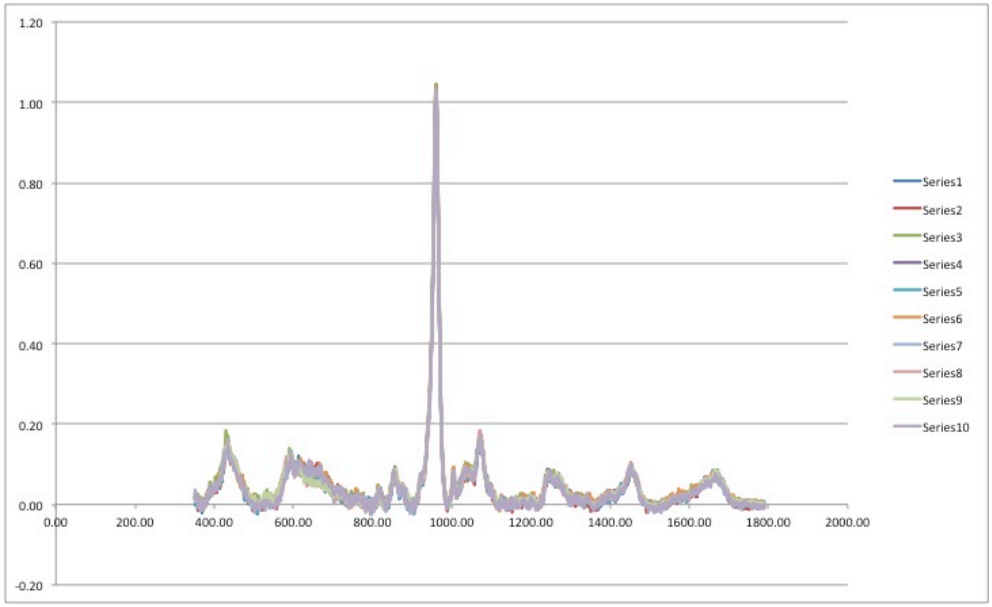

Figure 4.6: Ten spectra recorded one after another on the same piece of bone.

	REPEATABILITY
Phosphate/Amide I	13.2(0.2)
Carbonate/Amide I	2.1(0.1)
Carbonate/Phosphate	0.15(0.001)

Table 3: The mean ratios (standard deviation) for phosphate/amide I; carbonate/amide I; carbonate/phosphate are shown.

In order to assess reproducibility a spectrum was recorded from a specimen (cadaveric femur), the sample was then removed, and subsequently placed back on the stage, so that the laser illuminated roughly the same area, and another spectrum was recorded. Ten spectra were obtained this way. Since it was impossible to probe the exact same piece of bone material, the variation between these plots was larger that in repeatability measurements. However the spectra were again very similar and the amide I band did not change shape. Band ratios are given in **Table 4**.

	REPRODUCIBILITY
Phosphate/Amide I	12.9(0.3)
Carbonate/Amide I	2.2(0.2)
Carbonate/Phosphate	0.17(0.002)

Table 4: The mean ratios (standard deviation) for phosphate/amide I; carbonate/amide I; carbonate/phosphate are shown.

4.2.2 Raw Spectral Signatures

The Raman spectra from each cohort were averaged and compared (**Figures 4.7 to 4.14**). Ten independent spectra were acquired per core, therefore 20 spectra per tibial plateau (total 400 spectra). By eye there are few differences between the OA and non-OA, however, subtle differences are difficult to identify by observing only the average spectra from each data set. To improve discrimination multivariate analysis was required to quantify the subtle differences across the spectrum as a whole. The main biological peaks of interest are shown in the following figures and include phosphate (960 cm^{-1}), Amide I ($\approx$1660 cm^{-1}), Amide III ($\approx$1275 cm^{-1}) and carbonate (1070 cm^{-1}).

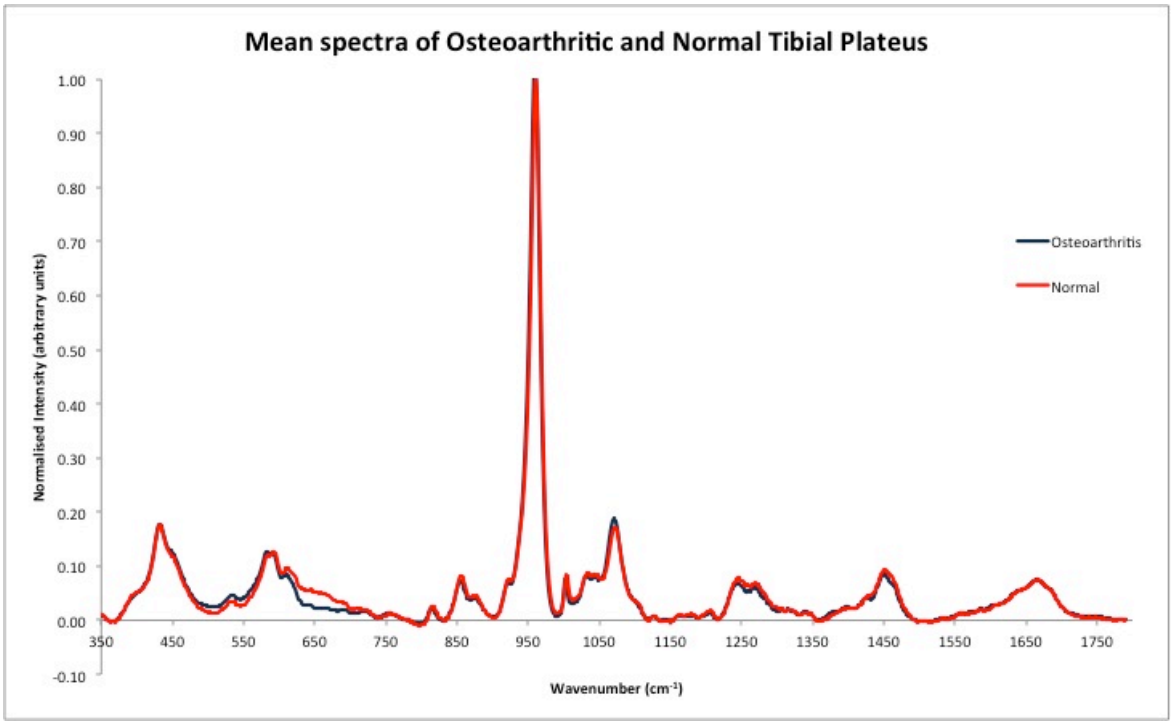

Figure 4.7: Mean Spectra (20 spectra per tibial plateau) for osteoarthritic compared to control/normal (fresh and cadaveric) tibial plateaus. Small differences can be identified by naked eye at the carbonate and amide peaks. The Raman intensity (a.u.) has been normalised to the phosphate peak at wavenumber 961cm^{-1}.

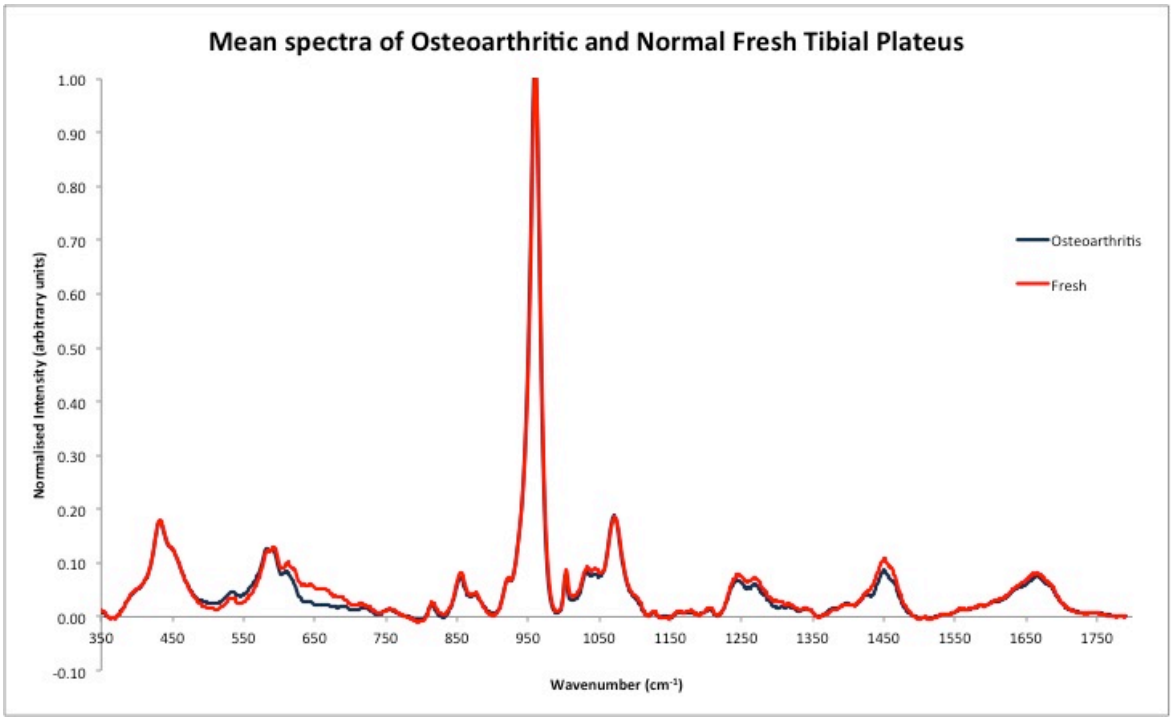

Figure 4.8: Mean Spectra (20 spectra per tibial plateau) for osteoarthritic compared to fresh control (normal) tibial plateaus. Differences predominantly seen at amide peaks. The Raman intensity (dimensionless) has been normalised to the phosphate peak at wavenumber 961cm^{-1}.

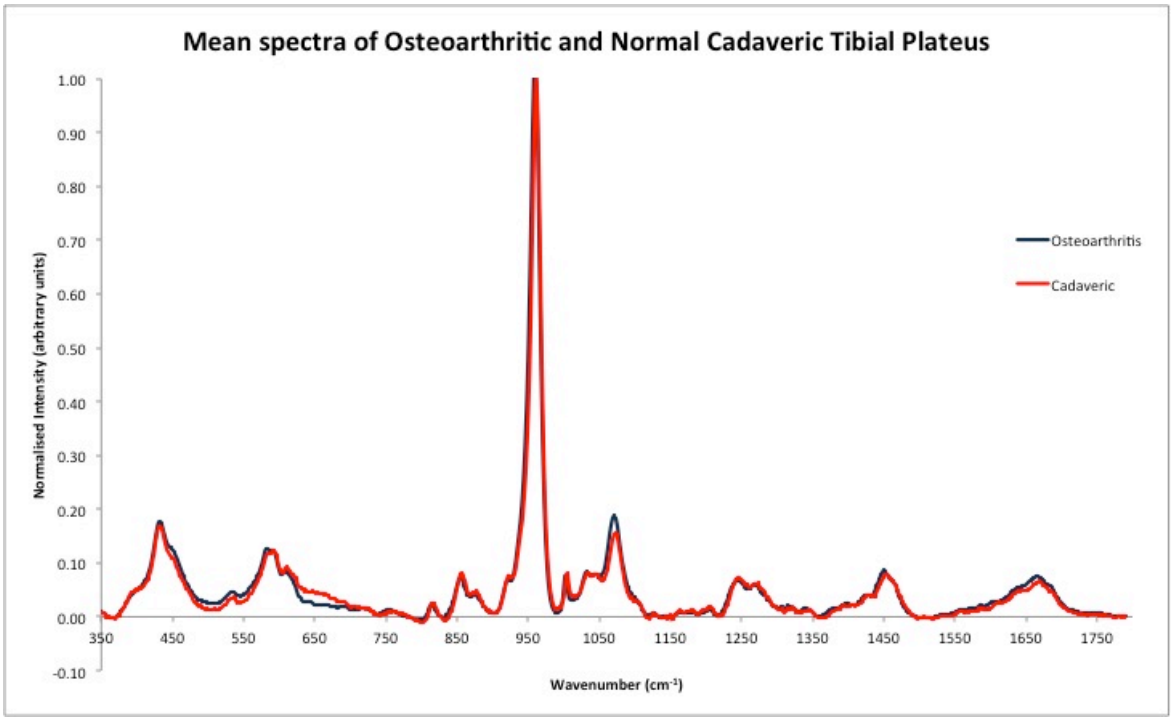

Figure 4.9: Mean Spectra (20 spectra per tibial plateau) for osteoarthritic compared to cadaveric control (normal) tibial plateaus. Main difference, for the biological peaks of interest, is seen by naked eye at carbonate peak. The Raman intensity (dimensionless) has been normalised to the phosphate peak at wavenumber 961.36cm^{-1}.

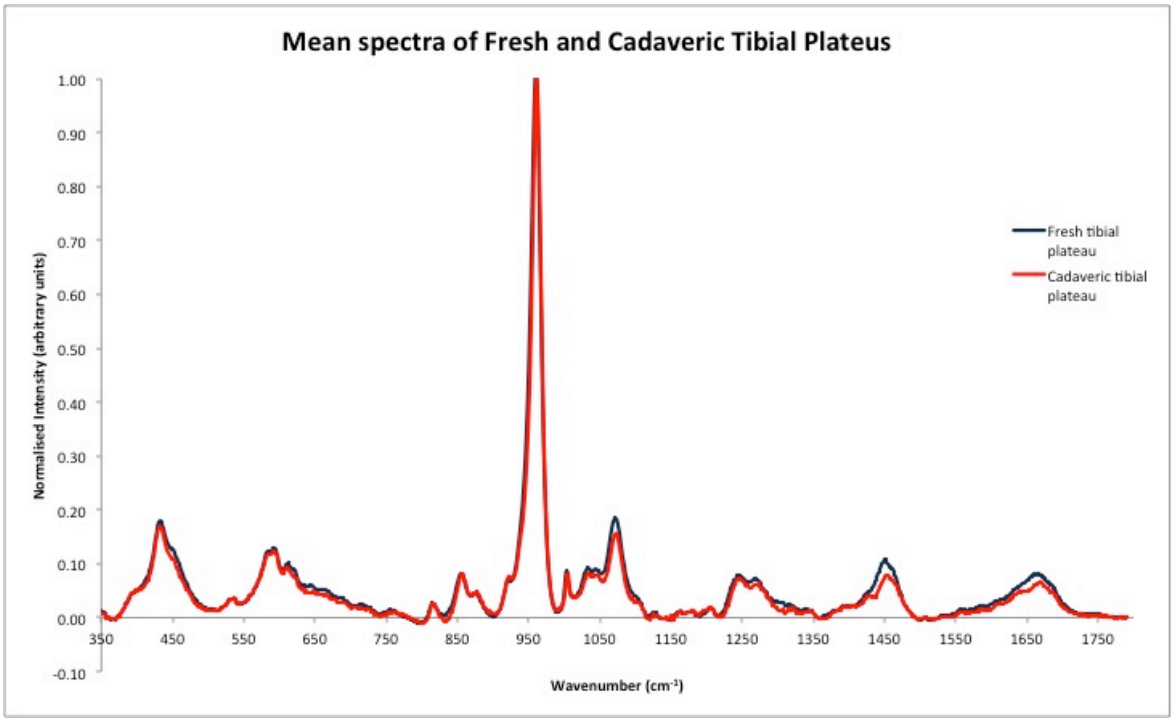

Figure 4.10: Mean Spectra (20 spectra per tibial plateau) for fresh control (normal) compared to cadaveric control (normal) tibial plateaus. Differences observed in carbonate, amide I and amide III peaks. The Raman intensity (dimensionless) has been normalised to the phosphate peak at wavenumber 961.36cm^{-1}.

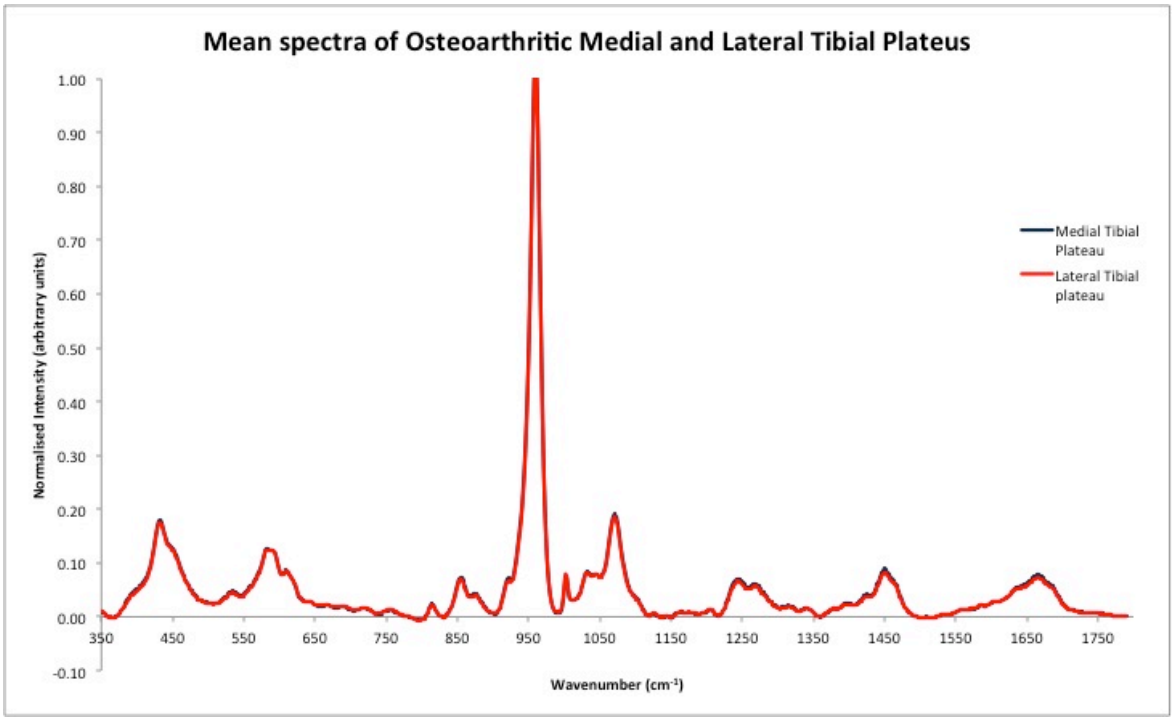

Figure 4.11: Mean Spectra (10 spectra per tibial plateau compartment) for osteoarthritic medial compared to osteoarthritic lateral tibial plateaus. No detectable difference by naked eye. The Raman intensity (dimensionless) has been normalised to the phosphate peak at wavenumber 961.36cm^{-1}.

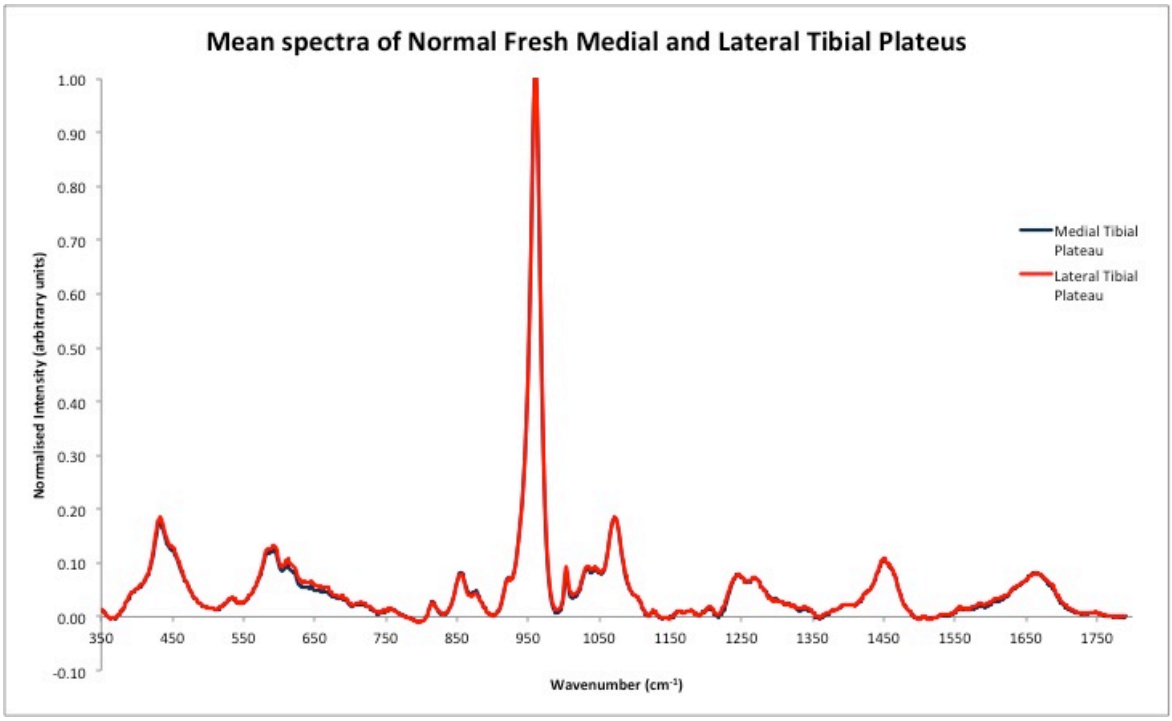

Figure 4.12: Mean Spectra (10 spectra per tibial plateau compartment) for control (fresh) medial compared to control (fresh) lateral tibial plateaus. No detectable difference by naked eye. The Raman intensity (dimensionless) has been normalised to the phosphate peak at wavenumber 961.36cm^{-1}.

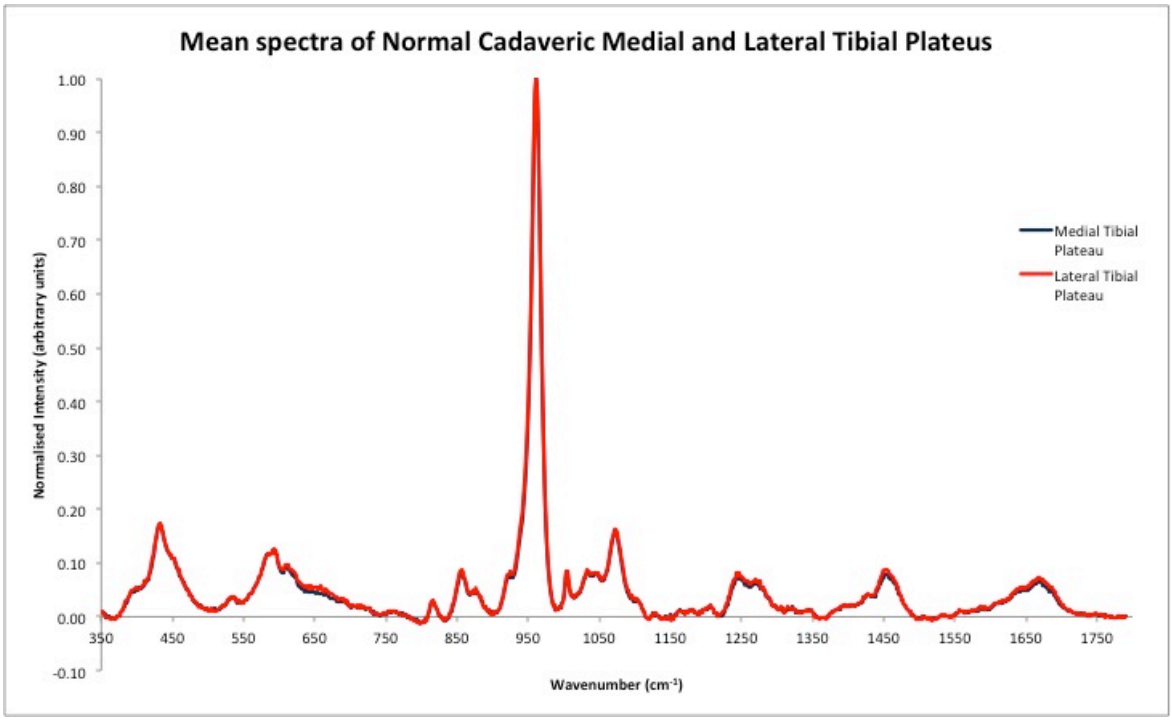

Figure 4.13: Mean Spectra (10 spectra per tibial plateau compartment) for control (cadaveric) medial compared to control (cadaveric) lateral tibial plateaus. No detectable difference by naked eye. The Raman intensity (dimensionless) has been normalised to the phosphate peak at wavenumber 961.36cm^{-1}.

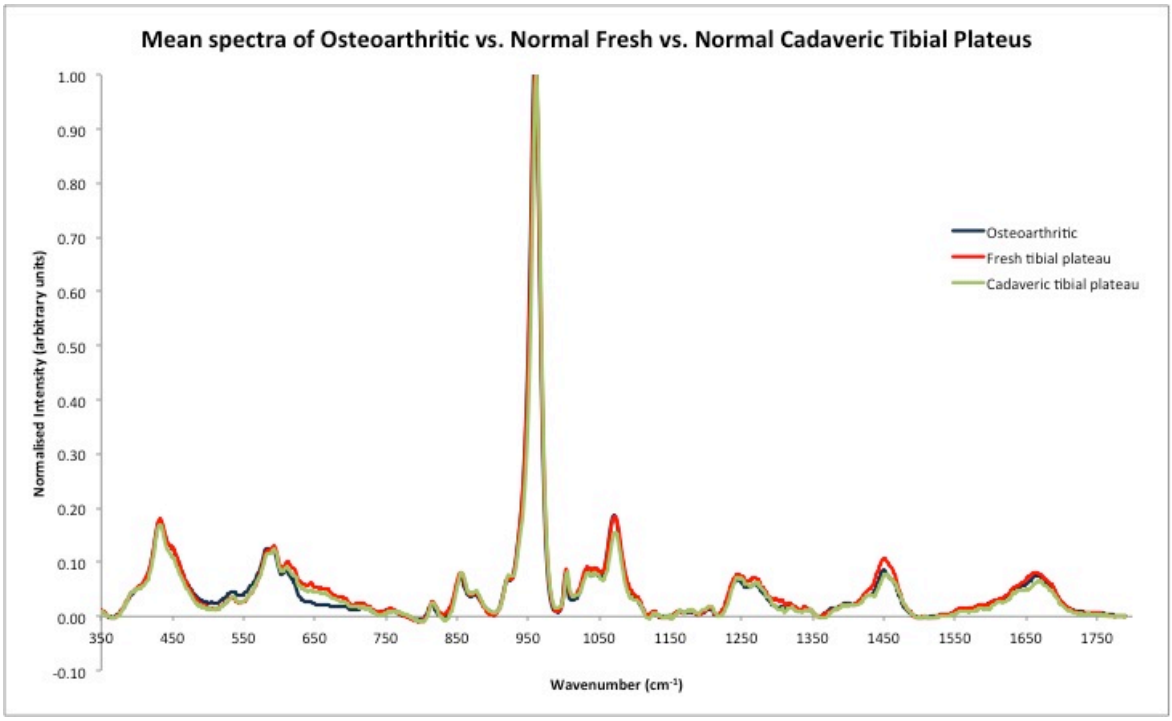

Figure 4.14: Mean Spectra (20 spectra per tibial plateau) for osteoarthritic compared to fresh control and cadaveric control tibial plateaus. Predominant difference, for the biological peaks of interest, is observed in relation to amide I peak. The Raman intensity (dimensionless) has been normalised to the phosphate peak at wavenumber 961.36cm^{-1}.

4.2.3 Mineral Volume Ratios determined by the Phosphate to Amide I Peak Magnitude Ratio (level of mineralisation) – Univariate Analysis

There was no statistically significant difference between OA lateral and OA medial tibial plateaus (**p=0.08**). Moreover, there was no difference when comparing control medial to control lateral. **Figures 4.15** to **4.16** summarise the comparisons in terms of the degree of mineralisation for the various specimen combinations. **Table 5** summarises the statistical significance values for the various comparisons.

Comparison	Phos:amide
OA (l+m) vs. N (l+m)	0.04
OA l vs. N l	0.005
OA m vs. N m	0.04
OA l vs. OA m	0.08
N l vs. N m	0.281

Table 5: Statistical significance values for phosphate: amide I ratio comparisons. OA=osteoarthritic; N=normal (fresh and cadaveric together); l=lateral; m=medial

When comparing lateral tibial plateaus and medial tibial plateaus separately between osteoarthritic samples and control (fresh and cadaveric combined) there was a statistically significant difference (p=0.005 and p=0.04 respectively) with higher phosphate to amide I ratio in the OA groups; a comparison of the entire tibial plateau (medial and lateral compartments together) between OA and controls (cadaveric and fresh together) also demonstrated statistical significance (p=0.04) with a lower ratio in the control group.

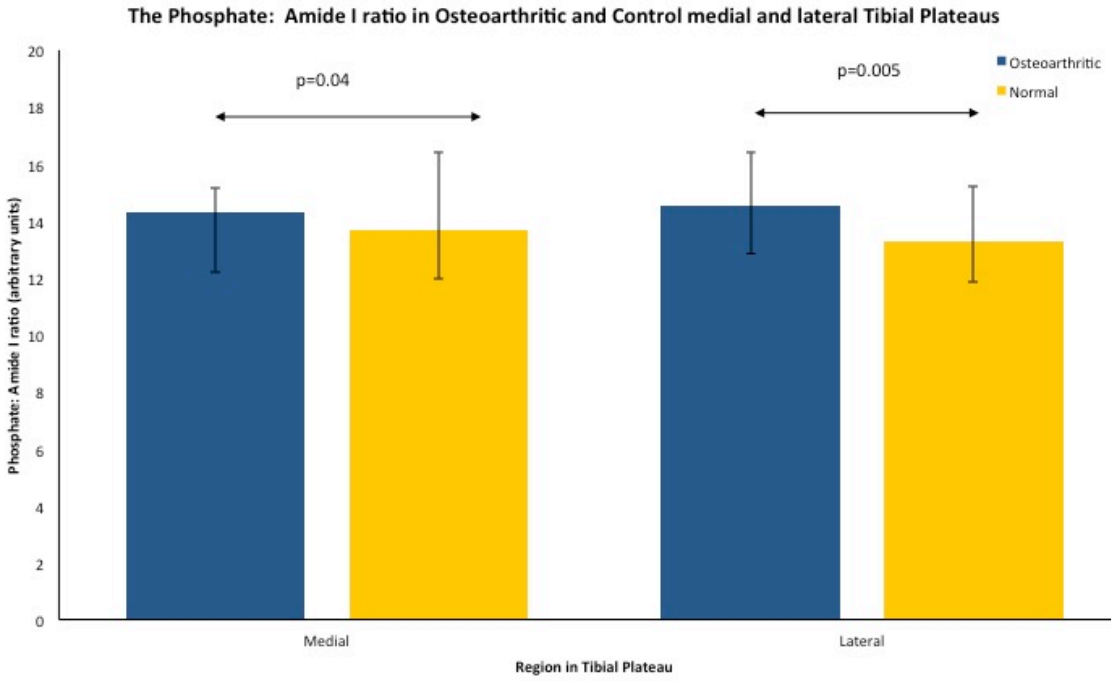

Figure 4.15: Phosphate: Amide I ratio in osteoarthritic and control (normal; fresh and cadaveric) medial and lateral tibial plateaus. The Phosphate: Amide I ratio indicates the degree of mineralisation. Median ratios (dimensionless) are presented to an accuracy of two decimal places. Error bars represent the inter-quartile range. p values are given only for the statistically significant comparisons.

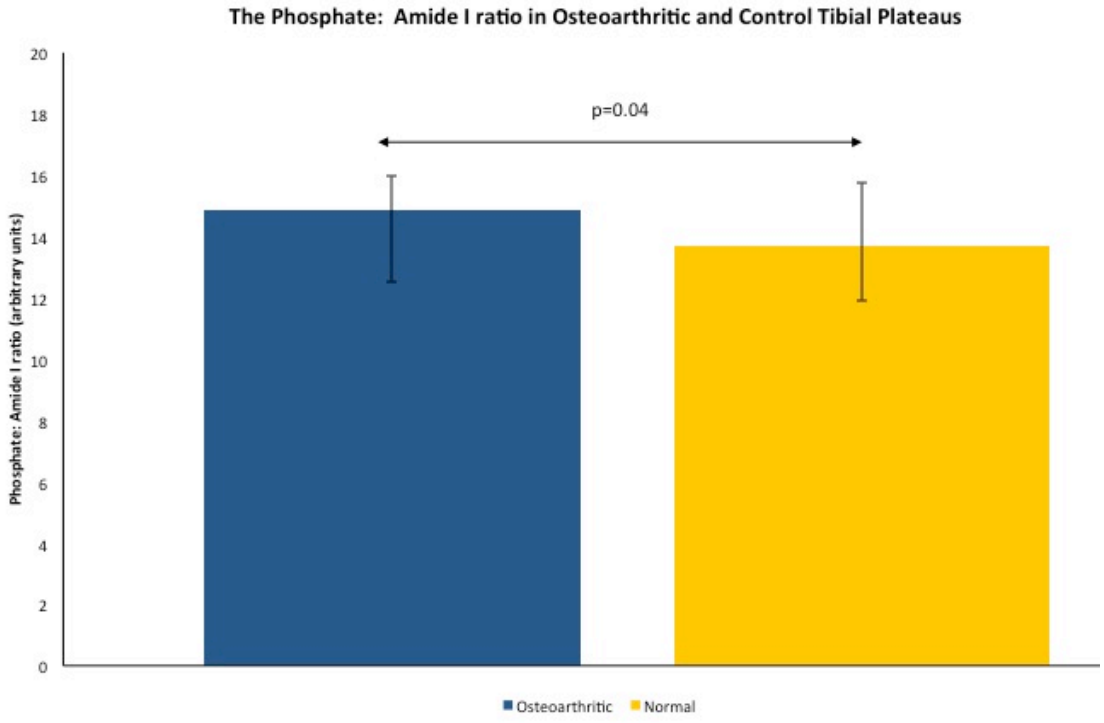

Figure 4.16: Phosphate: Amide I ratio in osteoarthritic and normal (fresh and cadaveric) tibial plateaus irrespective of laterality. The Phosphate: Amide I ratio indicates the degree of mineralisation. Median ratios (dimensionless) are presented to an accuracy of two decimal places. Error bars represent the inter-quartile range. Significant difference observed between OA and normal tibial plateaus irrespective of compartment.

4.2.4 Carbonate to Phosphate Ratio as Indicative of Carbonate Substitution – Univariate Analysis

There was no statistically significant difference in the extent of carbonate substitution in the lattice structure of the apatite crystals, between OA lateral and OA medial tibial plateaus (**p=0.6**) and control (fresh and cadaveric) medial and control lateral tibial plateaus (**p=0.3**). **Table 6** summarises the statistical significance values for the various comparisons.

Comparison	Carb:Phos
OA (l+m) vs. N (l+m)	p<0.001
OA l vs. N l	0.016
OA m vs. N m	p<0.001
OA l vs. OA m	0.6
N l vs. N m	0.3

Table 6: Statistical Significance Values for carbonate to phosphate ratio comparisons. OA=osteoarthritic; N=normal (fresh and cadaveric together); l=lateral; m=medial

Carbonate substitution was lower in osteoarthritic samples compared to controls (fresh and cadaveric combined) with a statistically significant difference between the lateral tibial plateaus (**p=0.016**), medial tibial plateaus (**p<0.001**) and entire tibial plateaus (irrespective of laterality) (**p<0.001**).

Figures 4.17 and **4.18** summarise the comparisons in terms of the extent of carbonate substitution in the lattice structure of the apatite crystals.

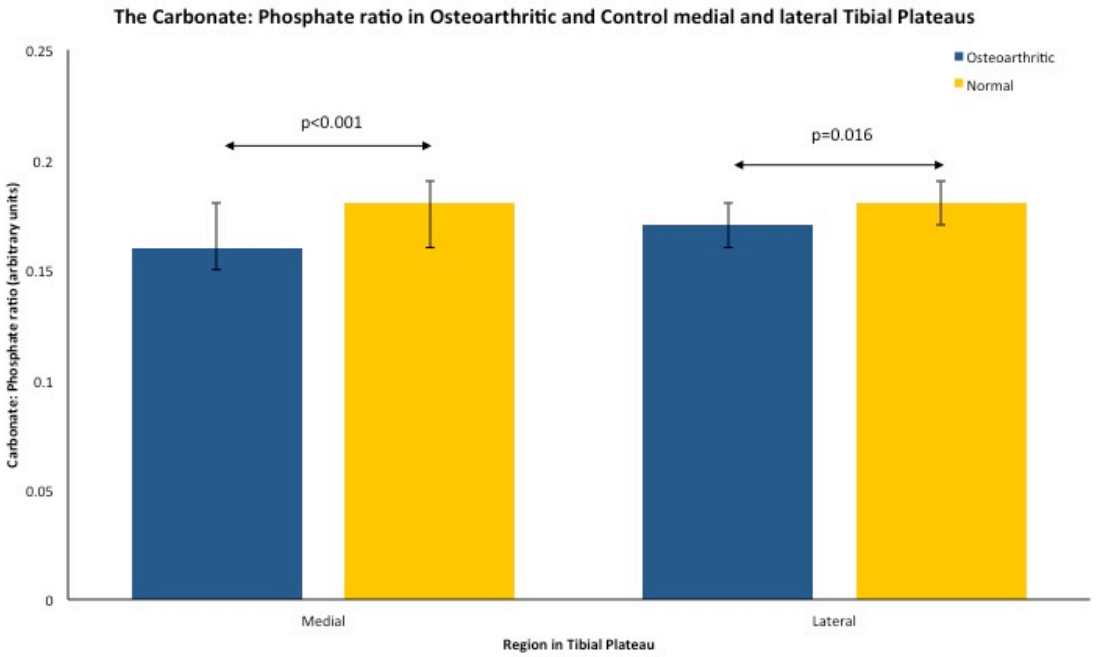

Figure 4.17: Carbonate to Phosphate ratio in osteoarthritic and control (fresh and cadaveric) medial and lateral tibial plateaus. The Carbonate to Phosphate ratio indicates the extent of carbonate substitution in the apatite crystals. Median ratios (dimensionless) are presented to an accuracy of two decimal places. Error bars represent the inter-quartile range. OA specimens exhibit lower carbonate substitution hence greater degree of mineralisation.

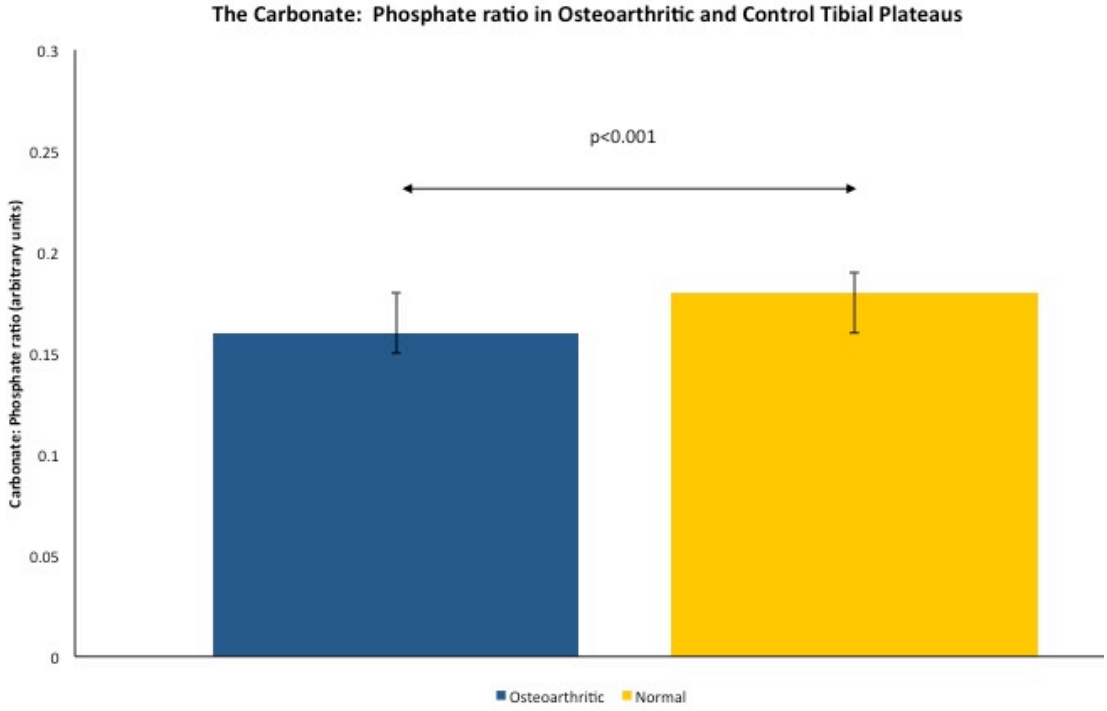

Figure 4.18: Carbonate to Phosphate ratio in osteoarthritic and control (fresh and cadaveric) tibial plateaus irrespective of compartment. The Carbonate to Phosphate ratio indicates the extent of carbonate substitution in the apatite crystals. Median ratios (dimensionless) are presented to an accuracy of two decimal places. Error bars represent the inter-quartile range. Controls exhibit greater carbonate substitution compared to OA.

4.2.5 Carbonate to Amide I Ratio as Indicator of Remodelling – Univariate Analysis

Carbonate to amide I ratio has been suggested as a potential marker for bone remodelling (McCreadie et al. 2006). There was no significant difference between OA lateral and OA medial tibial plateaus and control (fresh and cadaveric) medial to control lateral. **Table 7** summarises the statistical significance values for the various comparisons.

Comparison	Carb:Amid
OA (l+m) vs. N (l+m)	p<0.001
OA l vs. N l	p<0.001
OA m vs. N m	0.009
OA l vs. OA m	0.058
N l vs. N m	0.927

Table 7: Statistical Significance Values for carbonate to amide I ratio comparisons. OA=osteoarthritic; N=normal (fresh and cadaveric together); l=lateral; m=medial

When comparing osteoarthritic samples to controls (fresh and cadaveric combined), carbonate to amide I ratio was higher in the OA cohort with a statistically significant difference between the lateral tibial plateaus (**p<0.001**), medial tibial plateaus (**p=0.009**) and entire tibial plateaus (irrespective of laterality) (**p<0.001**).

Figures 4.19 and **4.20** summarise the comparisons in terms of the degree of bone remodelling for the various specimen combinations.

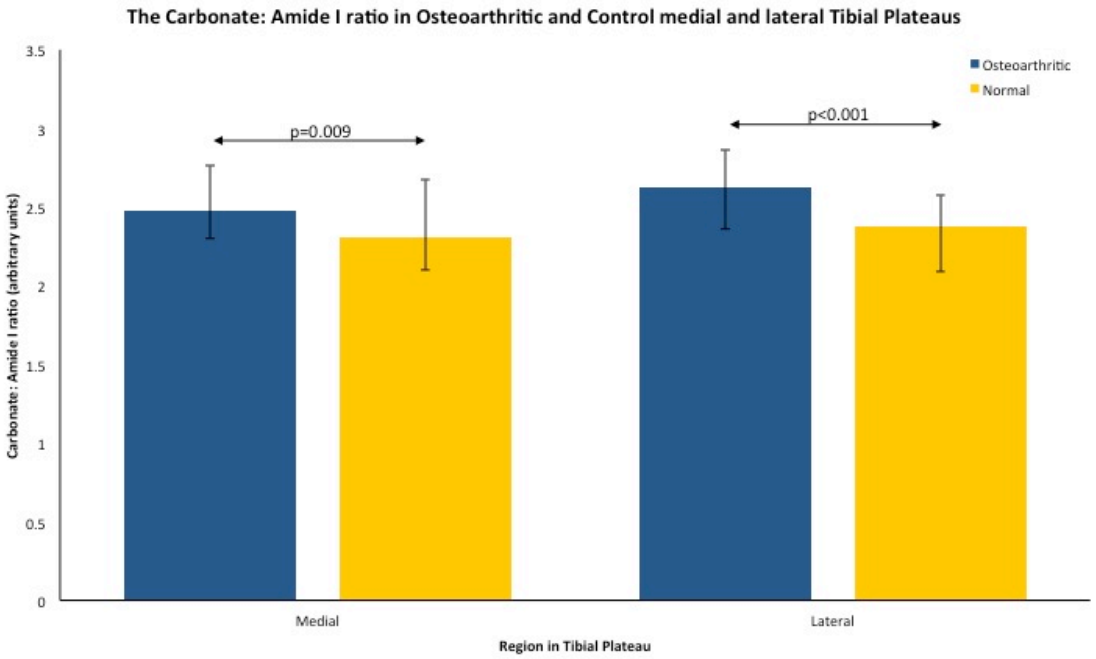

Figure 4.19: Carbonate to Amide I ratio (may indicate bone remodelling) in osteoarthritic and control (fresh and cadaveric) medial and lateral tibial plateaus. Median ratios (dimensionless) are presented to an accuracy of two decimal places. Error bars represent the inter-quartile range. OA demonstrates higher carbonate to amide I ratio compared to controls (fresh and cadaveric combined).

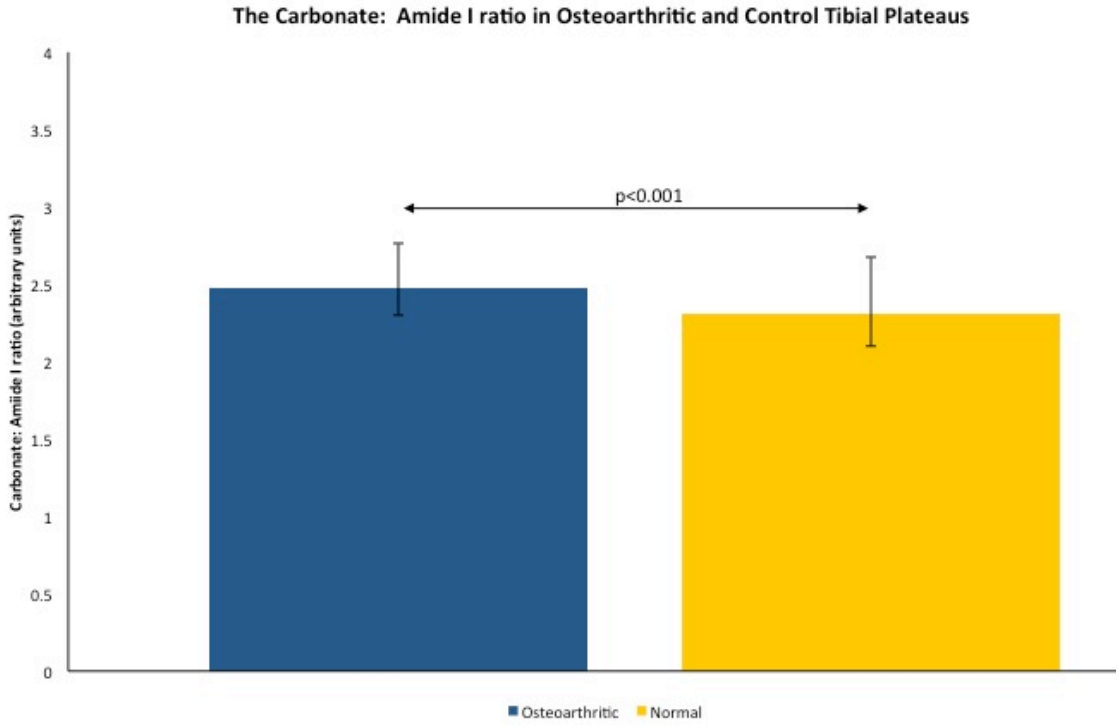

Figure 4.20: Carbonate to Amide I ratio (may indicate bone remodelling) in osteoarthritic and control (fresh and cadaveric) tibial plateaus irrespective of laterality. Median ratios (dimensionless) are presented to an accuracy of two decimal places. Error bars represent the inter-quartile range. Carbonate to amide I ratio is higher in the OA cohort compared to the control cohort irrespective of compartment.

4.2.6 Amide I to Amide III Ratio as Indicator of Collagen's Secondary Structure – Univariate Analysis

The collagen quality parameter used in Raman spectroscopy investigates the collagen's secondary structure and the degree of distortion of collagen crosslinks in bone matrix. This parameter could be obtained by studying the amide I or amide III envelopes(Morris 2011). Overall amide I or amide III envelope analysis should be used with caution. In our study we used amide I to amide III ratio as a potential indicator of collagen secondary structure.

There was no significant difference between OA lateral and OA medial tibial plateaus and between control (fresh and cadaveric) medial and control lateral. **Table 8** summarises the statistical significance values for the various comparisons.

Comparison	Amide I:Amide III
OA (l+m) vs. N (l+m)	p<0.001
OA l vs. N l	p<0.001
OA m vs. N m	p<0.001
OA l vs. OA m	0.097
N l vs. N m	0.706

Table 8: Statistical Significance Values for amide I to amide III ratio comparisons. OA=osteoarthritic; N=normal (fresh and cadaveric together); l=lateral; m=medial

When comparing osteoarthritic samples to controls (fresh and cadaveric combined) there was a statistically significant difference, with higher ratio in OA samples, between the lateral tibial plateaus (**p<0.001**), medial tibial plateaus (**p<0.001**) and entire tibial plateaus (irrespective of laterality) (**p<0.001**).

Figures 4.21 to **4.22** summarise the comparisons in terms of amide I to amide III ratios for the various sample combinations.

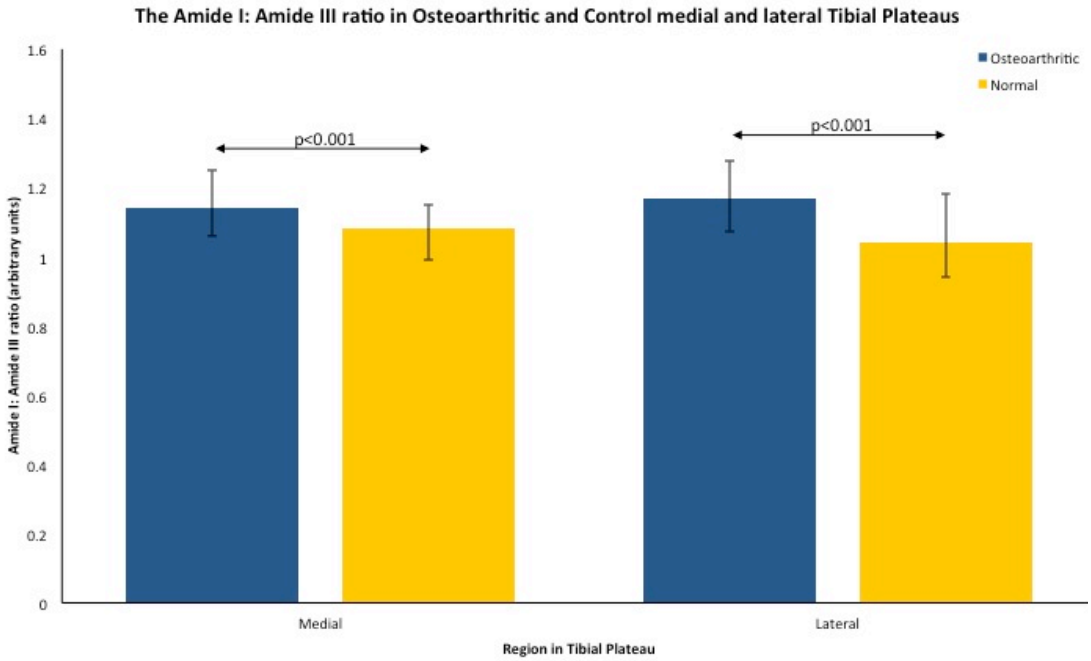

Figure 4.21: Amide I: Amide III ratio (potential marker of collagen I secondary structure) in osteoarthritic and control (fresh and cadaveric) medial and lateral tibial plateaus. Median ratios (dimensionless) are presented to an accuracy of two decimal places. Error bars represent the inter-quartile range. Higher ratio seen in OA when compared to controls (combined fresh and cadaveric).

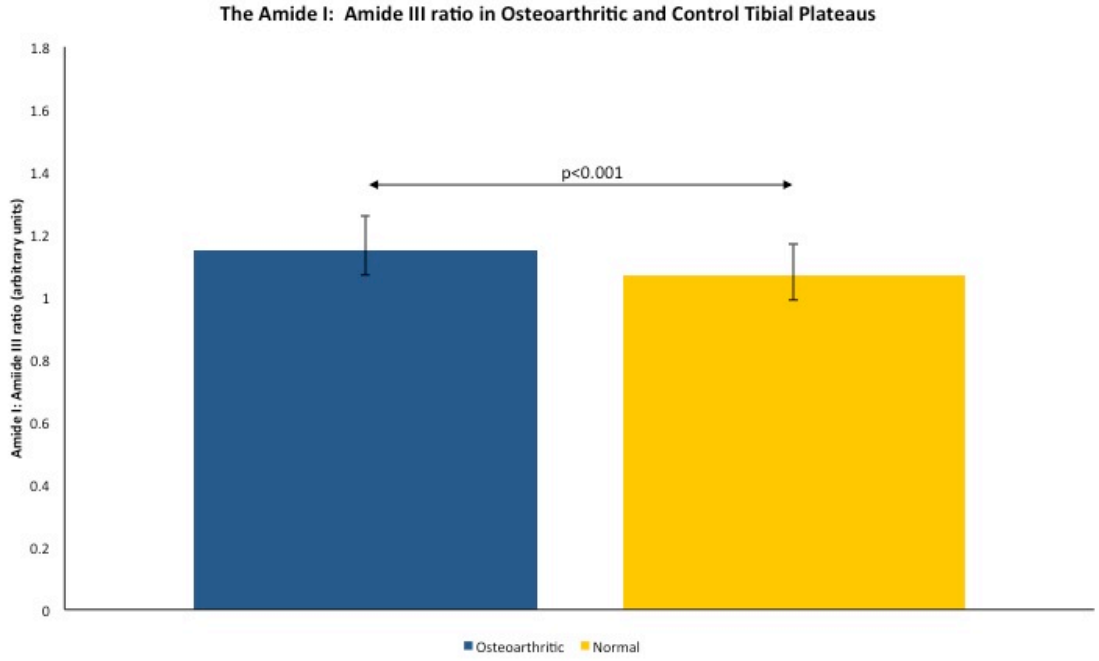

Figure 4.22: Amide I: Amide III ratio (potential marker of collagen I secondary structure) in osteoarthritic and control (fresh and cadaveric) tibial plateaus irrespective of laterality. Median ratios (dimensionless) are presented to an accuracy of two decimal places. Error bars represent the inter-quartile range. Higher ratio in the OA cohort compared to the control cohort.

4.3 Multivariate Analysis

Multivariate analysis was performed on the Raman spectral data sets, with the aim of identifying, in an unsupervised (PCA) and supervised (LDA) manner, the similarities and differences inherent in the spectra.

4.3.1 PCA

Figures 4.23 and **4.24** depict the PCA-scores plot obtained from the multivariate analysis, looking at all specimens. A 3D scatter plot of the scores (a scores plot) allows for differences to be identified because the distance between the scores (points; each point represents a spectrum) on the plot directly relate to the biochemical similarities, i.e., the closer together two scores are in the plot the more similar they are biochemically and vice versa. **Figure 4.23** demonstrates separation between OA group and control group (fresh and cadaveric combined). **Figure 4.24** shows the spread of the data and reveals that the OA, control (normal) fresh and control (normal) cadaveric separate into three distinct groups with little overlap. The reasons for the spectral differences resolved from PCA are identified from interpretation of **Figure 4.25** (corresponding to PCA of **Figure 4.23**) and **Figure 4.26** (corresponding to PCA of **Figure 4.24**). The first axis (PC1) shows that the phosphate band (954 and 966 cm^{-1}) is different between all the cohorts. In **Figure 4.25**, PC2 reveals that the second largest difference between the groups is Amide I (1668 and 1685 cm^{-1}) and phosphate

shoulder (941 cm^{-1}); PC3 shows that the next difference is related to broad differences across ~1597 cm^{-1}.

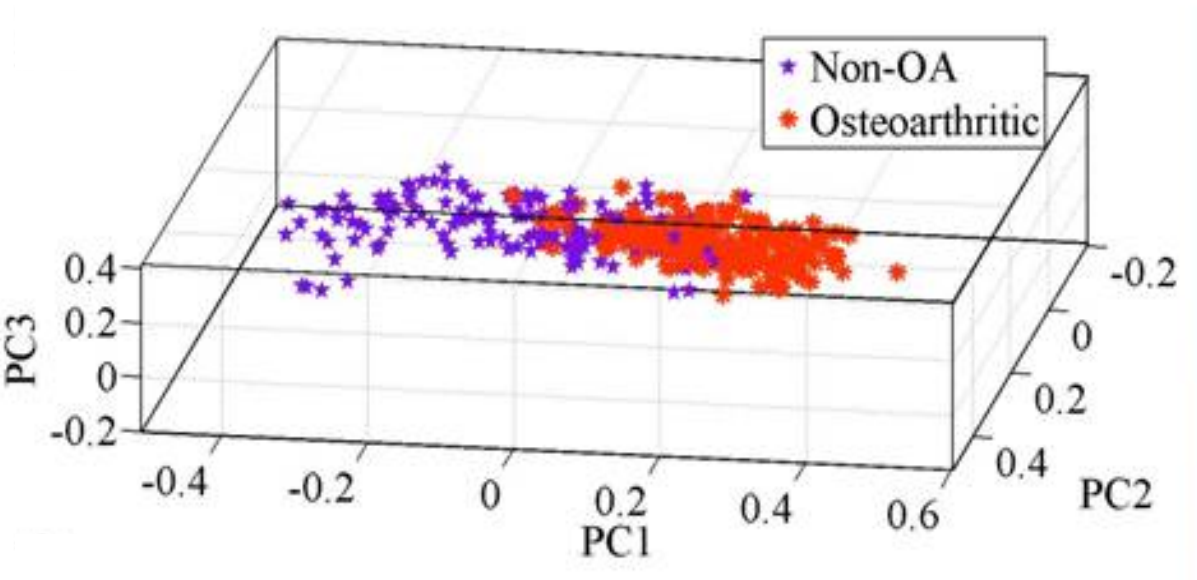

Figure 4.23: 3D –PCA score plot of non –OA vs. OA.

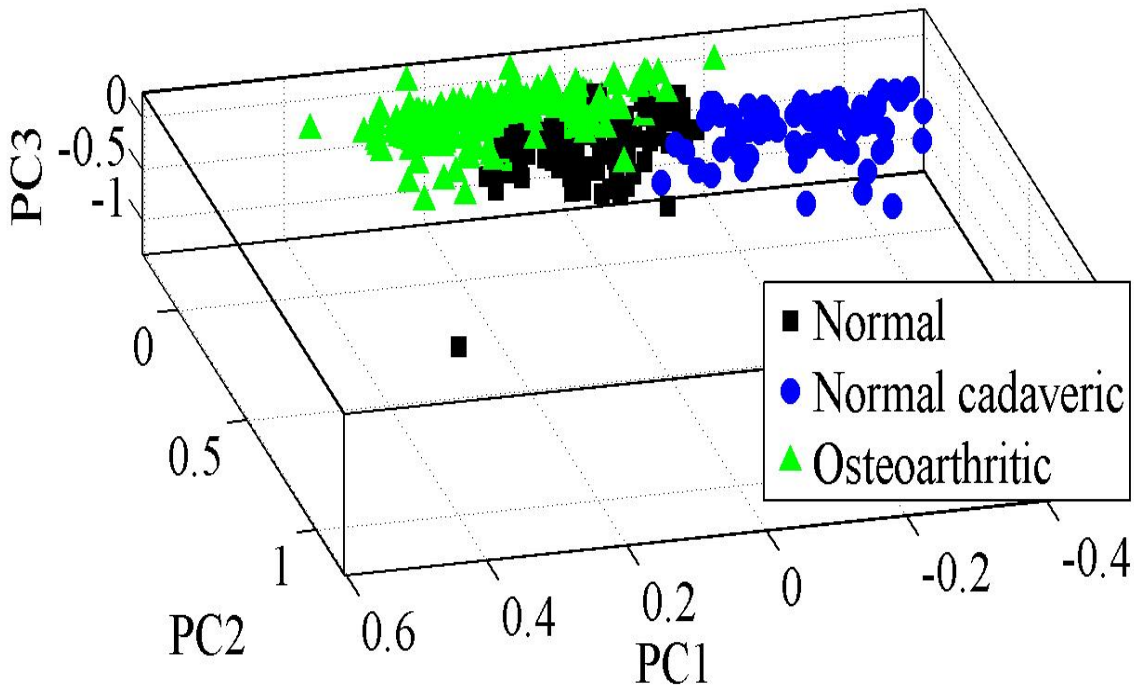

Figure 4.24: 3D - PCA score plot for control (normal – fresh), control (normal – cadaveric) and osteoarthritic specimens.

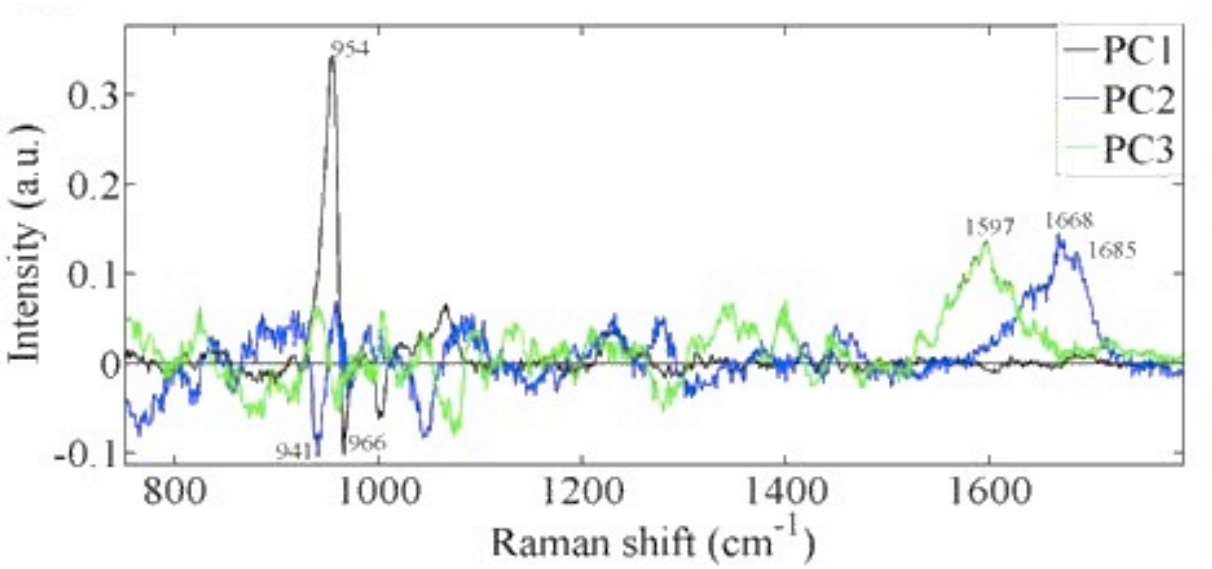

Figure 4.25: PCA loadings for control (fresh and cadaveric) vs. osteoarthritic specimens.

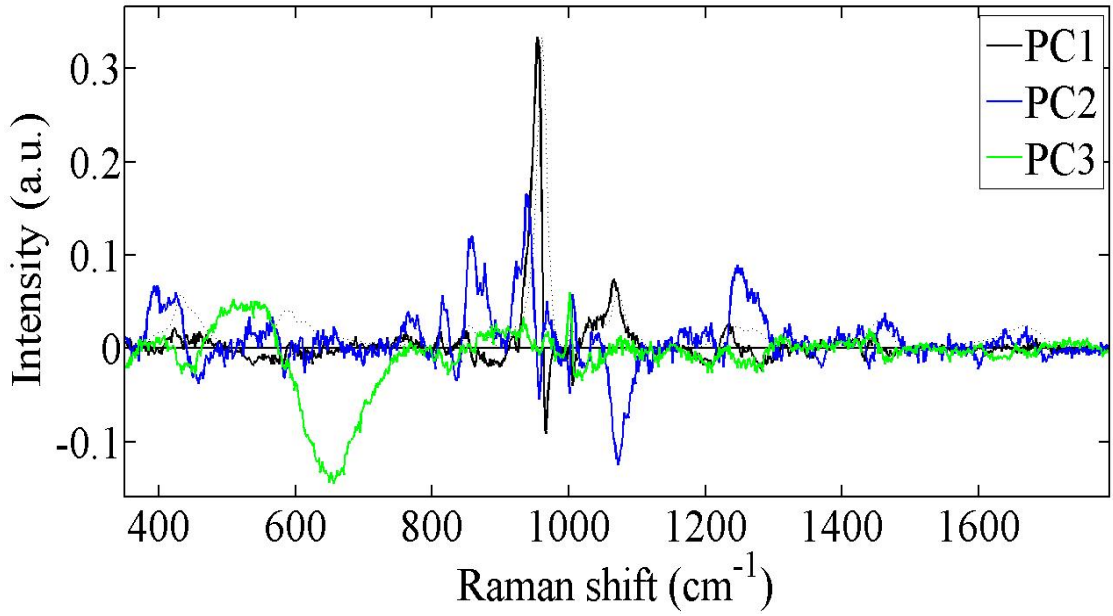

Figure 4.26: PCA loadings for control (fresh) vs. control (cadaveric) vs. OA.

Figure 4.27 depicts the PCA-score plot of PC1 *vs.* PC2 vs. PC3 obtained from the multivariate analysis, looking specifically at normal

fresh vs. normal cadaveric tibial plateaus. Despite some overlap, a separation among specimens can be observed along the PC1-axis. In **Figure 4.28** the PC-loading values are plotted, which represent the regions of the Raman spectra where the differences among cohorts are more evident. The main difference relates predominantly to the phosphate peak (954 and 966 cm^{-1}) and this is smaller compared to the one observed in **Figure 4.25**

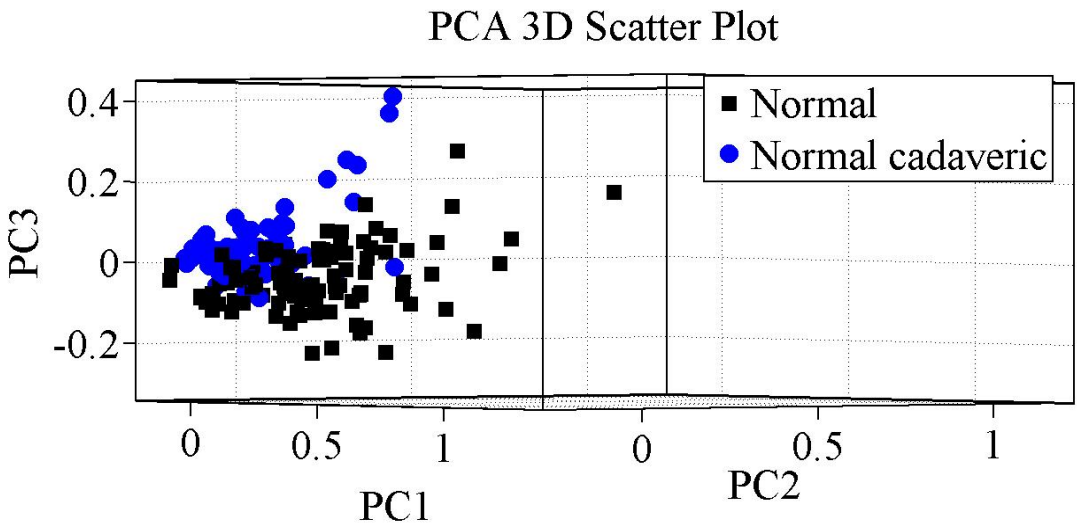

Figure 4.27: 3D - PCA score plot for normal fresh and normal cadaveric specimens.

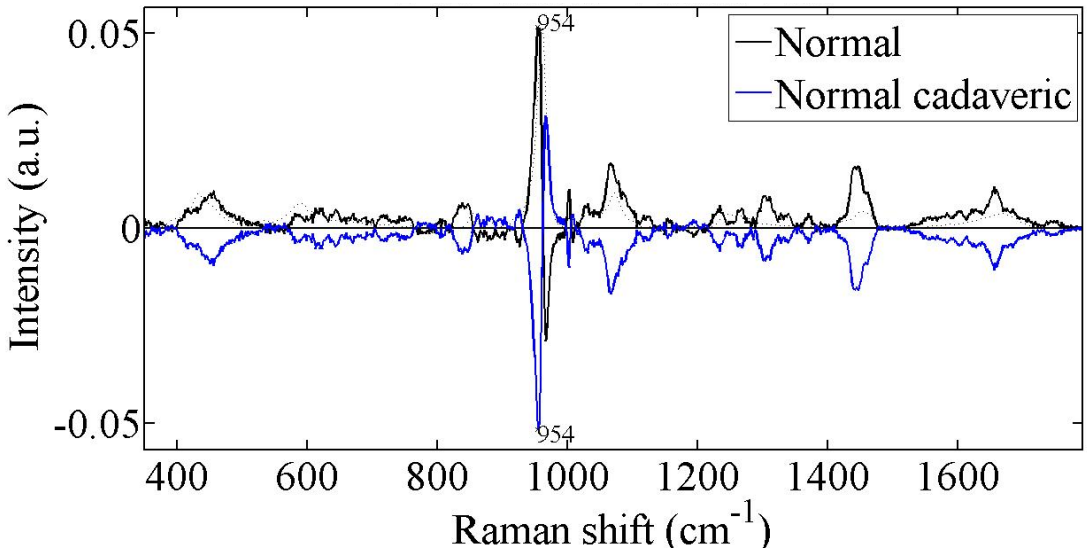

Figure 4.28: PCA loadings for normal fresh and normal cadaveric specimens. The main difference relates predominantly to the phosphate peak (954 and 966 cm^{-1}).

4.3.2 PCA – LDA

Figure 4.29 presents the PCA-LDA scores of all the specimens analysed. The formation of three clusters is observed, corresponding to normal fresh, normal cadaveric and osteoarthritic tibial plateaus. While the cluster of the normal cadaveric tibial plateaus is well separated, some overlapping between the normal fresh and the osteoarthritic tibial plateaus is observed. Furthermore, if you consider the fresh and cadaveric to be one cluster there is good separation from the OA cluster. **Figure 4.30** depicts the loadings plot for the PCA-LDA analysis and represents the regions of the Raman spectra where the differences among specimens can be identified. Interpretation of **Figure 4.30** shows that the main differences among the tibial plateaus analyzed are localized in the 900- 980 cm^{-1} region.

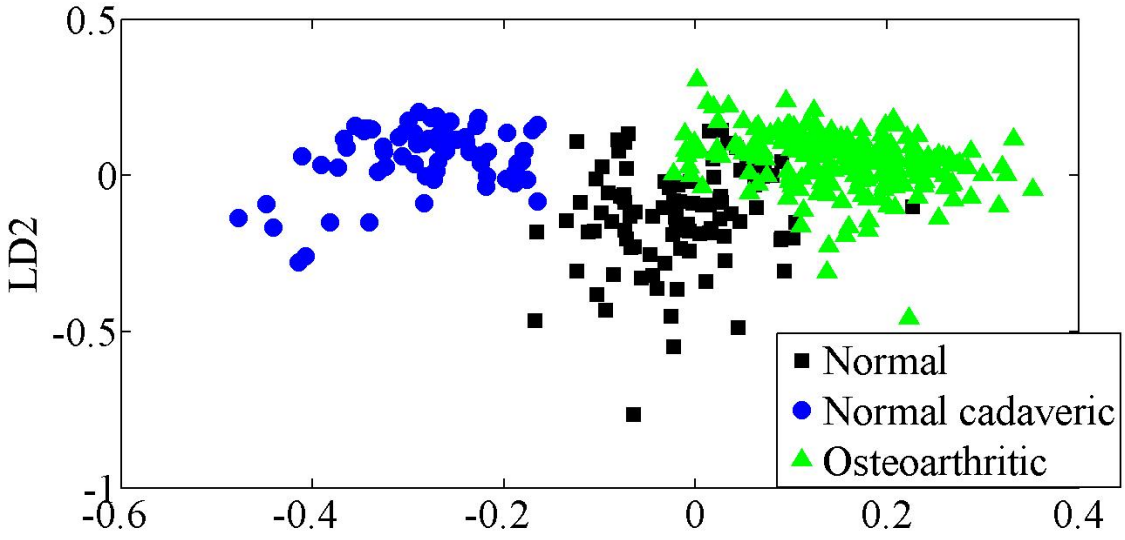

Figure 4.29: PCA-LDA scores plot for osteoarthritic, normal cadaveric and normal fresh specimens. The formation of three clusters is observed. While the cluster of the normal cadaveric tibial plateaus is well separated, some overlapping between the normal fresh and the osteoarthritic tibial plateaus is observed.

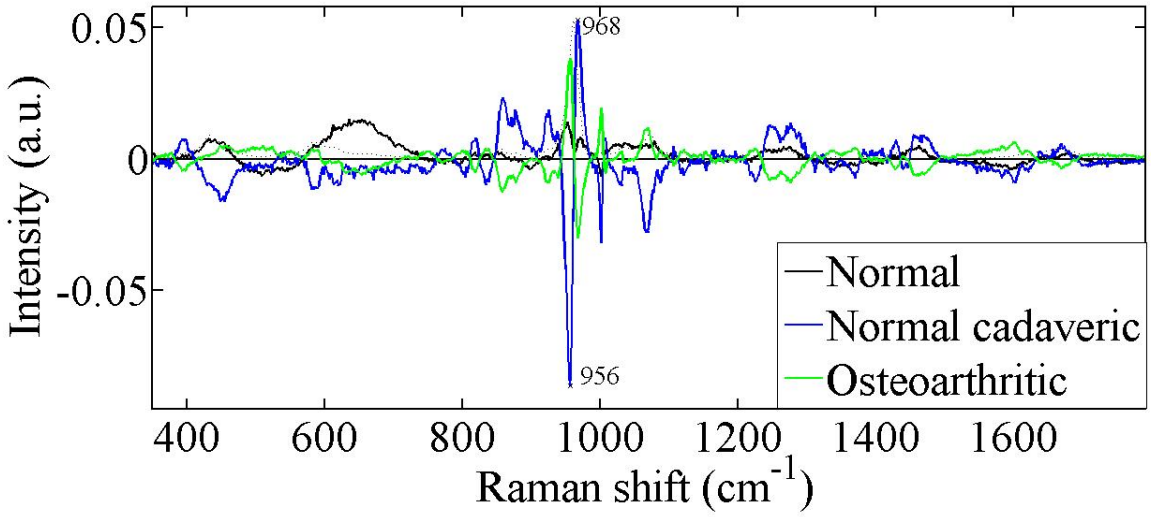

Figure 4.30: PCA-LDA loadings plot for osteoarthritic, normal fresh and normal cadaveric specimens. The main differences among the tibial plateaus analyzed are localized in the 900- 980 cm^{-1} region.

Figure 4.31 is a PCA-LDA scores plot for medial and lateral compartments of non-OA and OA specimens. It emphasises the differences between non-OA and OA while confirming that there are no differences between compartments within each cohort, as previously seen with the univariate analysis.

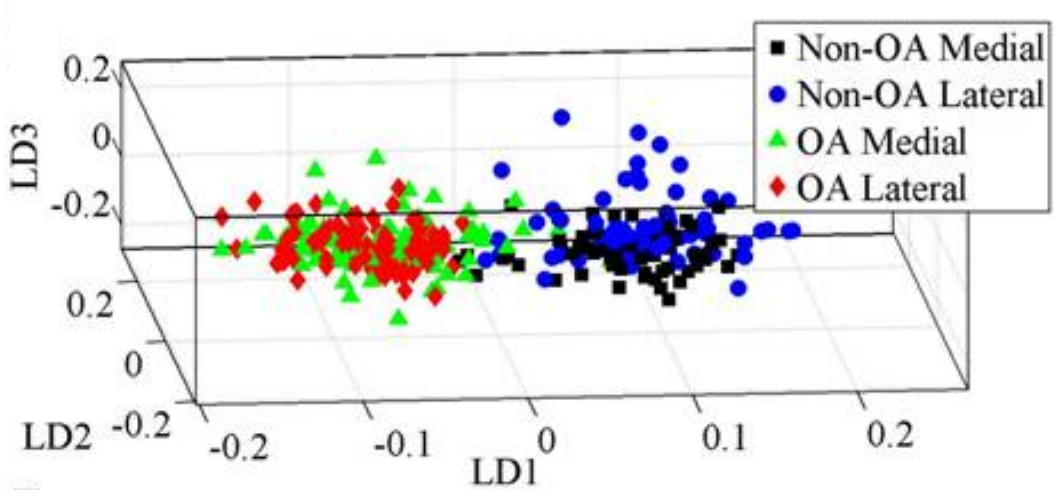

Figure 4.31: PCA-LDA scores plot for non-OA medial *vs.* non-OA lateral *vs.* OA medial *vs.* OA lateral.

4.4 Collagen Alpha Chain Analysis

Figures 4.32 to **4.37** display the individual bands obtained from electrophoresis. The difference in the α1-chain to α2-chain ratios between OA and normal samples was found to be statistically significant (**p = 0.021**) with the OA samples showing higher α1-chain to α2-chain ratio. The OA samples had a median α1-chain to α2-chain ratio of 3.05:1 (IQR 3.95:1 – 2.4:1), which is above the normal ratio level for heterotrimeric collagen of two alpha 1 to one alpha 2 (standard 2.476:1). The maximum OA ratio analysed was 11.5:1 and the minimum 1.8:1. On the other hand, the pooled normal samples had a median α1-chain to α2-chain ratio of 1.75:1 (IQR 3.17:1 – 1.42:1). The maximum normal ratio analysed was 5.9:1 and the minimum 1.4:1.

Comparisons of the α1-chain to α2-chain ratios between the medial and lateral sides of the OA tibial plateaus found no significant difference. However both medial and lateral mean ratios were above the normal level for heterotrimeric collagen of 2:1 (standard 2.476:1) at 4.087:1 and 3.573:1 respectively ($p>0.05$).

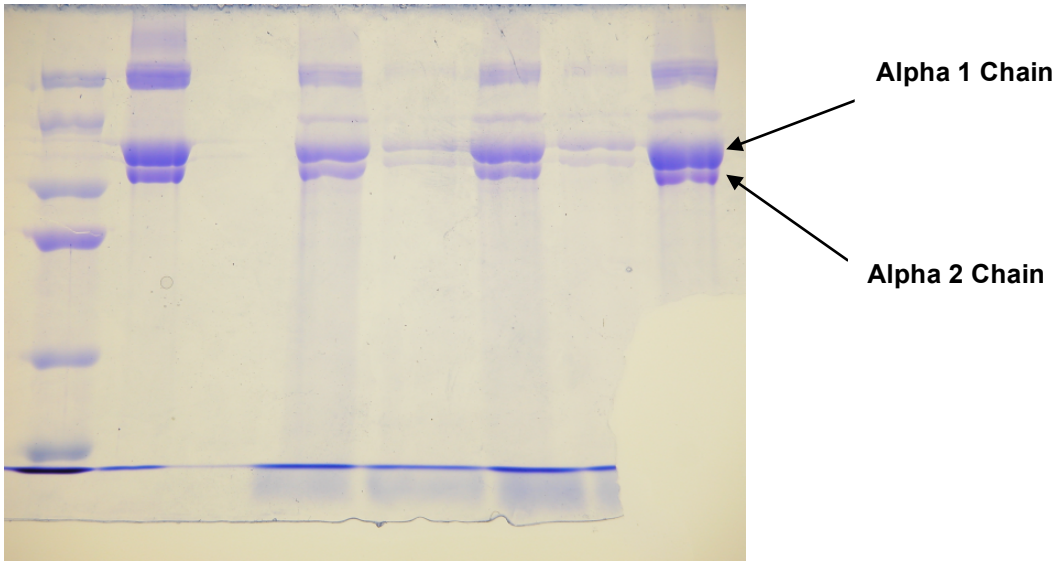

Figure 4.32: SDS PAGE bands. From left to right: molecular weight standard, collagen standard, OA specimen 1 medial (3.3:1), OA specimen 1 lateral (3.8:1), OA specimen 2 medial (3.7:1), OA specimen 2 lateral (3.1:1), OA specimen 3 medial (9.4:1).

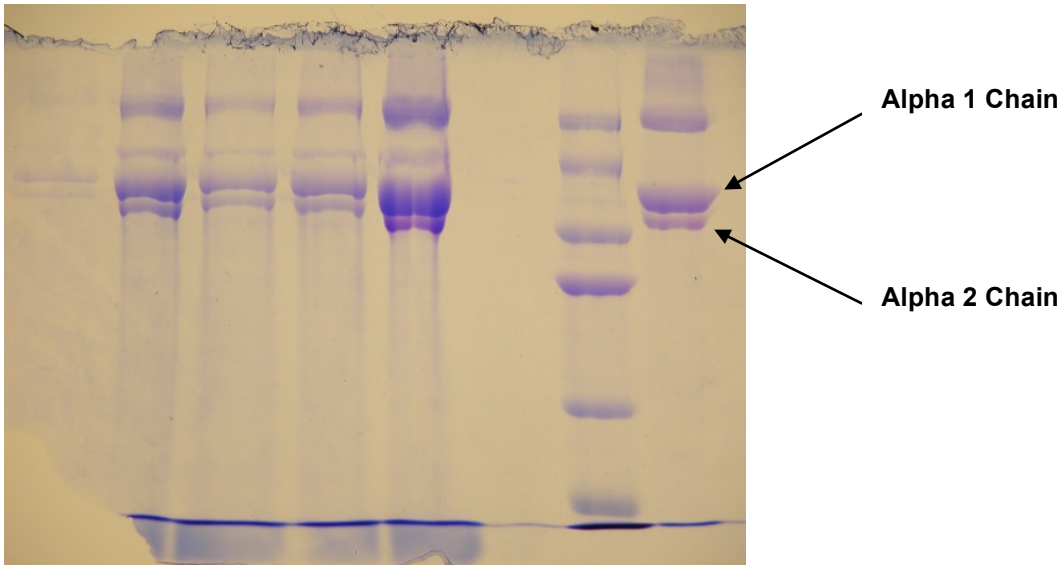

Figure 4.33: SDS PAGE bands. From left to right, OA specimen 5 lateral (2.6:1), OA specimen 5 medial (4.8:1), OA specimen 4 lateral (2.2:1), OA specimen 4 medial (3.3:1), OA specimen 3 lateral (11.5:1), molecular weight standard, collagen standard.

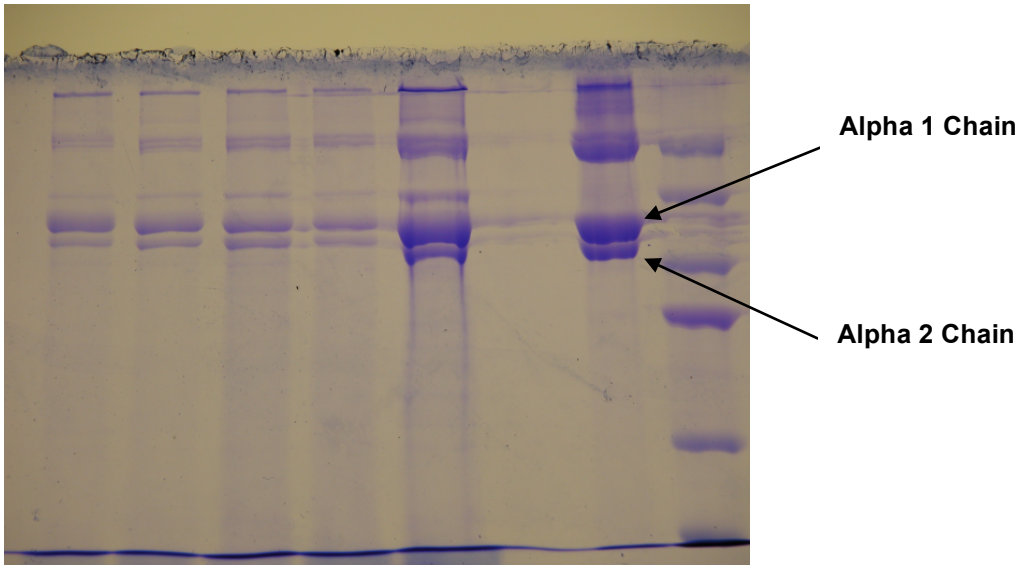

Figure 4.34: SDS PAGE bands. From left to right: OA specimen 8 medial (4.0:1), OA specimen 7 lateral (3.0:1), OA specimen 7 medial (1.8:1), OA specimen 6 lateral (2.4:1), OA specimen 6 medial (6.4:1) collagen standard, molecular weight standard.

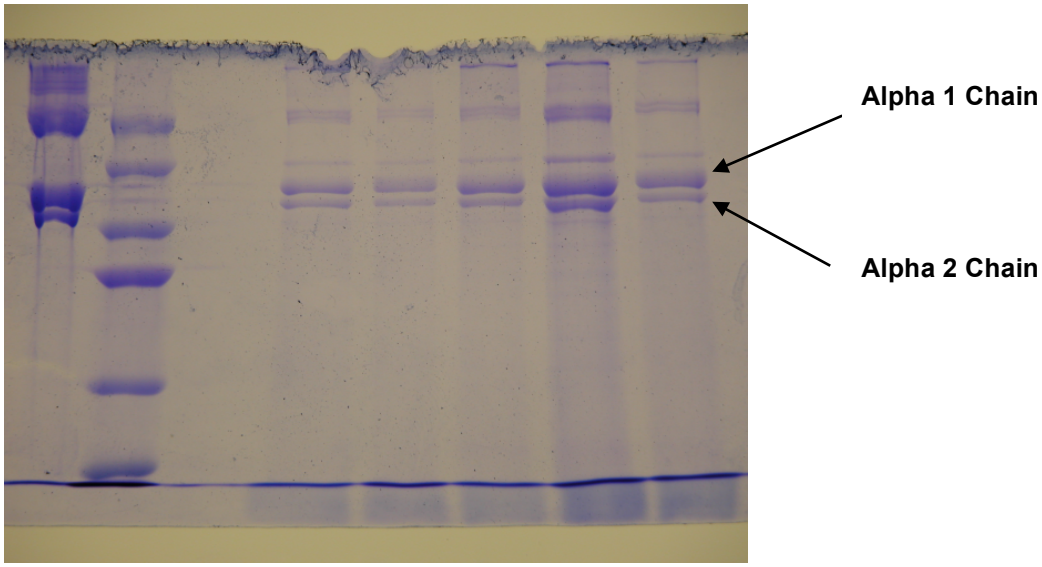

Figure 4.35: SDS PAGE bands. From left to right: collagen standard, molecular weight standard, OA specimen 8 lateral (1.9:1), OA specimen 9 medial (2.4:1), OA specimen 9 lateral (2.7:1), OA specimen 10 medial (1.8:1), OA specimen 10 lateral (2.6:1).

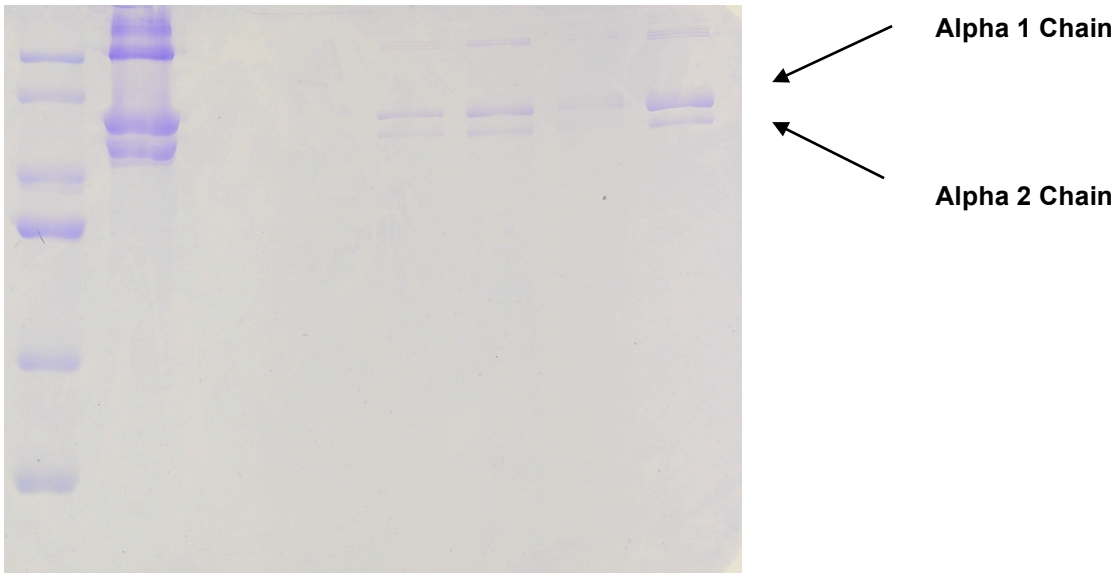

Figure 4.36: SDS PAGE bands. From left to right: molecular weight standard, collagen standard, normal fresh specimen 1 medial, normal fresh specimen 1 lateral (1.4:1), normal fresh specimen 2 medial (1.8:1), normal fresh specimen 2 lateral (2.2:1), normal fresh specimen 3 lateral (3.5:1).

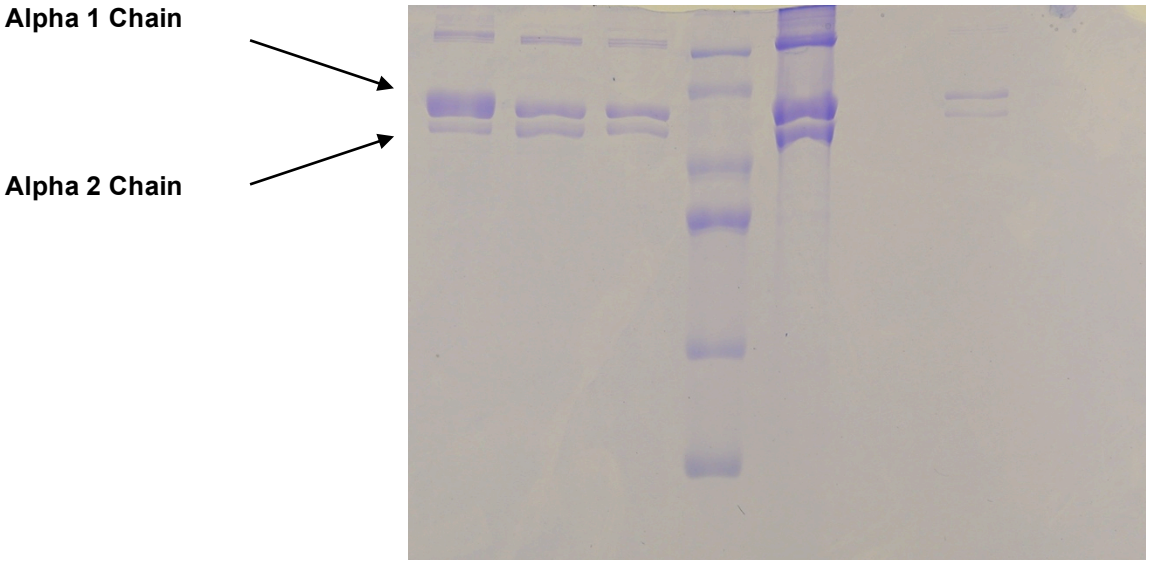

Figure 4.37: SDS PAGE bands. From left to right: normal fresh specimen 4 lateral (5.9:1), normal fresh specimen 5 medial (1.5:1), normal fresh specimen 5 lateral (1.7:1), molecular weight standard, collagen standard, normal fresh specimen 1 lateral repeat (1.4:1).

Figure 4.38 summarises the comparison between the OA and normal tibial plateaus.

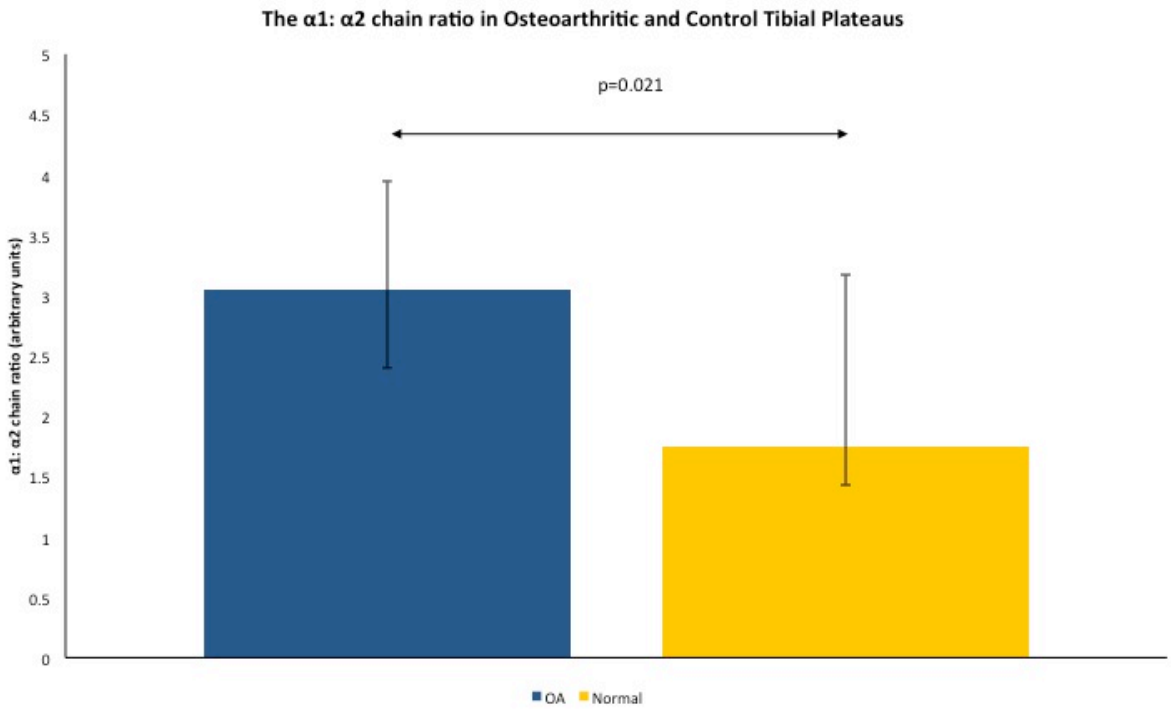

Figure 4.38: a1: a2 chain ratio between the osteoarthritic and normal (fresh and cadaveric) tibial plateaus. Median ratios (dimensionless) are presented to an accuracy of two decimal places. Error bars represent the inter-quartile range.

CHAPTER 5 – DISCUSSION

5.0 Overview

Osteoarthritis (OA) is a chronic, slowly progressive, degenerative joint disease, leading to pain and disability. It is characterized by the degeneration of the articular cartilage and changes in the structure of calcified cartilage and underlying subchondral bone. There are several proposed pathogenetic mechanisms, attempting to explain the initiation of OA. One of them considers that bone may be the primary organ triggering OA, with stiffening of the subchondral bone leading to a decrease in shock absorbency and eventually cartilage damage due to overloading.

Spectroscopic methods including infrared and Raman spectroscopy have been used to study cartilage and bone tissue. They give information about the structure and composition of studied material at the molecular level, data are obtained in a noninvasive manner or minimally invasive method and there is no limit to the size, allowing a study of a large area of a sample. Properties of Raman spectroscopy (micro-Raman spectroscopy) that make it more attractive than infrared spectroscopy for direct analysis of biological tissues include high spatial resolution (0.5 to 1 μm) and limited spectral interference from water.

Better understanding of the role of subchondral bone in OA disease progression, through examination of compositional and structural changes, is very important in analyzing the etiology of arthritis,

developing novel therapeutic targets and monitoring treatment in patients. Raman spectroscopy may help by providing insight into the chemistry of the subchondral bone and hence its contribution to the pathogenesis of OA. This technology has the potential to be used as a minimally invasive method to interrogate the inorganic and organic phases of bone matrix in patients. The goal of this work was to examine the chemical composition and molecular structure of extracellular matrix in subchondral bone from human osteoarthritic tibias using Raman spectroscopy.

5.1 Volumetric Bone Mineral Density

5.1.1 Appraisal of pQCT Method

The software used was designed to take into account the porosity and structure of the trabeculae and so even if the quality was the same between two regions, the vBMD would be different if one region was more porous than the other. Moreover, the apparent vBMD was measured. This is the wet weight divided by the total volume occupied by bone and pore spaces. A more accurate and valid measure of vBMD is ash density which is ash weight divided by the actual volume of bone tissue(Johanson 1993). The reproducibility of the regions of interest is also a limitation. Neither the area nor the dimensions of the rectangular regions of interest are specified in the software. Instead, each region of interest had to be re-drawn and matched in terms of size as closely as possible to the previous one. Slight differences in the size of the

rectangles are inevitable and this will have led to subtle differences in the vBMD. Moreover, the tibial plateaus were of different sizes, some larger than others. Consequently, there was no way of ensuring that regions of interest corresponded to an exact location in each specimen.

5.1.2 Discussion of pQCT Results

The vBMD is greater in OA specimens than controls; the subchondral sclerosis, which occurs in OA, could account for this increase. The thickness of the subchondral bone, as expected, is equal across both compartments of the control samples but thicker in the medial compartment of the OA specimens ($p < 0.001$) compared to the lateral compartment.

The variation of bone mineral density in OA subchondral bone was considerable. This was illustrated by a relatively large IQR error bar. It would be worthwhile to investigate whether this variation is linked to the severity of OA. The results are consistent with the hypothesis and what has been established from previous studies. Dequeker and Johnell found an increase in bone density in OA and suggested that this is protective against hip fractures(Dequeker 1993). Jones et al. also found an increase in bone density in OA but were sceptical as to whether this provides a protective function(Jones 1995). Moreover, the differences in vBMD between individual OA specimens were found to be insignificant ($p=0.745$) despite their differences in age, sex, severity of OA, loading history and so on. All of these factors potentially could have been major confounders but the statistical insignificance allows us to assume their impact on the data is limited.

Despite the results confirming previous reports, one puzzling question still remains: vBMD measures the mineral density and hypomineralisation has been found in OA, why then is the vBMD higher in OA than controls? This apparent contradiction can be explained by distinguishing apparent structural density from material density. The apparent density of bone is the wet weight divided by the total volume occupied by bone and pore spaces(Johanson 1993). The total volume increases in OA by 10-15% because of a thickening of the trabeculae(Li 1997). This is identified radiologically as subchondral sclerosis. However, Grynpas et al. measured the mineral content in bone through density fractionation, and found the OA subchondral bone (both the cortical plate and the underlying cancellous bone) to contain less mineral content than age-matched controls(Grynpas 1991). Therefore, from a material perspective, and contrary to intuition, bone mineral density actually decreases in OA. Why does it decrease? Burr suggests subchondral bone is constantly remodeling (in a damage and repair cycle) with a high turnover rate, preventing the matrix from fully mineralising(Burr 2004). Consequently, subchondral bone has a lower material density in OA so the total volume, which is related to the apparent density, must increase significantly to provide a sufficient degree of stiffness. Therefore, the apparent structural density has to increase in OA, to compensate for the reduced material density, in order to provide an acceptable level of structural stiffness(Burr 2004).

5.1.3 Summary for Volumetric Bone Mineral Density and Wider Implications

1. The thickness of the subchondral bone is equal across both compartments of the non-OA samples but thicker in the medial compartment of the OA specimens.
2. The subchondral bone in the medial compartment is statistically significantly denser than the lateral compartment. These measurements of the bone are taking into account the bone as a material and a structure.
3. The OA medial compartments are thicker and denser than the lateral and overall denser than the non-OA specimens.

5.2 Raman Spectroscopy

5.2.1 Appraisal of Raman Spectroscopy Method

Ratio parameters were used instead of absolute band intensities because the latter is affected by the efficiency of Raman scattering, the refractive index and the surface roughness (Morris 2011). The ratios were calculated by using the actual heights of the bands. A better technique would have been to use the areas of the bands. The area of a particular band could be obtained by fitting a Gaussian curve(Morris 2011). The ratio parameters used were carefully considered before selection. There is evidence to suggest that the carbonate to amide I ratio may reflect bone remodelling (McCreadie 2006) but more validation is required. The amide I band was also used to represent the matrix in the mineral to matrix ratio. According to Morris, an informal consensus is

forming around the use of proline and hydroxyproline bands as a more accurate measure of matrix content(Morris 2011; Karampas 2012). However, further validation is still required. Equally there is no consensus in the literature as to the best way of assessing collagen secondary structure. In this study we used the amide I to amide III ratio as a potential marker of collagen differences between cohorts, however this is not validated in the literature. The technique used to baseline correct the data has some flaws(Schulze 2005). There are newer and perhaps better ways to baseline correct the data so as to account for fluorescence. Zhang et al. have recently developed a novel algorithm that does not require user intervention(Zhang 2010).

Finally laser polarization and orientation of the specimen can potentially have an effect on the spectra acquired. In this work all specimens were orientated in a given way with no variations during measurements, however the absolute effect of different specimen orientations was not formally assessed.

5.2.2. Discussion of Spectroscopy Results

5.2.2.1 Mineral Volume Ratios Determined by the Phosphate to Amide I Peak Magnitude Ratio (level of mineralisation)

The phosphate to amide I ratio indicates the degree of mineralisation. The levels of mineralisation were not significantly greater in OA medial (macroscopically affected) compared to OA lateral (macroscopically normal) tibial plateaus but were significantly higher when the whole OA specimen was compared to the control tibial

plateaus (fresh and cadaveric together) as well as when comparison was between OA cohort and control fresh and OA and control cadaveric. These findings disagree with the hypothesis and contradict the literature suggesting that OA subchondral bone is in fact hypermineralised.

The majority of the literature suggests OA bone should be hypomineralised. Mansell and Bailey found lower levels of mineralisation in OA(Mansell 1998). Although the phosphate to amide I ratio has been used and validated in previous studies(Morris 2011), there may be other bands in the spectra that reflect the matrix content better than the amide I band. Buchwald et al. used the phosphate to amide III band as an indicator of mineralisation ratio and found OA subchondral bone to be less mineralised than controls(Buchwald 2012). They concluded that hypomineralisation of OA subchondral bone was a consequence of increased turnover and remodelling. Furthermore, Grynpas et al. found that despite an increased thickness, the subchondral cortical plate in OA was deficient in mineral(Grynpas 1991). Ageing is known to increase mineral content and can therefore influence the mineral to matrix ratio(Grynpas 1991). One could therefore argue that the observed difference between the OA specimens and the control fresh specimens could be a result of ageing, given that the control fresh cohort had a lower mean age compared to the OA cohort. This however does not explain the difference between OA and control cadaveric; two cohorts that were age matched.

5.2.2.2 Carbonate to phosphate ratio as indicative of carbonate substitution

The carbonate to phosphate ratio reflects the extent of carbonate accumulation in the apatite crystals. Carbonate accumulation was significantly lower in OA subchondral bone than controls. This was the case when comparing the OA cohort with the control cohort (fresh and cadaveric combined). Comparison of the medial to the lateral tibial plateau in OA specimens did not demonstrate a statistically significant decrease.

It is believed that carbonate substitution into the apatite crystals increases as a response to a decline in mineralization(Buchwald 2012). Carbonate ions may replace phosphate ions in apatite crystals as an attempt to limit mineral loss. These findings further support the hypermineralisation found in OA subchondral bone.

Putting the results so far together, they suggest the presence of hypermineralisation in OA subchondral bone with high levels of phosphate and low levels of carbonate in the apatite crystals. The findings do not support the hypothesis. The lower levels of carbonate accumulation in OA were unexpected. Buchwald et al. found carbonate accumulation to be significantly higher in OA subchondral bone than controls(Buchwald 2012).

5.2.2.3 Carbonate to Amide I Ratio as Indicator of Remodeling

It has been suggested that the carbonate to amide I ratio is a marker for bone remodeling(McCreadie 2006). The carbonate to amide I ratio was significantly higher in osteoarthritic subchondral bone when

compared to controls (fresh and cadaveric combined). The results suggest that bone remodeling is higher in OA than controls. This is consistent with the literature. Woods et al. found similar carbonate to amide I ratios in OA specimens(Woods 2011). Grynpas et al. discovered increased levels of bone remodeling in the weight-bearing regions of OA subchondral bone compared to non-weight bearing regions(Grynpas 1991). Furthermore, Mansell and Bailey also found OA bone to be more metabolically active than controls, and the rate of turnover to decrease distally(Mansell 1998). The polarisation in OA bone turnover could precipitate joint deformity as the levels of bone remodeling can influence the morphology. Indeed, knee joint deformity is regularly seen in end-stage OA. Joint deformity could aggravate the disease process by increasing the stress on subchondral bone.

The increase in subchondral bone turnover in OA is not due to a remodeling of microfractures (Burr 2004), as first envisaged by Radin and Rose(Radin 1986). Burr proposes that microcracks, instead of microfractures, may play a physiological role. Mechanically overloading the joint may result in microcracks, which disrupt the canalicular processes resulting in apoptosis of osteocytes. This brings the continuous release of sclerostin by osteocytes to a halt. This somehow, for reasons not completely understood, stimulates bone remodeling. Perhaps, when the inhibitory effect of sclerostin is lost, osteoblasts can express RANKL on their cell-surface. RANKL can bind to RANK, which is on the surface of osteoclast-precursor cells. This interaction stimulates the latter to differentiate into mature osteoclasts, which can

then resorb bone. Indeed, osteoclasts are seen leading the cutting cones and residing in resorption pits. They help remove microcracks and eventually the damage is repaired by osteoid-secreting osteoblasts. Therefore, the presence of microcracks in OA results in an increased rate of subchondral bone turnover, which in turn, leads to a decrease in the material density(Burr 2004).

5.2.2.4 Amide I to Amide III as indicator of collagen's secondary structure

Diagnosis and monitoring of collagen defects poses a challenge, especially for sub-clinical patients, since several inter-related biochemical, environmental and genetic factors may lead to collagen damage. Genetic and acquired abnormalities in types I, II and IX collagen cause a range of skeletal diseases, such as early-onset osteoarthritis, Stickler's syndrome and osteogenesis imperfecta (OI)

Amide I to amide III ratio was used in this study as a potential marker of collagen I secondary structure. When comparing osteoarthritic samples to normal (fresh and cadaveric combined) there was a statistically significant difference with a higher ratio in the OA group. This can potentially and cautiously be interpreted as a reflection of collagen differences between the OA and control groups.

Raman spectroscopy of proteins has shown that changes in the secondary structure, due to environmental, mechanical, or chemical stresses, will be reflected in the amide III and amide I bands(Morris 2011). These alterations may be observed as changes in band position,

band area ratio, or band intensity ratio.

The value of the amide I to amide III ratio was expected to remain consistent, regardless of the type of tissue examined. Nevertheless, the observed difference clearly supports and extends earlier observations(Morris 2011) that Raman spectroscopy is able to identify collagen disorders. Therefore, amide I and amide III Raman bands can be used to identify and possibly quantify disorders in the secondary structure of collagen protein in osteoarthritic tissue.

Loss of collagen fiber elasticity from normal ageing could be the cause of the spectroscopic changes that are observed in the amide I and amide III bands. However in our cohort OA samples had similar ages with the normal cadaveric samples and yet there was statistically significant difference in the amide ratio between these two groups.

5.2.3 Multivariate Analysis

PCA and PCA-LDA were used to try and determine if there were differences between non-OA and OA specimens across the whole spectrum, as well as at *a priori* bands.

When comparing OA to control (fresh and cadaveric together), irrespective of compartment, two distinct groups form. This is consistent with OA being a whole joint disease, something that has been implied by the results of the univariate analysis so far.

Furthermore, if we divide the control group to control fresh and control cadaveric (age-matched to OA) again we can easily identify

three groups with some degree of overlapping between the OA and control fresh group. An attractive explanation for this would be that the control cadaveric group, being older has not so far developed clinical OA and likely would not do so. Instead the younger, control fresh group, may be predisposed to OA and the subtle changes in the subchondral bone that reflect this predisposition may well be detected by Raman.

The changes observed between the non-OA and OA specimens using multivariate analysis, both with specimens divided into medial and lateral compartments as well as analysed as a whole compartment, in combination with the findings from the univariate analysis have shown that the whole joint is affected, and perhaps at different stages of disease. Multivariate analysis has shown that the main differences are due to phosphate and Amide I. This suggests that there are changes in collagen, specifically affecting mineralisation of the subchondral bone.

5.2.4 Summary for Raman Spectroscopy Results and Wider Implications

OA tibial plateaus (irrespective of compartment) did demonstrate higher phosphate to amide ratio (higher mineralization), lower carbonate to phosphate ratio (higher mineralization), higher carbonate to amide I ratio (higher remodeling), higher amide I to amide III ratio (alterations in collagen structure) when compared to control groups.

Comparison of the medial to the lateral tibial plateau in OA specimens did not demonstrate any statistically significant difference for phosphate to amide I ratio, carbonate to phosphate ratio, carbonate to

amide I ratio and amide I to amide III ratio. This is not consistent with the macroscopic, clinical findings of cartilage loss affecting the medial tibial plateau with relative preservation of the lateral compartment. This discrepancy could be explained by the notion that osteoarthritis is indeed a whole joint disease affecting equally the subchondral bone in both medial and lateral compartments but with clinical disease becoming apparent first in the main load bearing part of the joint (i.e. medial side).

5.3 Collagen Alpha Chain Analysis

5.3.1 Appraisal of Collagen Alpha Chain Analysis

5.3.1.1 Tissue Preparation

Pepsin was used to digest proteins and liberate collagen. In reality, pepsin does not digest all non-collagenous proteins. This means that collagen which was still locked in the matrix after pepsin treatment, was lost from the sample when the pellet was discarded. It is widely documented that tropocollagen is highly resistant to digestion from most proteases with the exception of collagenases(Bannister 1972). However, it has been reported that subtle differences occur to tropocollagen after treatment with pepsin; such as the release of telopeptide regions which are critical for crosslinking α chains(Steven 1965).

5.3.1.2 SDS PAGE

The majority of OA samples stained quite well whereas the majority of the normal samples failed to stain. It may be that the OA samples, because of their superior turnover rate, dissolve more readily in pepsin. Perhaps the normal samples could have been left in pepsin for longer but this would be a risky strategy. On the other hand, more concentrated solutions could have been made by dissolving in less sample buffer, or a greater volume could have been loaded onto the gels. Either would have increased the quantity of collagen loaded. However, increasing the concentration or volume also increases the risk of overloading the gel. In hindsight, almost all of the normal samples failed to stain whilst at the same concentration and volume as OA sample. This strongly suggests that the problem was not the concentration or volume used but the solubility of the normal collagenous proteins in pepsin. A final criticism of the methodology is that the G-force, which is critical to centrifugation, should have also been assessed in addition to the speed, time and temperature.

5.3.2 Discussion of Collagen Alpha Chain Analysis Method

The difference in the α_1-chain to α_2-chain ratio between OA and normal samples was found to be statistically significant. A normal type I collagen heterotrimer consists of two α_1-chains and one α_2-chain in the triple helix secondary structure. The OA samples had a median α_1-chain to α_2-chain ratio of 3.05:1 (IQR 3.95:1 – 2.4:1), which is above the normal level for heterotrimeric collagen of 2:1 (standard 2.476:1). On the contrary, Bailey et al. found ratios in the range of 4:1 – 17:1 in OA samples(Bailey 2002). One could argue that the amount of homotrimer

depends on the severity of OA. However, all ten patients had Grade IV OA. In addition Bailey and his coworkers used an area of cancellous bone distant to the joint surface for their measurements, which is in contrast with the area used in this current study (defined within 3mm from the joint surface). Nevertheless, our results suggest that homotrimeric collagen is not always present in OA to the extent that was initially anticipated.

The increase in α_1-chain to α_2-chain ratio detected supports previous work (Bailey 2002; Troung 2006; Couchourel 2009). Troung et al. investigated bone at a site distant from the active site of the disease, whereas Couchourel et al. and Bailey et al., investigated bone from the active site of OA and found higher ratios. It was expected that the ratio of alpha 1 to alpha 2 chains would be closer to the results of Bailey et al. and Couchourel et al. However Bailey et al. obtained cores from femoral heads at a location greater than 3 mm from the joint surface, which is what has been used in this study as definition of subchondral bone.

On the other hand the observed increase in the alpha 1 to alpha 2 ratio may be exaggerated. It is worth noting that the alpha 1 chain is 139 kDa whilst the alpha 2 chain is 129kDa. The larger weight of the alpha 1 chain may cause the band to appear larger than it actually is. This would make the ratio higher; and this also may be the reason that the mean collagen standard ratio is 2.476:1 rather than the expected 2:1.

5.3.3 Summary of Collagen Alpha Chain Analysis and Wider Implications

This is the first report of an increase in the ratio of alpha 1 to alpha 2 collagen I chain ratio in subchondral bone from human osteoarthritic knees. Collagen I homotrimer has been previously been reported for the hip joint. Our samples reflect true subchondral bone and this finding can an extra piece in the interpretation of the pathophysiological changes associated with OA as well as potentially forming a therapeutic target in the future.

5.4 OA IS A WHOLE JOINT DISEASE

Raman spectroscopy used in this study, found no difference between medial and lateral osteoarthritic tibial plateaus. This was expected for the control specimens but not for the OA where the medial has so clearly advanced grade IV macroscopic disease and the lateral does not. These findings suggest that OA of the knee is a total joint disease, with the subchondral bone exhibiting chemical changes in the entirety of the tibial plateau but with the load-bearing side being macroscopically affected first leading to degradation of the articular cartilage.

Furthermore, Raman spectroscopy can detect these changes and possibly at an early stage of disease in the subchondral bone, prior to cartilage degradation. Future efforts will assess spatially offset Raman spectroscopy, a technique offsetting the collection of Raman photons and therefore allowing study of materials several millimetres beneath a surface (skin), for both characterising and detecting osteoarthritis during the early subclinical phase.

5.5 CONCLUSIONS

In summary this study supports the following findings:

1. OA of the knee is a total joint disease, affecting not only the articular cartilage but the underlying subchondral bone as well. Chemical alterations in the subchondral bone appear to pre-date any cartilage damage and affect both the medial and lateral compartments of the knee joint, irrespective of the overlying macroscopic degree of cartilage loss.
2. Raman spectroscopy can detect changes at an early stage of clinical disease in the subchondral bone matrix chemistry, prior to cartilage degradation. Indeed the differences in OA and non OA cohorts may be inherent and allow screening of individuals at risk.
3. subchondral bone has a crucial role in the development of OA. It is highly likely that it is the principal tissue involved in the aetiopathogenesis of osteoarthritis and therefore an important future target for novel diagnostic and therapeutic approaches.

5.6 WIDER IMPLICATIONS

The findings of this study contribute to the current body of knowledge surrounding subchondral bone in OA. The increase in the carbonate to amide I ratio in OA specimens may reflect an increase in bone turnover. This finding agrees with several previous reports of increased turnover in subchondral bone. Perhaps now is the time to ask

whether we should start targeting subchondral bone turnover when treating OA. This study has further validated Raman Spectroscopy at a time where research is entering the translational phase and SORS is being considered as a tool for diagnosing bone disorders.

Can SORS be used to measure mineral to collagen ratio differences (and hence mechanical property differences) non-invasively in vivo? Can SORS be used to measure amide I band profile changes in vivo in diseased or aged bones? A clinical trial of SORS, which looks into answering these and other questions, is currently underway at the UCL Institute of Orthopaedics and Musculoskeletal Science at the Royal National Orthopaedic Hospital (Stanmore).

5.7 FUTURE WORK

Some of the findings could be correlated with other more established techniques. For instance, the hypermineralisation detected by Raman spectroscopy could be correlated against levels of mineralisation determined through biochemistry. Alternatively, the mineral-to-matrix ratio could be calibrated against measured materials such as the ash weight of bone.

Moreover validation of the spectroscopic findings in terms of matrix mineralization can be performed in the future by looking at the material properties of the subchondral bone. Mechanical properties of bone are a combination of bone structure and material properties, where the material properties are determined by the chemical composition and microstructural organization of the extracellular matrix. While an

increasing level of bone mineralization is accompanied by an increase in the stiffness of the bone, it comes at the cost of reduced toughness (energy required to cause a fracture) of the bone. In other words, as mineralization increases, the tissue becomes more brittle and requires less energy to fracture. Therefore, it is possible for a bone that is hypermineralized to be more fragile than a bone with a lower degree of mineralization. Time unfortunately did not allow testing of the mechanical properties of subchondral bone but this investigation is currently being undertaken in our laboratory.

5.8 FUTURE DIRECTIONS

It is intriguing to conceptualize the application of Raman spectroscopy as a diagnostic modality given its ease of use, non-invasiveness and safety. The carbonate to phosphate band area ratio is calculated using bands that are not obscured by collagen protein signal. Observation of the strong phosphate band at 958 cm^{-1} and the carbonate band at ~1070 cm^{-1} in spectra that have not been baseline corrected indicates that calculation of this ratio would be possible in specimens with a thicker articular cartilage layer, therefore allowing interrogation of subchondral bone even in those cases where the cartilage is not lost due to the osteoarthritic process. Fiber-optic technology is frequently used through arthroscopes to evaluate knee, hip, shoulder and ankle joints. Silica fiber optic Raman probes have been used to evaluate coronary artery calcifications in a clinical experimental setting(Brennan 1997), as well as in animal studies to

diagnose cellular dysplasia in cancer models(Schut 2000). The non-destructive nature and sensitivity of Raman spectra to subtle tissue changes are attractive features in developing clinically relevant platforms such as a fiber-optic insert within an arthroscope. Potentially, Raman spectroscopy could be utilized through a combined arthroscopic imaging/Raman spectroscopic fiber optic system to diagnose early OA, or follow the response of damaged cartilage or subchondral bone to therapeutic intervention.

REFERENCES

Ager, J. (2005). "Deep-ultraviolet Raman spectroscopy study of the effect of aging on human cortical bone." Journal of Biomedical Optics **10**(3).

Akkus, O. (2003). "Aging of microstructural compartments in human compact bone." Journal of Bone and Mineral Research **18**(6): 1012-1019.

Akkus, O. (2004). "Age-related changes in physicochemical properties of mineral crystals are related to impaired mechanical function of cortical bone." Bone **34**(3): 443-453.

Anderson-MacKenzie, J. (1999). "Collagen remodelling in the anterior cruciate ligament associated with developing spontaneous murine osteoarthritis." Biochem Biophys Res Commun **258**: 763-767.

Bailey, A. (1997). "Do subchondral bone changes exacerbate or precede articular cartilage destruction in osteoarthritis of the elderly. ." Gerontology **43**: 296-304.

Bailey, A. (1999). "Age-related changes in the biochemical properties of human cancellous bone collagen: Relationships to bone strength." Calcif Tissue Int **65**: 203-210.

Bailey, A. (1999). "Molecular changes in bone collagen in osteoporosis and osteoarthritis in the elderly." Experimental Gerontology **34**: 337-351.

Bailey, A. (2002). "Phenotypic expression of osteoblast collagen in osteoarthritic bone: production of type I homotrimer." International Journal of Biochemistry & Cell Biology **34**(2): 176-182.

Bailey, A. (2004). "Biochemical and mechanical properties of subchondral bone in osteoarthritis. ." Biorheology **41**: 349-358.

Bannister, D. (1972). "Pepsin Treatment of Avian Skin Collagen - Effects on Solubility, Subunit Composition and Aggregation Properties." Biochemical Journal **129**(3).

Banse, X. (2002). "The cross-link profile of bone collagen correlates with the structural organization of the trabeculae." Bone **31**: 70-76.

Banse, X. (2002). "Mechanical properties of adult vertebral cancellous bone: Correlation with collagen intermolecular cross-links." Journal of Bone Mineral Research **17**: 70-76.

Bella, J. (1995). "Hydration structure of a collagen peptide." Structure **3**: 893-906.

Billingham, M. (1998). Value of animal models of osteoarthritis in the search for disease modifying anti-osteoarthritic drugs. Osteoarthritis. M. D. KD Brandt, LS Lohmander. Oxford, Oxford University Press.

Blake, G. (1997). "Technical principles of dual energy x-ray absorptiometry." Seminars in nuclear medicine **27**(3): 210-228.

Boivin, G. (1990). "Transmission electron microscopy of bone tissue. A review." Acta Orthop Scand **61**(2): 170-180.

Boivin, G. (2002). "Changes in bone remodelling rate infuence the degree of mineralization of bone." Connective Tissue Research **43**(2-3): 535-537.

Boskey, A. L. (2001). Bone Mineralization. Bone Mechanics Handbook. S. C. Cowin, CRC Press, Boca Raton, FL., USA.

Brennan, J. (1997). "Near-infrared Raman Spectrometer Systems for Human Tissue Studies." Applied Spectroscopy **51**(2): 201-208.

Brereton, R. (2003). Chemometrics, data analysis for the laboratory and chemical plant. New York, Wiley.

Bruyere, O. (2003). "Subchondral tibial bone mineral density predicts future joint space narrowing at the medial femoro-tibial compartment in patients with knee osteoarthritis. ." Bone **32**(5): 541-545.

Buchwald, T. (2012). "Identifying compositional and structural changes in spongy and subchondral bone from the hip joints of patients with osteoarthritis using Raman spectroscopy." Journal of Biomedical Optics **17**(1).

Buckland-Wright, J. (1994). " Quantitiative microfocal radiographic assessment of osteoarthritis of the knee from weight bearing tunnel and semi-flexed standing views." J. Rhematol. **21**: 1734-1741.

Buckland-Wright, J. (2004). "Subchondral bone changes in hand and knee osteoarthritis detected by radiography." Osteoarthritis and Cartilage **12**(Suppl A): S10-S19.

Burr, D. (1997). "The involvement of subchondral mineralized tissues in osteoarthrosis: Quantitative microscopic evidence. ." Microscopy Research and Technique **37**(4): 343-357.

Burr, D. (1998). "The importance of subchondral bone in osteoarthrosis." Curr Opinions Rheum **10**: 256-262.

Burr, D. (2003). Subchondral bone in the pathogenesis of osteoarthritis. Mechanical aspects. Osteoarthritis 2nd edition. M. D. KD Brandt, LS Lohmander. Oxford, Oxford University Press**:** 125-133.

Burr, D. (2004). "The importance of subchondral bone in the progression of osteoarthritis." Journal of Rheumatology **31**: 77-80.

Carey, P. (1982). Chapter 1. Biochemical Applications of Ramannand Resonance Raman Spectroscopies. N.Y. USA, Academic Press.

Carlson, C. (1996). "Osteoarthritis in cynomolgus macaques. III: Effects of age, gender, and subchondral bone thickness on the severity of disease." J Bone Miner Res **11**(9): 1209-1217.

Carmejane, O. D. (2005). "Bone chemical structure response to mechanical stress studied by high pressure Raman spectroscopy." Calcif Tissue Int **76**(3): 207-213.

Cawston, T. (1996). "Metalloproteinase inhibitors." Pharmacol Ther **70**: 163-188.

Chipman, S. (1993). "Defective pro-α2(I) collagen synthesised in a recessive mutation in mice. A model for human osteogenesis imperfecta." Proc. Natl. Acad. Sci. **90**: 1701-1705.

Cohen, J. (1988). Statistical Power Analysis for the Behavioural Sciences Lawrence Erlbaum Associates.

Cohen, N. P. (1998). "Composition and Dynamics of Articular Cartilage: Structure, Function, and Maintaining Healthy State." Journal of Orthopaedic and Sports Physical Therapy **28**(4): 203-212.

Couchourel, D. (2009). "Altered mineralization of human osteoarthritic osteoblasts is attributable to abnormal type I collagen production." Arthritis & Rheumatism **60**(5): 1438-1450.

Cowin, S. C. (1999). "Bone Poroelasticity." Journal of Biomechanics **32**: 217-238.

Cowman, M. K. (2005). "Experimental approaches to hyaluronan structure." Carbohydrate Research **340**(5): 791-809.

Currey, J. (2006). Bones: structures and mechanics, 2nd edition, Princeton University Press, princeton, N.J., USA.

Danese, R. (2001). "Ultrsound of the skeleton: review of its clinical limitationsand pitfalls." Current Rheumatology Reports **3**(3): 245-248.

Day, J. (2004). "Adaptation of subchondral bone in osteoarthritis." Biorheology **41**: 359-368.

Dequeker, J. (1993). "Generalised OA associated with increased insulin-like growth factor I and II and transforming growth factor-β in cortical bone from the iliac crest." Arthritis & Rheumatism **36**: 1702-1708.

Dequeker, J. (1993). "Osteoarthritis protects against femoral neck fracture: the MEDOS study experience." Bone (NY) **14**: S51-S56.

Dieppe, P. (1993). "Prediction of the Progression of Joint Space Narrowing in Osteoarthritis of the Knee by Bone-Scintigraphy." Annals of the Rheumatic Diseases **52**(8): 557-563.

Dieppe, P. (2005). "Pathogenesis and management of pain in osteoarthritis." The Lancet **365**: 965-973.

Donnelly, E. (2010). "Effects of tissue age on bone tissue material composition and nanomechanical properties in the rat cortex." Journal of Biomedical Materials Research **92**(3): 1048-1059.

Draper, E. (2005). "Novel assessment of bone using time-resolved transcutaneous Raman spectroscopy." Journal of Bone and Mineral Research **20**(11): 1968-1972.

Esbensen, K. (2005). Multivariate Data Analysis - In Practice. Denmark, CAMO Process AS.

Fam, H. "Rheological properties of synovial fluids." Biorheology **44**(2): 59-74.

Felson, D. (2000). "Osteoarthritis: new insights. Part 1: the disease and its risk factors." Ann Intern Med **133**(8): 635-646.

Felson, D. (2004). "Osteoarthritis: Is it a disease of cartilage or of bone? ." Arthritis & Rheumatism **50**(2): 341-344.

Ferguson, V. L. (2003). "Nanomechanical properties and mineral concentration in articular calcified cartilage and subchondral bone." Journal of Anatomy **203**: 191-202.

Fermor, B. (1998). "Primary human osteoblast proliferation and prosaglandin E2 release in response to mechanical strain in vitro." Bone **22**: 637.

Fratzl, P. (1993). "Collagen packing and mineralization; An xray scattering investigation of turkey leg tendon." Journal of Biophysics **64**: 260-266.

Fratzl, P. (2004). "Structure and mechanical quality of the collagen-mineral nanocomposite in bone." Journal of Materials Chemistry **14**: 2115.

Freeman, J. (2001). "Raman spectroscopic detection of changes in bioapatite in mouse femora as a function of age and in vitro fluoride treatment." Calcif Tissue Int **68**(3): 156-162.

Gabriel, S. (2001). Epidemiology of Osteoarthritis. *Kelley's Textbook of Rheumatology 6th edition*. E. H. J. S Ruddy, CB Sledge, JS Sergent, RC Budd. Philadelphia, W.B. Saunders**:** 324-327.

Gamsjaeger, S. (2010). "Cortical bone composition and orientation as a function of animal and tissue age in mice by Raman spectroscopy." Bone **47**: 392-399.

Garnero, P. (1998). "The collagenolytic activity of cathepsin K is unique among mammalian proteinases." J Biol Chem **273**: 32347-32352.

Genant, H. (1996). "Advances in the noninvasive assessment of bone density, quality and structure." Calcif Tissue Int **59**: S10-S15.

Glanville, R. (1983). "Completion of the amino acid sequence of the alpha 1 chain from type I calf skin collagen. Amino acid sequence of alpha 1(I)B8." The Biochemical Journal **215**: 183-189.

Goodship, A. E. (1979). "Functional adaptation of bone to increased stress - An experimental study." The Journal of Bone and Joint Surgery (Am) **61**(4): 539-546.

Gregg, E. (1997). "The epidemiology of quantitative ultrasound: a review of the realtionships with bone mass, osteoporosis and fracture risk." Osteoporosis International **7**(2): 88-89.

Grynpas, M. (1991). "Subchondral bone in osteoarthritis." Calcif Tissue Int **49**: 20-26.

Grynpas, M. (1993). "Effect of age and osteoarthritis on bone mineral in rhesus monkey vertebrae." J Bone Miner Res **8**(8): 909-917.

Guccione, A. (1994). "The effects of specific medical conditions on the functional limitations of elders in the Framingham Study." Am J Public Health **84**(3): 351-358.

Hair, J. (1998). Multivariate Data Analysis. UK, Prentice hall.

Heaney, R. (2005). "BMD: The problem." Osteoporosis International **16**(9): 1013-1015.

Hendrick, R. (1994). "The AAPM/RSNA Physics Tutorial for Residents - Basic Physics of MR Imaging - An Introduction." Radiographics **14**(4): 829-846.

Hilal, G. (1998). "Osteoblastic-like cells from human subchondral osteoarthritic
bone demonstrate an altered phenotype in vitro: possible role of subchondral bone sclerosis." Arthritis & Rheumatism **41**: 981-999.

Hochberg, M. (2012). "Genetic epidemiology of osteoarthritis: recent developments and future directions." Curr Opin Rheumatol.

Holmgren, S. (1998). "Code for collagen stability deciphered." Nature **392**: 666-667.

Huerre, C. (1982). "Human type I procollagen genes are located on different chromosomes." Proceedings of the National Academy of Sciences of the United States of America **79**: 6627-6630.

Hulmes, D. (1995). "Radial packing, order and disorder in collagen fibrils." Biophysical Journal **68**(5): 1661-1670.

Hunter, D. (2003). "Evidence of altered bone turnover, vitamin D and calcium regulation with knee osteoarthritis in female twins. ." Rheumatology (Oxford) **42**(11): 1311-1316.

Jay, G. D. (2007). "Association between friction and wear in diarthrodial joints lacking lubricin." Arthritis & Rheumatism **56**(11): 3662-3669.

Johanson, N. (1993). "Femoral neck bone density. Direct measurement and histomorphometric validation." J Arthroplasty **8**(6): 641-652.

Johnson, L. (1962). "Joint remodelling as a basis for osteoarthritis." J. Amer. Vet. Med. Assoc. **141**: 1237-1241.

Jollife, I. (1986). Principal Component Analysis. New York, Springer, New York.

Jones, G. (1995). "Osteoarthritis, Bone-Density, Postural Stability, and Osteoporotic Fractures - A Population-Based Study." Journal of Rheumatology **22**(5): 921-925.

Jones, H. (1987). "Inactivation of antithrombin III in synovial ¯uid from patients with rheumatoid arthritis. ." Ann Rheum Dis **57**: 162-165.

Karampas, I. (2012). "A quantitative bioapatite/collagen calibration method using Raman spectroscopy of bone." J Biophotonics **doi: 10.1002/jbio.201200053**.

Kavukcuoglu, N. (2007). "Nanomechanics and Raman spectroscopy of fibrillin 2 knock-out mouse bones." Journal of Materials Science **42**(21): 8788-8794.

Kazanci, M. (2007). "Raman imaging of two orthogonal planes within cortical bone." Bone **41**(3): 456-461.

Kelly, J. (2010). Infrared microspectroscopy of cancerous and non-cancerous cells
, University of Lancaster.

Kim, H. M. (1996). "X-Ray Diffraction, Electron Microscopy, and Fourier Transform Infrared Spectroscopy of Apatite Crystals Isolated From Chicken and Bovine Calcified Cartilage." Calcified Tissue International **59**(1): 58-63.

Knott, L. (1998). "Collagen cros-links in mineralising tissues: a review of their chemistry, function and clinical relevance." Bone **22**: 181-187.

Kohn, D. (2009). "Exercise alters mineral and matrix composition in the absence of adding new bone." Cells Tissues Organs **189**: 33-37.

Krishnan, R. (1981). "Raman effect: History of the discovery." Journal of Raman Spectroscopy **10**: 1-8.

Kubisz, L. (2007). "FT NIR Raman studies on gamma-irradiated bone, Spectrochimica Acta Part A - Molecular and Biomolecular." Spectroscopy **66**(3): 616-625.

Kucharz, E. J. (1992). The Collagens: Biochemistry and Pathophysiology. Berlin, Springer-Verlag.

Kurhanewicz, J. (1996). "Three - dimensional H-1 MR spectroscopic imaging of the in situ human prostate with high (0.24 - 0.1 cm3) spatial resolution." Radiology **198**(3): 795-805.

Kvistad, K. (1999). "Characterization of neoplastic and normal human breast tissues with in vivo H - 1 MR spectroscopy." Journal of Magnetic Resonance Imaging **10**(2): 159-164.

Lahm, A. (2004). "Articular cartilage degeneration after acute subchondral bone damage: an experimental study in dogs with histopathological grading. ." Acta Orthop Scand **75**(6): 762-767.

Lanyon, L. (1996). "Using functional loading to in¯uence bone mass and architecture." Bone **18**: 375-435.

Lees, S. (1977). "The role of collagen in the elastic properties of calcified tissues." Journal of Biomechanics **10**: 473-486.

Lees, S. (1987). "Considerations regarding the structure of the mammalian mineralized osteoid from viewpoint of the generalised packing model." Connective Tissue Research **16**(4): 281-303.

Lees, S. (1990). "BAPN dose dependence of mature crosslinking in bone matrix collagen of rabbit compact bone: Corresponding variation of sonic velocity and equatorial diffraction spacing." Connective Tissue Research **24**: 95-105.

Li, B. (1997). "Composition and Mechanical Properties of Cancellous Bone from the Femoral Head of Patients with Osteoporosis or Osteoarthritis. ." Journal of Bone and Mineral Research **12**(4): 641-651.

Li, B. (1999). "The electron microscope appearance of the subchondral bone plate in the human femoral head in osteoarthritis and osteoporosis." Jounal of Anatomy **195**: 101-110.

Long, D. (2002). The Raman Effect: A Unified Treatment of the Theory of Raman Scattering by Molecules. Chichester, U.K., John Wiley & Sons.

Mahesh, M. (2002). "The AAPM/RSNA physics tutorial for residents - Search for isotropic resolution in CT from conventional through multiple - row detector." Radiographics **22**(4): 949-962.

Mansell, J. (1998). "Abnormal cancellous bone collagen metabolism in osteoarthritis." J Clin Invest **101**(8): 1596-1603.

Mansell, J. (2007). "Bone, not cartilage, should be the major focus in osteoarthritis." Nat Clin Pract Rheumatol **3**(6): 306-307.

Marieb, E. N. (1998). Human Anatomy and Physiology. Menlo Park, CA, Benjamin Cummings Science Publishers.

Martens, H. (1989). Multivariate Calibration. Chichester, England, Wiley.

Mason, D. (1997). "Mechanically regulated expression of a neural glutamate transporter in bone. A role for excitatory amino acids as osteotropic agents." Bone **20**: 199-205.

Matousek, P. (2006). "Noninvasive Raman spectroscopy of human tissue in vivo." Applied Spectroscopy **60**(7): 758-763.

Matsui, H. (1997). "Cartilage and subchondral bone interaction in osteoarthrosis of human knee joint: A histological and histomorphometric study. ." Microscopy Research and Technique **37**(4): 333-342.

McCreadie, B. (2006). "Bone tissue compositional differences in women with and without osteoporotic fracture." Bone **39**(6): 1190-1195.

Miller, T. (1996). "Clinical aspects of emission tomography." Radiographics **16**(3): 661-668.

Miller, T. (1998). "Xanthine oxoreductase catalyses the reduction of nitrates to nitric oxide under hypoxic conditions. ." FEBS Letters **427**: 225-228.

Morris, M. (2004). "Bone tissue ultrastructural response to elastic deformation probed by Raman spectroscopy." Faraday Discussions **126**: 159-168.

Morris, M. (2004). "Kerr-gated picosecond Raman spectroscopy and Raman photon migration of equine bone tissue with 400-nm excitation." Proceedings of the SPIE - Biochemical Vibrational Spectroscopy and Biohazard Detection Technologies **5321**: 164-169.

Morris, M. (2005). "Kerr-gated time-resolved Raman spectroscopy of equine cortical bone tissue." Journal of Biomedical Optics **10**(1).

Morris, M. (2005). "Picosecond time-gated Raman spectroscopy for transcutaneous evaluation of bone composition." Proceedings of the SPIE - Optical Tomography and Spectroscopy of Tissue VI **5693**: 344-350.

Morris, M. (2011). "Raman Assessment of Bone Quality." Clinical Orthopaedics and Related Research **469**(8): 2160-2169.

Murray, D. (1990). "The effect of strain on bone cell prostaglandin-E2 releaseÐa new experimental method." Calcif Tissue Int **47**: 35-39.

Neumann, A. (1999). "High molecular weight hyaluronic acid inhibits advanced glycation endproduct-induced NF-kB activation and cytokine expression." FEBS Letters **453**(3): 283-287.

Newberry, W. (1997). "Subfracture insult to a knee joint causes alterations in the bone and in the
functional stiffness of overlying cartilage." J Orthop Res **15**: 450-455.

Oegema, T. (1997). "The interaction of the zone of calcified cartilage and subchondral bone in osteoarthritis." Microscopy Research and Technique **37**(4): 324-332.

Oxlund, H. (1995). "Reduced concentration of collagen cross-links are associated
with reduced strength of bone." Bone **17**(Suppl 4): 365S-371S.

Penel, G. (2005). "Composition of bone and apatitic biomaterials as revealed by intravital Raman microspectroscopy." Bone **36**(5): 893-901.

Pfeilschifter, J. (1998). "Concentration of transforming growth factor beta in human bone tissue: relationship to age, menopause, bone turnover and bone volume." J Bone Miner Res **13**: 716-730.

Polomska, M. (2010). "Fourier Transform Near Infrared Raman Spectroscopy in Studies on Connective Tissue." Acta Physica Polonica **118**(1): 136-140.

Pooley, R. (2005). "The AAPM/RSNA physics tutorial for residents - Fundamental physics of MR imaging." Radiographics **25**(4): 1087-1099.

Quasnichka, H. (2000). The role of knee cruciate ligament in a spontaneous model of osteoarthritis [Abstract]. 17th Federation of European Connective Tissue Societies. Athens.

Quasnichka, H. (2006). "Subchondral bone and ligament changes precede cartilage degradation in guinea pig osteoarthritis." Biorheology **43**: 389-397.

Radin, E. (1986). "Role of subchondral bone in the initiation and progression of cartilage damage." Clin Orthop Relat Res **213**: 34-40.

Ramachandran, G. (1973). "A hypothesis on the role of hydroxyproline in stabilising the collagen structure." Biochim. Biophys. Acta 166-171.

Raman, C. (1928). "A New Radiation." Indian Journal of Physics **2**: 387-398.

Raman, C. (1928). "A New Type of Secondary Radiation." Nature **121**(3048): 501-502.

Reinmann, I. (1997). "Quantitative histologic analyses of articular cartilage and subchondral bone
from osteoarthritic and normal human hips." Acta Orthop Scand **48**: 63-67.

Ritchie, R. O. (2009). "Plasticity and Toughness in Bone." Physics Today: 41-47.

Rizzoli, R. (2003). "Bone strength and its determinants." Osteoporosis International **14**(3): 13-18.

Saied, A. (1997). "Assessment of articular cartilage and subchondral bone: subtle and progressive changes in experimental osteoarthritis using 50 MHz echography in vitro." J Bone Miner Res **12**: 1378-1386.

Schulmerich, M. (2006). "Transcutaneous fiber optic Raman spectroscopy of bone using annular illumination and a circular array of collection fibers." Journal of Biomedical Optics **11**(6).

Schulmerich, M. (2006). "Transcutaneous Raman spectroscopy of bone tissue using a non-confocal fiber optic array probe." Proceedings of the SPIE - Biochemical Vibrational Spectroscopy III: Advances in Research and Industry.

Schulze, G. (2005). "Investigation of selected baseline removal techniques as candidates for automated implementation." Applied Spectroscopy **59**(5): 545-574.

Schut, T. B. (2000). "In Vivo Detection of Dysplastic Tissue by Raman Spectroscopy." Anal Chem **72**(24): 6010-6018.

Sedlin, E. D. (1966). "factors affecting the determination of the physical properties of femoral cortical bone." Acta Orthopaedica Scandinavica **37**: 29-48.

Senior, K. (2000). "Osteoarthritis research: on the veerge of a revolution." Lancet **355**: 208(Editorial).

Shingleton, W. (1996). "Collagenase: a key enzyme in collagen turnover." Biochem Cell Biol **74**: 759-775.

Skerry, T. (1997). "Mechanical loading of bone: what sort of exercise is bene®cial to the skeleton." Bone **20**: 179-181.

Smith, E. (2005). Modern Raman Spectroscopy: a practical approach. Chichester, U.K., John Wiley & Sons.

Smith, J. (1968). "Molecular Pattern in Native Collagen." Nature **219**: 157-158.

Steven, F. (1965). "Cleavage of Tyrosyl Peptides by Pepsin from Collagen Solubilised by Nishihara Technique." Biochimica et Biophysica Acta **97**(3).

Tarnowski, C. (2002). "Mineralization of developing mouse calvaria as revealed by Raman microspectroscopy." Journal of Bone and Mineral Research **17**(6): 1118-1126.

Thompson, J. (2010). Netter's Concise Orthopaedic Anatomy. Philadelphia, Saunders Elsevier.

Thurner, P. (2009). "Atomic force microscopy and identation force measurement of bone." Engineering **1**(6): 624-649.

Thurner, P. (2009). "Atomic force microscopy and indentation force measurement of bone." Engineering **1**(6): 624-649.

Troung, L. (2006). "Differential gene expression of bone anabolic factors and trabecular bone architectural changes in the proximal femoral shaft of

primary hip osteoarthritis patients." Arthritis Research and Therapy **8**(6): R188.

Turner, C. H. (1993). "Basic biomechanical measurements of bone: a tutorial " Bone **14**: 595-608.

Veis, A. (1997). "Collagen fibrillar structure in mineralised and nonmineralised tissues." Current Opinion in Solid State and Materials Science **2**: 370-378.

Viguet-Carrin, S. (2006). "The role of collagen in bone strength." Osteoporosis International **17**: 319-336.

Votaw, J. (1995). "The AAPM/RSNA Physics Tutorial for Residents. Physics of PET." radiographics **15**(5): 1179-1190.

Wagermaier, W. (2006). "Spiral twisting of fiber orientation inside bone lamellae." Biointerphases **1(1)**: 1-5.

Walton, A. (1970). "Raman Spectroscopy of Calcified Tissue." Calcif Tissue Int **167**: 162-167.

Wang, C. T. (2006). "High molecular weight hyaluronic acid down-regulates the gene expression of osteoarthritis- associated cytokines and enzymes in fibroblast-like synoviocytes from patients with early osteoarthritis." Osteoarthritis and Cartilage **14**(12): 1237-1247.

Webb, R. (2004). "Opportunities for prevention of 'clinically significant' knee pain: results from a population- based cross sectional survey." J Public Health (Oxf) **26**(3): 277-284.

Webster, S. S. J. (2001). Integrated Bone Tissue Physiology. Bone Mechanics Handbook 2nd edition. S. C. Cowin, CRC Press, Boca raton, FL., USA.

Weiner, S. (1992). "Bone structure: From angstroms to microns." The FASEB Journal **6**(879-885).

Weiner, S. (1998). "The Material Bone: Structure-Mechanical Function Relations." Annual Review of Materials Science **28(1)**(271-298).

Westacott, C. (1997). "Alteration of cartilage metabolism by cells from osteoarthritic bone." Arthritis & Rheumatism **40**: 1282-1291.

Wilson, E. E. (2006). "Three structural roles for water in bone observed by solid-state NMR." Biophysical Journal **90**: 3722-3371.

Woods, C. (2011). Investigation of selected baseline removal techniques as candidates for automated implementation. IOMS, UCL. London, UCL, UoL. **MSc**.

Young, M. F. (2003). "Bone matrix proteins: their function, regulation and relationship to osteoporosis." Osteoporosis International **14**(3): S35-S42.

Zhang, Z. (2010). "Baseline correction using adaptive iteratively reweighted penalized least squares." Analyst **135**(5): 1138-1146.